The electrodynamic response of heavy-electron compounds

L. Degiorgi

Laboratorium für Festkörperphysik ETH-Zürich, CH-8093 Zürich, Switzerland

This review discusses the heavy-electron compounds and related materials from the perspective of their electrodynamic response. The investigation of the electrodynamic response by means of optical methods, extending over a very broad spectral range, should reveal, in principle, the complete excitation spectrum. This study incorporates several important sources of information on the intrinsic properties of the investigated materials. In particular, attention will be focused on the optical properties of prototype heavy-electron systems and on Kondo systems with low-temperature non-Fermi-liquid behavior or insulating characteristics. In the discussion, the electrodynamic response will be related to other relevant results arrived at by various experimental methods and to the theoretical state of the art. [S0034-6861(99)00303-7]

CONTENTS

I. INTRODUCTION

Highly correlated states of condensed matter have opened new chapters in physics. Examples of particular interest include the so-called Kondo or heavy-electron materials, which were discovered in the late seventies. The class of strongly correlated systems also includes the transition-metal oxides, including d-electron (Mott-Hubbard) systems as well as the high-temperature superconducting cuprates, quasi-one-dimensional materials, such as organic Bechgaard salts, and possibly the carbon fullerenes. It would be hopeless to try to address, even superficially and only from the optical point of view, all of these topics. Due to space limitations, the present review will be focused only on heavy-electron and related materials.

Heavy-electron systems are electrically conducting materials with peculiar low-temperature physical properties that distinguish them from ordinary metals (Ott and Fisk, 1987; Fisk *et al.*, 1988). In fact, the conduction-electron specific heat is typically some 100 times larger than that found in most metals. Similarly, the magnetic susceptibility can be two or more orders of magnitude larger than the temperature-independent Pauli susceptibility observed in conventional conducting materials.

The prototype heavy-electron materials include actinide and rare-earth alloys, mostly containing U and Ce, respectively, like $CeAl_3$, $CeCu_6$, UBe_{13}, and UPt_3.

At high temperatures, these systems behave as a weakly interacting collection of *f*-electron moments and conduction electrons with quite ordinary masses; at low temperatures, the *f*-electron moments become strongly coupled to the conduction electrons and to one another, and the conduction-electron effective mass is typically 10 to 100 times the bare electron mass. This obviously leads to an enhanced Sommerfeld coefficient γ of the linear T term associated with the electronic contribution to the specific heat. Alternatively, such an enhancement of the γ values indicates a large electronic density of states at the Fermi level E_F.

Heavy-electron materials constitute a formidable challenge to condensed-matter physicists not only with respect to their normal properties but also to their superconducting and magnetic properties, which are not yet fully understood. Particularly, the coexistence of heavy-electron behavior with magnetic ordering or superconductivity (or both) has attracted a lot of interest. In fact, although magnetic ordering and heavy-electron behavior (possibly together with superconductivity) seem, at first sight, to be mutually exclusive, various experimental observations in recent years indicate that this is not necessarily so (Ott and Fisk, 1987; Fisk *et al.*, 1988). Both magnetic ordering out of a heavy-electron state and the formation of a heavy-electron state in a magnetically ordered matrix seem possible. Examples of these two distinctly different situations are realized in the low-temperature properties of U_2Zn_{17} and UCu_5, which order antiferromagnetically at 9.7 and 15 K, respectively. Also of interest are those heavy-electron materials showing the coexistence of superconductivity with magnetic ordering (Maple *et al.*, 1986). In this respect, URu_2Si_2 attracted a lot of attention as the first heavy-electron metal with superconductivity ($T_c = 1$ K), developing in an antiferromagnetically ordered matrix ($T_N = 17.5$ K). More recently, a systematic search (Geibel, Schank, *et al.*, 1991; Geibel, Thies, *et al.*, 1991) led to the discovery of the coexistence of antiferromagnetism and superconductivity in UNi_2Al_3 ($T_N = 4.6$ K and $T_c = 1$ K) and UPd_2Al_3 ($T_N = 14$ K and $T_c = 2$ K), as well. On the other hand, superconductivity also manifests itself in some of the more "conventional" heavy-electron materials, e.g., $CeCu_2Si_2$, UPt_3, and UBe_{13}.

Another major issue and a current topic of debate in the field of highly correlated electron systems is the fundamental question of whether these systems, in their normal state, may be described as simple Fermi liquids. For some heavy-electron compounds (e.g., UPt_3) this seems indeed to be the appropriate picture. Specific-heat $C(T)$ and resistivity $\rho(T)$ data, supported by results of de Haas-van Alphen experiments, may be explained in this way, if strongly renormalized Fermi-liquid parameters are introduced. More recent experimental work (Maple *et al.*, 1994, 1995) has indicated, however, that several heavy-electron compounds and related alloys display quite remarkable properties, which may be much less well related to "conventional" Fermi-liquid behavior. Problems with Fermi-liquid-type descriptions of relevant data have been encountered on different occasions, involving materials like $UCu_{5-x}Pd_x$ for $x = 1$ and 1.5, $CeCu_{5.9}Au_{0.1}$, $U_xY_{1-x}Pd_3$ ($x < 0.2$), $Th_{1-x}U_xRu_2Si_2$ ($x < 0.07$), and $U_{1-x}Th_xPd_2Al_3$ ($x > 0.4$). In these compounds, specific-heat, magnetic susceptibility, and resistivity measurements were found to be at variance with the usual temperature dependence expected for these quantities in Fermi-liquid-type systems.

Among the highly correlated electron systems, various rare-earth compounds known as hybridization gap semiconductors or Kondo insulators have also attracted some interest recently (Aeppli and Fisk, 1992). These semiconductors are, with one exception, cubic, and their lattice parameters indicate a mixed-valence character for the *f* element in all cases in which comparisons can be made. Recent studies have reported on the properties of two Ce members of this class of narrow-gap semiconductors, and the conceptual simplicity of the Ce $4f^1 \leftrightarrow 4f^0$ configuration fluctuations has led to renewed interest in the several-decades-old hybridization gap problem. Within this class of so-called Kondo insulators, one finds a large variety of compounds, for instance, $Ce_3Bi_4Pt_3$, CeNiSn, SmB_6, TmSe, YbB_{12}, UNiSn, etc.

This work will review the current understanding of electrodynamic responses in conventional or prototype heavy-electron materials, non-Fermi-liquid Kondo alloys, and Kondo insulators. The electrodynamics of heavy-electron antiferromagnets have already been treated in a review (Degiorgi *et al.*, 1997) and various publications (Degiorgi, Dressel *et al.*, 1994; Degiorgi, Ott, Dressel *et al.*, 1994; Degiorgi, Ott, Dressel *et al.*, 1995; Thieme *et al.*, 1995). Measurements of the charge dynamics should help to address the crucial issue of the nature of the correlation effects. In our discussion, the information gained from the optical properties will be compared with information arrived at by other investigations. The comparison of experimental results will be complemented by a review of the theoretical background. The concluding section summarizes the principal findings and the major unresolved problems. The reader is referred to the book of Wooten (1972), and articles of Klein *et al.* (1993), Donovan *et al.* (1993), Dressel *et al.* (1993), and Degiorgi (1995) for a thorough presentation of the most commonly used experimental optical techniques.[1]

II. HEAVY-ELECTRON SYSTEMS

A. A phenomenological introduction

Heavy-electron materials can be considered as metals with strongly correlated, yet delocalized electrons. In order to understand this, we shall first compare this new kind of metal with "heavy electrons" to the more con-

[1]The optical properties are usually represented as a function of frequency (in cm^{-1} or Hz) or of photon energy (in eV). For clarity, the various conversion factors among the mostly used units are given here (Wooten, 1972): 12 400 Å$\rightarrow$1 eV$\rightarrow$8.065 48 $\times 10^3$ $cm^{-1} \rightarrow 1.5 \times 10^{15}$ $sec^{-1} \rightarrow 1.163 \times 10^4$ K.

ventional or ordinary metals (Ott and Fisk, 1987; Fisk *et al.*, 1988). Usually, metals are characterized by typical properties like increasing conductivity with decreasing temperature, small and temperature-independent magnetic susceptibility (i.e., Pauli paramagnetism), and linear temperature dependence for the specific heat $C_p(T)$ at low temperatures (i.e., for $T \ll E_F$, Θ_D, $C_p \sim T$, where E_F is the Fermi energy and Θ_D is the Debye energy).

In heavy-electron systems $\rho(T)$ does not change appreciably at high temperatures, and in several compounds it might even increase with decreasing temperature down to a characteristic temperature $T_{\max}$. Below $T_{\max}$ there is a strong decrease of the resistivity with decreasing temperatures. Furthermore, at very low temperatures one finds

$$\rho(T) \sim \rho_0 + A T^2, \tag{1}$$

where ρ_0 is the residual resistivity. Such a T^2 dependence in $\rho(T)$ at low temperatures is usually taken as the criterion for the identification of Fermi-liquid behavior in heavy-electron systems. The magnetic susceptibility $\chi(T)$ follows a Curie-Weiss law at high temperatures. However, the low-temperature behavior of $\chi(T)$ is not unique, and very often $\chi(T)$ saturates at a constant and usually quite enhanced value. The low-temperature specific-heat behavior of heavy-electron systems, while not universal, shows that there are far more low-lying excitations present than in an ordinary metal. C_p/T increases remarkably below $T_{\max}$ and can reach values as high as 1 J/mol K^2 (instead of mJ/mol K^2 for ordinary metals like Cu, with $\gamma \sim 0.69$ mJ/mol K^2).

The most interesting finding is that there seems to be a one-to-one correspondence between the low-lying excitations in heavy-electron systems and those in a nearly-free-electron gas when the parameters of the latter (e.g., the mass or the magnetic moment of the electrons) are properly renormalized. The name "heavy-electron" stems from the observation that an enormously large specific-heat coefficient γ implies an effective mass m^* of the quasiparticles, which is several hundred times the free-electron mass. Indeed, the most important experimental quantity by which to recognize heavy-carrier masses is the Sommerfeld coefficient γ of the electronic specific heat. In Fermi-liquid theory, γ is proportional to the quasiparticle density of states (DOS) at E_F or to the effective mass. Then, the free-electron formula

$$\gamma = \frac{\pi^2}{3} k_B^2 N_F = \frac{k_B^2}{3\hbar^2} k_F m^* \tag{2}$$

is used to give m^*, where N_F is the total quasiparticle DOS at the Fermi surface, $k_F^3 = 3\pi^2 n$ defines the Fermi wave vector, and n is the electronic density (Brandt and Moshchalkov, 1984; Ott and Fisk, 1987; Fisk *et al.*, 1988).

We can now understand, at least from a phenomenological point of view, the origin of the enhancement of the effective mass. The key is the presence of localized f electrons in all heavy-electron systems. These may be Ce ions with $4f$ electrons or U or Np ions with $5f$ electrons. Prominent examples of heavy-electron systems are $CeAl_3$, $CeCu_2Si_2$, $CeCu_6$, UBe_{13}, UPt_3, UCd_{11}, U_2Zn_{17}, and $NpBe_{13}$. The "heavy electron" can be considered as the $4f$ or $5f$ electron interacting with the bands of the delocalized electrons (d or s). It must be pointed out that, since the $5f$ wave function is much more spatially extended than the $4f$ one and direct overlap between actinide $5f$ wave functions seems possible, the actinide heavy electron really occupies a middle ground between a d-transition metal and a rare-earth element. However, both $4f$ and $5f$ heavy-electron systems present a large number of similarities, and therefore we shall first consider them from a very general and common point of view. Essentially, the interaction between f and delocalized band electrons is a hybridization with the band states near E_F via the Kondo spin fluctuations, which happen through constant exchange spin-flip transitions of f electrons and band electrons in the vicinity of the Fermi level (Brandt and Moshchalkov, 1984; Lee *et al.*, 1986; Rice, 1987; Fulde, 1988). It is precisely this process that leads to the strong mixing of the Fermi electrons with the localized f electrons. The final result is a renormalization of the Fermi surface and a drastic enhancement of the effective mass of free band electrons at E_F. In other words, the delocalized band electrons screen the localized f electrons, forming a singlet state also known as a Kondo cloud. The formation of such a cloud leads to a gain in energy per magnetic impurity of the order of

$$k_B T_K \sim E_F e^{-1/N(E_F)J}, \tag{3}$$

where J is the coupling between f and conduction electrons and $N(E_F)$ is the density of conduction-electron states at E_F. This is an important energy scale defining the so-called Kondo temperature T_K. It turns out that the electrons close to E_F will contribute most to the singlet formation because for them the energy involved in screening the f electron is small. The remarkable feature is the formation of a sharp and narrow resonance (with a width of approximately T_K for $T \ll T_K$) in the density of states $N(E)$ at E_F (Brandt and Moshchalkov, 1984). In the framework of a semiphenomenological model for $3d$ Kondo systems, the formation of a narrow resonance at E_F in the density of states was first proposed by Grüner and Zawadowski (1972) as a consequence of the resonance in electron scattering by magnetic impurities (see also Grüner, 1974; Zlatic *et al.*, 1974). They called such a peak in $N(E)$ an Abrikosov-Suhl resonance. The electrons sitting in this narrow resonance are the new "heavy" quasiparticles (i.e., with an enhanced effective mass), responsible for the low-temperature transport and thermodynamic properties.

The above scenario applies in the single-ion Kondo regime, where the formation of the Abrikosov-Suhl resonance reflects the screening of the f-localized moment by the free conduction electrons. The intersite interaction of the Kondo clouds is then an essential feature in the low-temperature behavior of a periodic Kondo system or Kondo lattice. From the density-of-states point of view, the lattice periodicity leads to struc-

TABLE I. Some relevant parameters for typical heavy-electron systems: the coefficient A of Eq. (1), the linear specific-heat term γ of Eq. (2), the $T\rightarrow 0$ magnetic susceptibility and the high-temperature magnetic moment μ. Multiple values separated by slashes indicate different crystallographic directions.

	A ($\mu\Omega$ cm K^{-2})	γ (mJ mol^{-1} K^{-2})	$\chi(T\rightarrow 0)$ (10^{-3} emu cm^{-3})	μ (μ_B)	Ref.
$CeAl_3$	35	1620	0.41	2.63	Fisk *et al.*, 1988
UPt_3	0.5	450	0.19/0.1	3	Fisk *et al.*, 1988
$CePd_3$		37			Brandt and Moshchalkov, 1984; Marabelli, 1989
UBe_{13}		1100	0.18	3.1	Fisk *et al.*, 1988
URu_2Si_2	0.17/0.1	180	0.03/0.1	3.51	Fisk *et al.*, 1988
UCu_5		250	0.18	3.52	Fisk *et al.*, 1988
U_2Zn_{17}		500	0.19/0.24	3.3	Fisk *et al.*, 1988
UPd_2Al_3	0.23	150		3.3	Fisk *et al.*, 1988; Giebel, Thies *et al.*, 1991; Dalichaouch *et al.*, 1992; Bakker *et al.*, 1993
$CeCu_6$		1300	0.28	2.6/2.67/2.46	Fisk *et al.*, 1988

tures in the Abrikosov-Suhl resonance. Moreover, there is a crossover to a low-temperature many-body coherent state, which develops below a characteristic temperature T_{co} (usually coinciding with T_{max}). However, for both single impurities and Kondo-lattice systems the heavy electrons obey Fermi statistics and follow Fermi-liquid behavior. The main difference between the two regimes is manifested by the low-temperature dependence of the resistivity, which increases or decreases with a T^2 behavior for an incoherent single Kondo impurity (at $T<T_K$) or coherent many-body Kondo-lattice (at $T\ll T_{co}<T_K$) situation, respectively (Cox and Grewe, 1988). Nevertheless, it is important to notice that in a Kondo lattice there is an additional competing interaction of a magnetic nature, induced by the periodic array of magnetic impurities. This corresponds to the Ruderman-Kittel-Kasuya-Yoshida (RKKY) interaction, which defines another relevant energy scale (Doniach, 1977):

$$k_B T_{RKKY} \sim J^2 N(E_F). \tag{4}$$

For small J, T_{RKKY} is larger than T_K and magnetic ordering is expected. Otherwise, for large J the formation of singlet Kondo clouds will lead to a larger energy gain than by magnetic ordering. Therefore in heavy-electron systems there is a balance between Kondo fluctuations and correlation effects of the impurity magnetic moments. Such a balance can also lead to the coexistence of various states, for example, a heavy-electron and magnetic order, or even to a non-Fermi-liquid state (see Sec. III).

B. The prototype heavy-electron systems

It is appropriate to review briefly some basic and well-known results, particularly with respect to the transport and thermodynamic properties, of the two "prototypical" heavy-electron systems, $CeAl_3$ and UPt_3. Table I summarizes some important parameters (e.g., γ and A) for various heavy-electron systems, which we shall also briefly discuss later in connection with the electrodynamic response of $CeAl_3$ and UPt_3.

1. $CeAl_3$

The $CeAl_3$ compound has a hexagonal crystal structure and its resistivity $\rho(T)$ is shown in Fig. 1 (Andres *et al.*, 1975). $\rho(T)$ displays the usual fingerprints mentioned above. Particularly for $T<0.3$ K, $\rho(T)$ follows the T^2 law of Eq. (1) (with $\rho_0=0.76\,\mu\Omega$ cm, $A=35\,\mu\Omega$ cm/K^2) and displays a broad maximum at $T_{max}\sim 35$ K. Besides $\rho(T)$, $\chi(T)$ and $C_p(T)$ also show the typical heavy-electron behavior. In fact, below 0.2 K

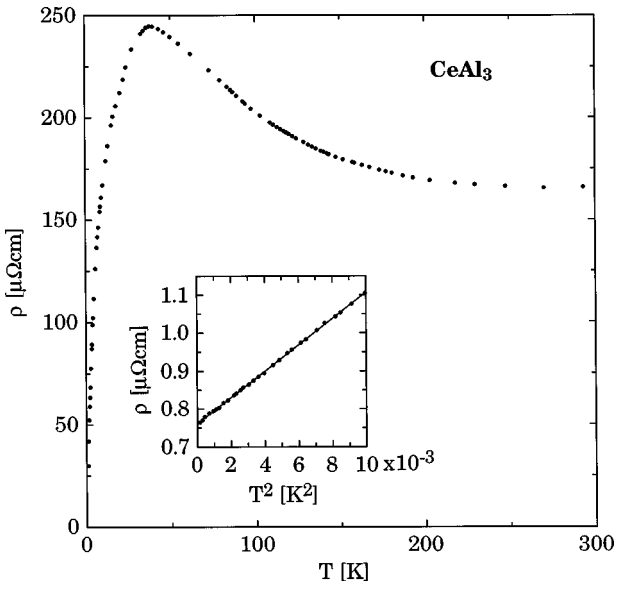

FIG. 1. Temperature dependence of the resistivity $\rho(T)$ for $CeAl_3$. The inset shows $\rho(T)$ vs T^2 with a fit after Eq. (1) (Andres *et al.*, 1975).

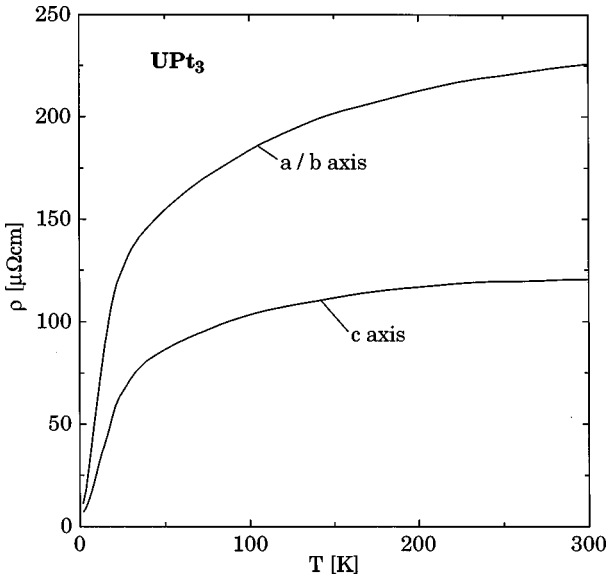

FIG. 2. Temperature dependence of the resistivity $\rho(T)$ for UPt_3 along the a and b axis, and the hexagonal c axis (de Visser *et al.*, 1984).

the linear specific-heat term is enormous, with $\gamma = 1620\,\mathrm{mJ/mol\,K^2}$. Thus transport and thermodynamic results are consistent with the scenario of $4f$ electrons obeying Fermi statistics at low temperatures with a very high effective mass of the quasiparticles (Andres *et al.*, 1975; Stewart, 1984).

2. UPt_3

The actinide UPt_3 also has a hexagonal structure and displays an anisotropic resistivity, as shown in Fig. 2, between the *ab* plane and along the hexagonal *c* axis (de Visser *et al.*, 1984). Once again, at low temperatures, the resistivity follows the T^2 behavior of Eq. (1), and the anisotropy of ρ is obviously also reflected in the prefactor A, which is 1.6 $\mu\Omega\,\mathrm{cm/K^2}$ for $\rho_\perp$, and 0.7 $\mu\Omega\,\mathrm{cm/K^2}$ for $\rho_\parallel$. These values are an order of magnitude smaller than that for the polycrystalline $CeAl_3$ mentioned above. Such an anisotropic behavior in $\rho(T)$ is also encountered in the magnetic spin susceptibility (Ott and Fisk, 1987).

The specific heat of UPt_3 also manifests the characteristic C^{el}_p/T upturn with decreasing temperatures in the liquid-helium temperature range and a subsequent transition to a superconducting state below 1 K. Concerning the normal-state properties, it has been shown that the total specific heat $C_p(T)$ of UPt_3 suggests a γ of approximately 450 $\mathrm{mJ/mol\,K^2}$ (Ott and Fisk, 1987; Fisk *et al.*, 1988). Moreover, $C_p(T)$ can be described by a model calculation appropriate for a metallic system in which the energy spectrum of the electrons is noticeably affected by spin fluctuations (Doniach and Engelsberg, 1966).

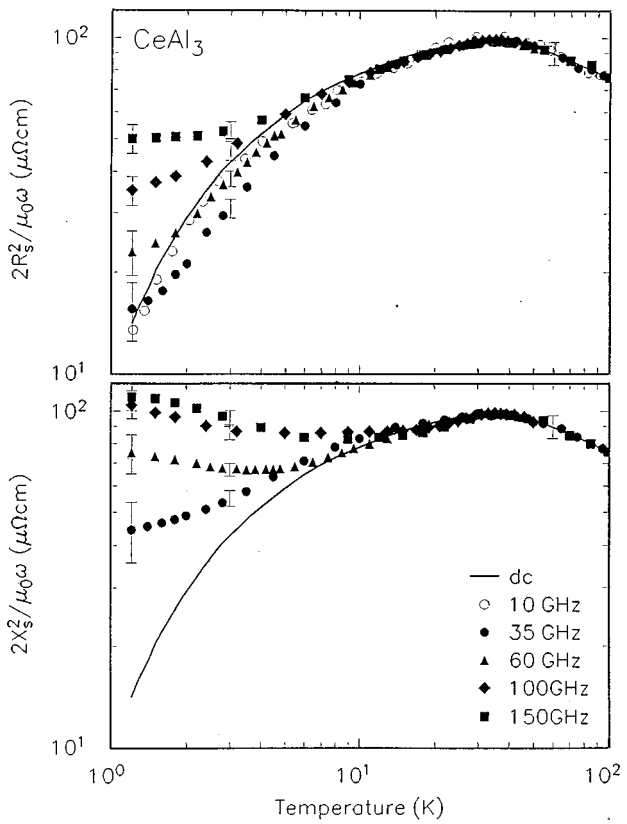

FIG. 3. Temperature dependence of the complex surface impedance of $CeAl_3$ at dc and selected millimeter and microwave frequencies. The choice of the particular representations of R_s and X_s is made to show the frequency independent behavior at high temperatures (above approximately 10 K) (Awasthi *et al.*, 1993).

C. The electrodynamic response of heavy-electron systems

This section discusses optical experiments on several prototype heavy-electron compounds. For $CeAl_3$, we shall present a full analysis of the experimental data, while for the other typical heavy-electron compounds (UPt_3, $CeCu_6$, and $CePd_3$) we shall limit our attention mainly to the final results. The onset of the many-body correlated state leads to the renormalization of several intrinsic parameters (e.g., the scattering rate and the plasma frequency associated with the charge carriers), which in turn, are expected to considerably affect the optical response.

1. $CeAl_3$

We start our presentation from the data collected in the micro- and millimeter wave spectral range (Awasthi *et al.*, 1993). By employing a cavity perturbation technique, Awasthi *et al.* were able to obtain both components of the surface impedance $Z_s = R_s + iX_s$ as a function of temperature at 35, 60, 100, and 150 GHz. At 10 GHz only the surface resistance (R_s) was measured (Buranov and Shchegolev, 1971; Awasthi *et al.*, 1989).

Figure 3 (Awasthi *et al.*, 1993) shows the measured

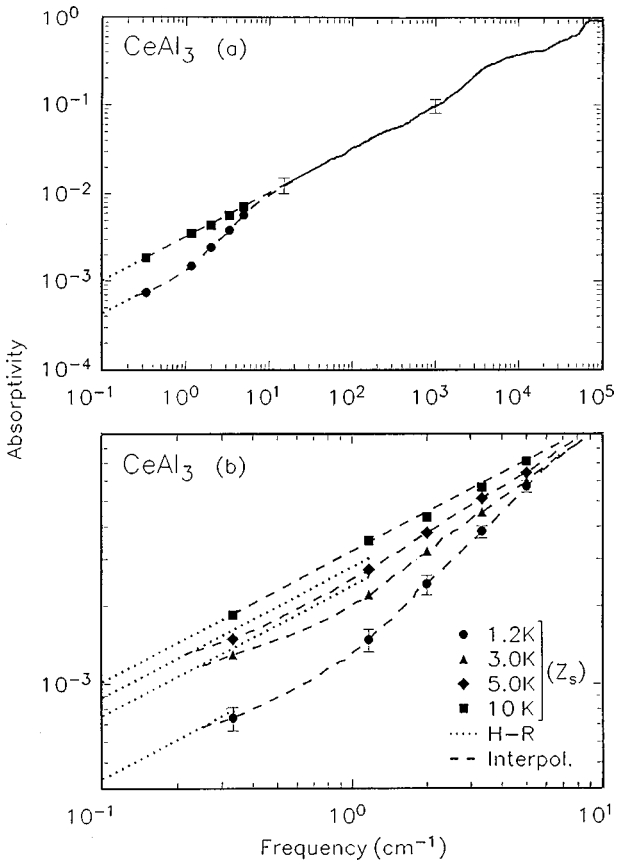

FIG. 4. Absorptivity in $CeAl_3$. (a) Frequency dependence of the absorptivity $A(\omega)=1-R(\omega)$ of $CeAl_3$ at 1.2 and 10 K. Both optical and microwave data are displayed in the figure. (b) Temperature variation of $A(\omega)$ in the 0.1–10 cm^{-1} range (Awasthi *et al.*, 1993).

surface resistance R_s and surface reactance X_s at micro- and millimeter-wave frequencies from 1.2 to 300 K. The data were normalized to the dc resistivity at approximately T_{max}. At low temperatures, the frequency dependent increase in the resistivity $(2R_s^2/\mu_0\omega)$ results from a steady loss of coherence, due to the ac perturbation. From the surface impedance we can directly determine the complex optical conductivity in the normal skin-depth regime (see below).

Above $T_{max}\sim 35$ K the temperature dependence of R_s and X_s at millimeter-wave frequencies were found to be the same within the experimental uncertainty (error bar in Fig. 3), suggesting a frequency independent response at high temperatures. This implies that in the high-temperature regime the scattering rate $(1/\tau)$ is significantly larger than the millimeter-wave frequencies, and σ_2 is negligible compared to σ_1. Consequently, the so-called Hagen-Rubens limit is valid at these temperatures. For the purpose of the Kramers-Kronig (KK) analysis, the millimeter-wave and microwave data were then joined with the reflectivity spectra $R(\omega)$ from the far infrared (IR) up to the ultraviolet (UV) in order to obtain the optical response over a broad spectral range. Figure 4 (Awasthi *et al.*, 1993) shows the absorptivity $A(\omega)=1-R(\omega)$ from microwave frequencies up to 12 eV.

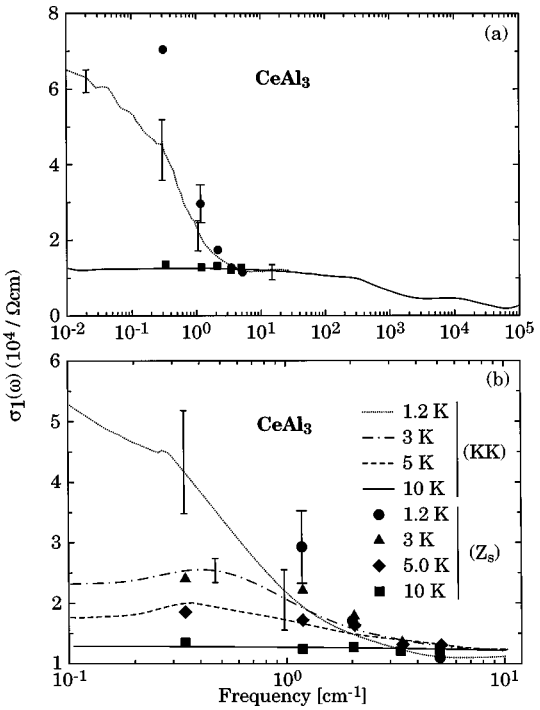

FIG. 5. Excitation spectrum of $CeAl_3$. (a) Real part of the optical conductivity $\sigma_1(\omega)$ obtained from the Kramers-Kronig analysis of the data in Fig. 4, and directly from the surface impedance measurements (Fig. 3). (b) An enlargement of the dynamical conductivity showing the development of the low-frequency resonance at low temperatures. The 10 GHz point from the surface resistance data is equal to $(2R_s^2/\mu_0\omega)^{-1}$ (Awasthi *et al.*, 1993).

Above 15 cm^{-1} the absorptivity spectrum does not show any temperature dependence. Results at microwave frequencies, however, show a strong frequency and temperature dependence below approximately 10 K (Fig. 4). At 10 GHz the measured absorptivity is close to the Hagens-Ruben extrapolation (dots in Fig. 4). To show the detailed temperature variation of the absorptivity, an enlargement of A in the 0.1–10 cm^{-1} range is plotted in Fig. 4(b). The error bars on the surface impedance data reflect the uncertainties in R_s at 1.2 K, whereas at higher temperatures, the symbol size itself is a measure of the uncertainty.

Figure 5 (Awasthi *et al.*, 1993) shows the real part of the optical conductivity $\sigma(\omega)=\sigma_1(\omega)+i\sigma_2(\omega)$, as obtained from the Kramers-Kronig analysis of the data in Fig. 4 and directly from R_s and X_s. The 10-GHz point [equal to $(2R_S^2/\mu_0\omega)^{-1}$] represents an upper bound on the conductivity rather than an exact value. Indeed, it was evaluated from the surface resistance data by assuming $R_s=X_s$. This point is shown only to provide an estimate of the maximum possible discrepancy that can be expected between the conductivity obtained directly from Z_s or from the Kramers-Kronig transformation. In fact, in the low-frequency regime the Hagen-Rubens limit might break down, and in principle both R_s and X_s components must be measured. Nevertheless, within the experimental accuracy both methods (i.e., the Kramers-Kronig transformation of the complete optical response or the direct measurement of Z_s) give the same

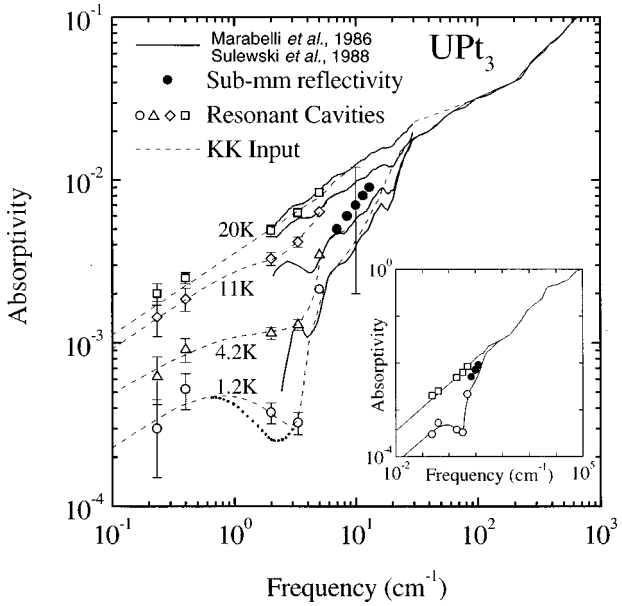

FIG. 6. The frequency dependence of the absorptivity $A(\omega)$ between 1.2 and 20 K. The solid curves are optical reflectivity and absorption data taken from Marabelli *et al.* (1986) and Sulewski *et al.* (1988); the open symbols are the results of microwave cavity perturbation measurements; the solid symbols are submillimeter reflectivity measurements at 4.2 K; and the dashed lines are the spectra used to calculate the conductivity through the Kramers-Kronig relation. The dotted line at 1.2 K between 0.7 and 3 cm^{-1} shows a second interpolation used. The inset shows the 1.2 and 20 K spectra over the entire frequency range (Donovan *et al.*, 1997).

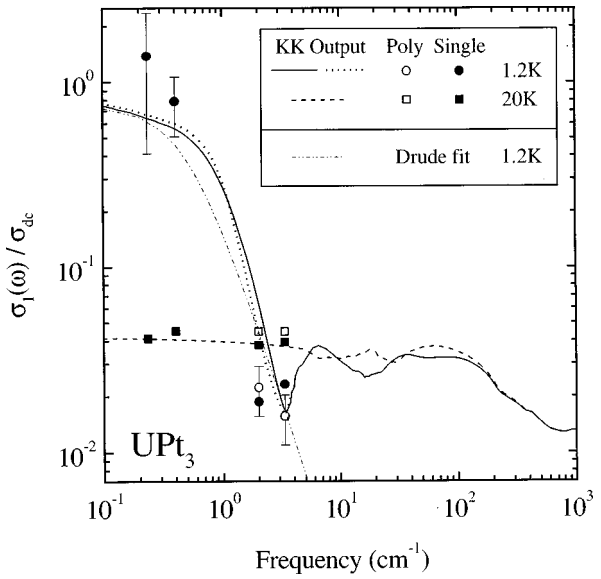

FIG. 7. The optical conductivity $\sigma_1(\omega)$ at 1.2 and 20 K, normalized to the 1.2 K dc conductivities, 2.5×10^5 $(\Omega\ cm)^{-1}$ and 6.5×10^5 $(\Omega\ cm)^{-1}$ for the polycrystalline and single crystal samples, respectively. The solid, dashed, and dotted lines are the results of a Kramers-Kronig calculation using the spectra in Fig. 6. The points at 2 and 3.3 cm^{-1} were calculated directly from R_s and X_s as well as from similar measurements of UPt_3 single crystals. The points at 0.25 and 0.4 cm^{-1} are simply $\mu_0\omega/2R_s^2$. The dot-dashed line is a fit to the low-frequency part of the 1.2 K spectrum with Eq. (32) (Donovan *et al.*, 1997).

frequency-dependent $\sigma_1(\omega)$ at different temperatures, and consequently it is believed that the signatures of the observed frequency dependent response are free of experimental ambiguities (Beyermann and Grüner, 1989; Sulewski and Sievers, 1989).

2. UPt_3

In analogy with $CeAl_3$ and in order to probe the electrodynamical response of UPt_3 over a broad frequency range ($0.2–10^5\ cm^{-1}$), data obtained using a variety of different experimental techniques have been combined. Early investigations by several groups (Marabelli *et al.*, 1986; Sulewski *et al.*, 1988; Awasthi *et al.*, 1989) have been carried out in the region between 2 and $10^5\ cm^{-1}$. The most recent experiment by Donovan *et al.* (1997) reported on new resonant measurements performed between 0.2 and 5 cm^{-1}, extending the previously measured frequency range by an order of magnitude. In this latter work, two different and complementary methods were used to extract the frequency-dependent conductivity from the measured surface impedance data. The first method is based on an evaluation of the absorptivity from the surface resistance. All of the results are displayed in Fig. 6 (Donovan *et al.*, 1997), together with those from previous measurements. An additional reflectivity measurement was carried out between 7 and 13 cm^{-1} in the submillimeter spectral range using a coherent-source spectrometer. Within experimental uncertainty, the results of this nonresonant measurement are temperature independent below 20 K. These data are also shown in Fig. 6 and are consistent with previous absorptivity measurements.

At each temperature an interpolation between the measured points was made, as shown in Fig. 6, and these values, together with suitable extrapolations at both low and high frequencies, were used to make the Kramers-Kronig transformation of the absorptivity. Both the real and imaginary parts of the optical conductivity were obtained in this manner, and in Fig. 7 (Donovan *et al.*, 1997) $\sigma_1(\omega)$ is displayed at both 1.2 and 20 K, normalized to the dc conductivity at 1.2 K. A somewhat different interpolation, shown by the dotted line, is also included, for reasons discussed below.

The second method of evaluating $\sigma_1(\omega)$ and $\sigma_2(\omega)$ uses both R_s and X_s. In order to extract absolute values it has been assumed that above 30 K UPt_3 behaves as a simple metal in the Hagen-Rubens limit, $\sigma_1(\omega)=\sigma_{dc} \gg \sigma_2(\omega)$. The data were normalized at 30 K using the dc resistivity. The results at 2 and 3 cm^{-1} are displayed in Fig. 7. At 0.25 and 0.4 cm^{-1} it was not possible to measure X_s, and the values of σ_1, which are shown in Fig. 7, are calculated assuming the Hagen-Rubens relation (Donovan *et al.*, 1997). Moreover, a thorough reanalysis of the data of Awasthi *et al.* (1989) at 3.3 and 5 cm^{-1} was made and compared with these new results at the same frequencies. It was found that within the experimental error, the two sets of data gave identical results.

It immediately appears that the absorptivity is different from that of a renormalized Drude metal. In particular, the 1.2 K absorptivity shown in Fig. 6 displays a well-defined minimum near 3 cm^{-1}. Such a minimum is a signature of the development of a pseudogap (see below). This is also clearly evident in the frequency dependence of the conductivity $\sigma_1(\omega)$, displayed in Fig. 7. This gap feature gradually disappears with increasing temperature, and at 20 K the conductivity is observed to be essentially independent of frequency.

There is, however, some difference in the precise shape of $\sigma_1(\omega)$. It is believed that this is related to the difficulties associated with the Kramers-Kronig analysis, in which interpolations have been used between data points available at fixed frequencies. In order to demonstrate this, Figs. 6 and 7 show two different interpolations at 1.2 K, leading to somewhat different $\sigma_1(\omega)$ curves, one of which shows a significantly improved agreement with the direct evaluation of $\sigma_1(\omega)$ from the measured R_s and X_s.

Besides the low-temperature minimum at about 3 cm^{-1} (which seems to be a peculiarity of UPt_3) the other striking feature is the development of a narrow mode at low temperature below the far-infrared range and extending down to the mm and microwave spectral range. This feature is obviously similar to what has been encountered before for $CeAl_3$ (Fig. 5) and seems to be a fingerprint of the excitation spectrum at low temperatures in highly correlated heavy-electron systems (for both poly- and single-crystalline specimens).

We also remark that in the far infrared and only at low temperatures Marabelli *et al.* (1986) identified another huge resonance at approximately 5 meV. This latter feature is, however, quite controversial and does not seem to be so relevant in the latest measurements (Donovan *et al.*, 1997). Moreover, the temperature dependence of the absorptivity of polycrystalline UPt_3, measured by Sulewski *et al.* (1988) between 2 and 100 cm^{-1}, displays a low-frequency narrow mode in $\sigma_1(\omega)$ at low temperatures, similar to the results of Fig. 7, with the apparent absence of the far-infrared resonance at 5 meV found by Marabelli *et al.* (1986).

Finally, we mention that the high-frequency spectral range, mainly dominated by electronic interband transitions, is not the central issue here. We refer the reader to the literature (Schoenes and Andres, 1982; Schoenes and Franse, 1985; Sulewski *et al.*, 1988; Awasthi *et al.*, 1989) for a comprehensive discussion of how to identify the electronic interband transitions in these compounds.

3. $CePd_3$ and $CeCu_6$

The results presented above for the prototype $CeAl_3$ and UPt_3 materials are very general and typical of a large variety of heavy-electron systems. Indeed, the formation of a narrow mode centered at zero frequency in $\sigma_1(\omega)$ at low temperatures is a common optical fingerprint of heavy-electron systems in their highly correlated ground state (i.e., at $T<T_{co}$). Here, we mention the results for two more compounds, $CePd_3$ and $CeCu_6$, for which Fig. 8 (Webb *et al.*, 1986; Awasthi *et al.*, 1989) and Fig. 9 (Marabelli *et al.*, 1988) display $\sigma_1(\omega)$, respectively. Once again the low-temperature data clearly show a fully developed narrow mode centered at zero frequency in $CePd_3$ (Fig. 8) and just the onset of it in $CeCu_6$ (Fig. 9). Moreover, a feature at approximately 5 meV also appears in $\sigma_1(\omega)$ of $CeCu_6$ (Marabelli *et al.*, 1988), similar to the situation encountered in the UPt_3 single crystal (Marabelli *et al.*, 1986).

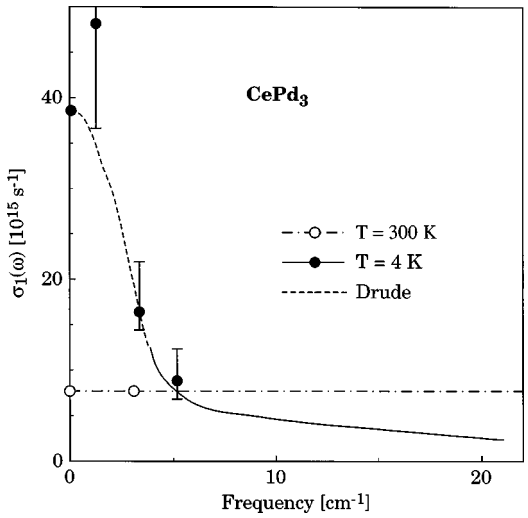

FIG. 8. $\sigma_1(\omega)$ of $CePd_3$ at 4 and 300 K from reflectivity and resonant cavity perturbation (dots) experiments (Webb *et al.*, 1986; Awasthi *et al.*, 1989).

D. Theoretical models for the optical properties of heavy-electron systems

Before discussing the optical properties summarized above and in order to have a theoretical background for comparison, we should like to briefly review the major theoretical results and models. Obviously, we do not

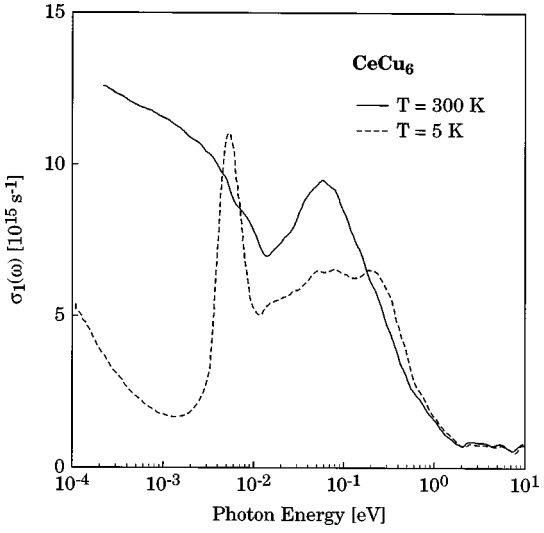

FIG. 9. $\sigma_1(\omega)$ of $CeCu_6$ at 5 and 300 K from reflectivity data (Marabelli *et al.*, 1988).

pretend to present an exhaustive theoretical review but will limit our attention to a few theoretical approaches that catch the essential features of the experimental excitation spectrum of the prototype heavy-electron systems.

Millis and Lee (1987) developed the most comprehensive theoretical calculation of the heavy-electron electrodynamic response. They performed a study of the low-temperature properties of the lattice Anderson Hamiltonian, in the Kondo limit, where it describes a band of nearly free electrons hybridizing with a very highly correlated band of f electrons. In the absence of this hybridization the f electrons would be confined, one to a site, in localized orbitals far below the Fermi energy. This model is believed to contain the essential physics of the currently interesting heavy-electron metals: a nonmagnetic ground state that behaves as a Fermi liquid with a large effective mass. In the $U=\infty$ limit, where U is the Coulomb repulsion between f electrons on the same site, the Hamiltonian may be written

$$H_A=\sum_{k\sigma}\varepsilon_{k\sigma}c^*_{k\sigma}c_{k\sigma}+\sum_{im}E_{0m}f^*_{im}f_{im}+\sum_{kim\sigma}(Ve^{ikR_i}c^*_{k\sigma}f_{im}+\text{H.c.}). \tag{5}$$

This Hamiltonian describes a band of conduction electrons (c electrons) with operator $c_{k\sigma}$ and energy $\varepsilon_{k\sigma}$, which hybridizes with a set of localized f electrons with operator f_{im} and energy E_{0m} via an interaction V, taken to be a constant for simplicity. The solution is subject to the constraint that each site may be occupied by at most one f electron (the $U=\infty$ limit):

$$\sum_m f^*_{im}f_{im}=n^i_f\leqslant 1. \tag{6}$$

Since the above constraint does not commute with H_A, a slave-boson formalism has been used to handle the Hamiltonian of Eq. (5). The analysis is then pursued using conventional quantum-field-theoretical techniques including a $1/N$ expansion, where N is the orbital degeneracy of the f state (Millis and Lee, 1987).

Here we are interested in the final results concerning $\sigma(\omega,T)$. In a perfect lattice, the dc conductivity is infinite, and in order to obtain sensible results, scattering must be incorporated. There are two possible sources of scattering of electrons. One is the scattering of electrons off of impurities; the other is scattering from boson fluctuations. This latter turns out to be in some ways analogous to electron-phonon scattering and corresponds to the fluctuations of the slave bosons with respect to their saddle-point value, i.e., a $1/N$ effect. In the following discussion, the validity of "Matthiessen's rule" (Ashcroft and Mermin, 1976), which asserts that the resistivities due to different scattering mechanisms add, is assumed. Thus, if in the presence of impurities only the conductivity is σ_i and in the presence of bosons only the conductivity is σ_b, then the total conductivity would be given by

$$\sigma^{-1}=\sigma_i^{-1}+\sigma_b^{-1}. \tag{7}$$

Matthiessen's rule is believed to be valid when the various scattering mechanisms are not momentum dependent and are weak.

At sufficiently low temperatures, only impurity scattering is relevant. To compute the corresponding "impurity component" $\sigma_i(\omega,T)$ of $\sigma(\omega,T)$, disorder must be coupled into the system. Millis and Lee (1987) assumed that the disorder is weak and on the conduction-electron sites only. The corresponding Hamiltonian is

$$H_{imp}=\sum_{kk'm}V_l c^*_{km}c_{k'm}, \tag{8}$$

where V_l is the impurity scattering amplitude. Moreover, Millis and Lee (1987) introduced an energy parameter ε_f, which is analogous to the Debye frequency in the electron-phonon interaction problem, in that it sets the scale for the energy of the boson propagator. However, unlike the electron-phonon problem, ε_f is also acting as the renormalized Fermi energy of the final ground state. The resulting flat band implies a large effective mass, so that

$$m^*\sim\frac{W}{N\varepsilon_f}, \tag{9}$$

where W is the bare bandwidth. For $\omega\ll\varepsilon_f$ and assuming that the impurity scattering is isotropic, $\sigma_i(\omega)$ reduces to

$$\sigma_i(\omega)=\frac{ne^2}{m_b}\frac{\tau_i}{1+(m^*/m_b)^2\omega^2\tau_i^2}=\frac{ne^2}{m^*}\frac{\tau_i^*}{1+(\omega\tau_i^*)^2}, \tag{10}$$

where Millis and Lee (1987) made use of the definition $\tau_i^*=(m^*/m)\tau_i$. Thus at dc the conductivity is what one would expect for a conventional, unenhanced metal, in agreement with the ideas of Varma (1985) and Fukuyama (1985). Note, however, that the quantity $n=Nk_F^3/6\pi^2$ in the prefactor is the area of the Fermi surface including both conduction and f electrons, in agreement with Luttinger's theorem. The new result (Millis and Lee, 1987) is that the frequency dependence is very strong (see Fig. 10). If the impurity scattering is weak, as in a good metal, the frequency $\omega^*=1/\tau_i^*$ at which $\sigma_1(\omega)$ (to be understood as the real part of $\sigma(\omega)$), has fallen to half of its dc value may be of order $10^9\,\text{Hz}\sim 0.3\,\text{cm}^{-1}$ (if $\varepsilon_f\sim 100\,\text{K}$), a remarkably small value.

Freytag and Keller (1990) also calculated the dynamical conductivity for heavy-electron systems, taking into account the effect of impurity scattering within a mean-field approximation of the Anderson Hamiltonian. Similarly to Millis and Lee (1987), they obtained a dynamical conductivity characterized by a narrow low-frequency Drude peak (with spectral weight scaling with the effective mass of the heavy quasiparticle) superimposed on a broad background with a minimum near k_BT_K. Freytag and Keller attribute this result to a mixture of the broadened interband transition and the Drude behavior of the conduction electrons.

Two characteristic plasma frequencies are then expected: the one at high frequency ($\omega_p^2=4\pi n_c e^2/m_b$),

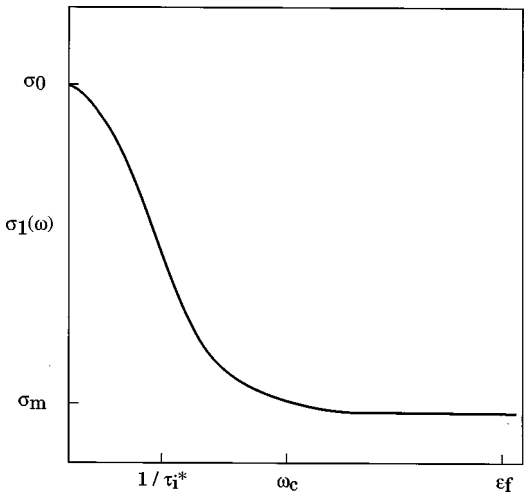

FIG. 10. Sketch of the calculated frequency-dependent conductivity $\sigma_1(\omega)$ after Millis and Lee (1987).

which identifies the uncorrelated conduction electrons, and the one at low frequency associated with the heavy plasmons:

$$\tilde{\omega}_p^* = \sqrt{6\left(1+\frac{n_f}{n_c}\right)}T^*, \tag{11}$$

where T^* is the renormalized Fermi temperature (usually identified with T_K), and $n=n_c+n_f$ is the total carrier density (conduction and f electrons), relevant to the low-frequency electrodynamics. The heavy-electron plasma mode ($\tilde{\omega}_p^*$) reflects not only the heavy-quasiparticle mass (m^*/m_b), but also the renormalized Coulomb screening (Millis, Lavagna, and Lee, 1987).

The plasma frequency $\tilde{\omega}_p^*$ is screened by the high-frequency excitations defining the broad background in $\sigma_1(\omega)$ (see, for example, Freytag and Keller, 1990) and should not be confused with the renormalized plasma frequency (or unscreened heavy plasmon):

$$(\omega_p^*)^2 = \left(\frac{4\pi n e^2}{m^*}\right), \tag{12}$$

which appears in Eq. (10) and corresponds to the spectral weight associated with the narrow Drude-like mode in $\sigma_1(\omega)$ (Fig. 10). In other words, assuming that the screening is mainly caused by the broad excitation (Δ_0) with onset near $k_B T_K$, one can find (Marabelli, 1989)

$$\frac{m^*}{m_b} \sim \left(\frac{\Delta_0}{T^*}\right)^2. \tag{13}$$

The next step concerns the inclusion of scattering off of bosons (σ_b). In light of the above discussion of Matthiessen's rule, the conductivity is simply formed by adding the c-electron self-energy due to electron-boson interactions. Moreover, because the f electrons are dispersionless in this approach, the applied model is not Galilean invariant. Keeping in mind that the umklapp process can occur at all nonzero temperatures and interpreting the imaginary part of the c-electron self-energy as a temperature and frequency-dependent scattering rate $1/2\pi\tau(\omega,T)$, Millis and Lee (1987) found

$$\frac{1}{\tau(\omega,T)} = \frac{1}{\tau_i} + \frac{m^*}{N m_b}\left(\frac{\omega^2+(\pi T)^2}{\varepsilon_f}\right). \tag{14}$$

Thus, at $T=0$ and for $\omega<\omega_c$, with

$$\omega_c^2 = \frac{N\varepsilon_f (m_b/m^*)}{\tau_i} \tag{15}$$

the impurity scattering dominates and Eq. (10) applies, but for larger ω one finds

$$\sigma_1(\omega) \sim \sigma_b \sim \frac{ne^2}{m_b}\frac{1}{N(m^*/m_b)\varepsilon_f} \sim \frac{ne^2}{m_b W}. \tag{16}$$

Therefore for $\omega>\omega_c$ the conductivity becomes very small (of the order of the Ioffe-Regel limit) and approximately independent of frequency. A sketch of the predicted $\sigma_1(\omega)$ is given in Fig. 10. The qualitative agreement with experiments is gratifying (see, for example Figs. 5 and 8).

We now consider the case $T>0$, and $\omega=0$. As can be seen from Eq. (14), the resistivity $\rho=\sigma^{-1}$ [after averaging Eq. (14) over the energies of thermally excited electrons] is

$$\rho = \frac{m_b}{ne^2}\left(\frac{1}{\tau}+\frac{4m^*(\pi T)^2}{3Nm_b\varepsilon_f}\right). \tag{17}$$

The coefficient of the T^2 term in the resistivity is large and scales as $(m^*/m_b)\varepsilon_f^{-1} \sim \varepsilon_f^{-2}$. To compare Eq. (17) with experiment it is convenient to differentiate Eq. (17) with respect to T^2 and make the dimensional factors explicit, obtaining

$$\frac{m^*}{N m_b \varepsilon_f} = 5A n_{22}. \tag{18}$$

Here n_{22} is the carrier density in units of 10^{22} particles/cm^3, ε_f is acting as the Kondo temperature in units of degrees Kelvin, and A is the coefficient of the T^2 term in the resistivity [Eq. (1)] in units of $\mu\Omega\,\mathrm{cm/K}^2$. For $CePd_3$, one finds $m^*/m_b=40$, which seems to have the correct order of magnitude (see below). It must be noted that because the details of Fermi-surface geometry, umklapp scattering, etc. have been ignored, one cannot expect Eq. (18) to hold precisely (Millis and Lee, 1987).

In conclusion, the results sketched here are valid only if the following chain of inequalities holds:

$$\frac{1}{\tau_i^*} \ll \omega_c \ll \varepsilon_f. \tag{19}$$

However, these conditions are equivalent to the simple condition

$$\varepsilon_f \tau_i^* \gg 1, \tag{20}$$

which should not be restrictive in practice.

Cox and Grewe (1988) also calculated the transport (dc and dynamical) properties for the Anderson lattice. They performed the calculation for the sixfold ($N=6$) degenerate case, which should be appropriate for the Ce ions. Moreover, coherence was explicitly included while the effects of intersite interactions, which may be re-

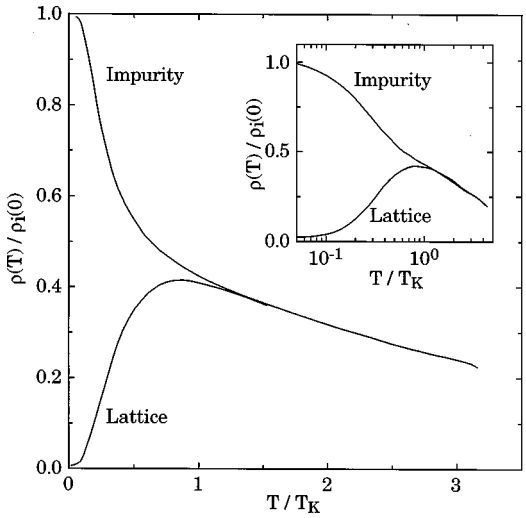

FIG. 11. Resistivity $\rho(T)$ of the sixfold degenerate Anderson lattice. The resistivity is measured in units of the dilute limit zero-temperature resistivity $\rho_i(0)$ per ion; for comparison, the full temperature dependence of the impurity resistivity is shown (the upper curve). Logarithmic behavior of both impurity and lattice curves is shown in the inset (Cox and Grewe, 1988).

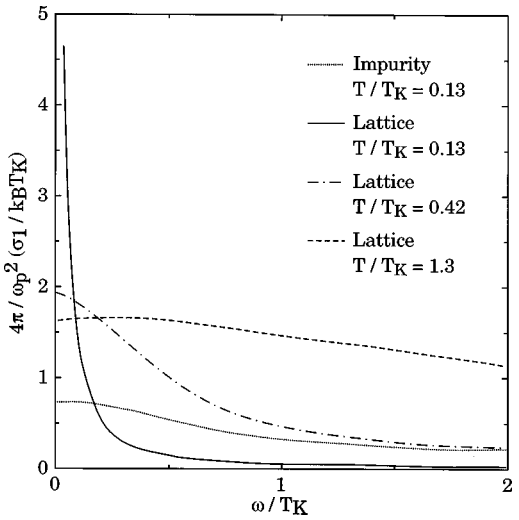

FIG. 12. Real part $\sigma_1(\omega,T)$ of the optical conductivity for sixfold degenerate Anderson lattice. The low-frequency narrow mode for the low-temperature (solid) curve arises from the strongly frequency-dependent quadratic electron-electron scattering. Upon warming, substantial broadening is visible. Note the large impurity/lattice discrepancy for low temperatures (Cox and Grewe, 1988).

sponsible for magnetic and superconducting instabilities, were neglected. The calculations were performed within the self-consistent noncrossing approximation perturbation theory. For the dc resistivity, the calculation demonstrates the crossover between incoherent single-ion scattering above the characteristic Kondo scale T_K and coherent ($\sim T^2$) scattering for $T\rightarrow 0$ (Fig. 11). In fact, the conductivity may be evaluated from the Kubo formula:

$$\sigma_{\mu\nu}(\omega,T)=\frac{1}{V}\int_0^\infty dt\, e^{-i\omega t}\int_0^\beta dt\langle j_{e\mu}(-i\hbar\tau)j_{e\nu}(t)\rangle, \tag{21}$$

where $j_{e\mu}$ is the electrical current, V is the system volume, and β the inverse temperature. With the simplifying assumption of isotropic dispersion and thus computing $\sigma(\omega,T)=Tr\sigma_{\mu\nu}(\omega,T)/3$, one can obtain the result

$$\sigma(\omega,T)=\frac{i\omega_p{}^2}{4\pi\omega}\int_{-\infty}^{\infty}d\varepsilon\,\frac{f(\varepsilon-\omega)-f(\varepsilon)}{\omega+\Sigma_c^A(\varepsilon-\omega,T)-\Sigma_c^R(\varepsilon,T)}, \tag{22}$$

where Σ_c is the band electron self-energy, ω_p is the Drude plasma frequency, and $f(\varepsilon)$ is the Fermi function. In the dc limit Eq. (22) reduces to the standard transport integral expression for the resistivity $\rho(T)$ given by

$$\rho(T)=\frac{1}{\sigma(0,T)}=\frac{4\pi}{\omega_p{}^2\langle\tau\rangle}, \tag{23}$$

where τ is given by

$$\langle\tau\rangle\sim\frac{1}{12A_f}\left(\frac{T_K}{k_BT}\right)^2, \tag{24}$$

where $A_f\sim 1/N(E_F)$.

The calculations of the optical conductivity are displayed in Fig. 12 (Cox and Grewe, 1988). For the purpose of comparison, a calculation for the "incoherent" model is included in which each site is treated as an Anderson impurity; although this model is unphysical, it is a useful reference for isolating the features due to coherence. The lattice curves for $\sigma_1(\omega,T)$ are seen to have the sharp falloff, arising from the rapid rise of scattering away from the Fermi level in the low-temperature limit. The optical conductivity changes from having a narrow low-frequency mode at low temperatures to a behavior with much broader response in energy above T_K, where the single-impurity results nearly coincide. As anticipated by Millis and Lee (1987) and Millis, Lavagna, and Lee (1987), the $\sigma_1(\omega,T)$ curve at $T\ll T_K$ saturates to a low plateau value at high frequencies. In contrast, the incoherent impurity scattering produces a broad monotonically decreasing conductivity. As the temperature is raised, the lattice curves broaden significantly until above the Kondo scale T_K, and the lattice curve and the impurity curve have similar shape. The broadening of the low-frequency (Drude-like) mode with increasing temperature indicates the gradual disappearance of correlation effects.

Cox and Grewe (1988) also calculated the effective mass $m^*(\omega)$ and the effective relaxation rate $\Gamma(\omega)\sim 1/\tau_{\rm eff}(\omega,T)$ functions at low temperatures for $N=6$. Despite the qualitative agreement between the calculated (Fig. 12) and the experimental $\sigma_1(\omega)$ (e.g., Figs. 5 and 8), $m^*(\omega)$ and $\Gamma(\omega)$ do not have the qualitative character of the experimental data (see below). In particular, the overall curvature of the effective mass is upwards (apart from an initial downturn, which may be a numerical artifact), and the overall character of the relaxation rate is that of a rather sharp peak instead of a saturated plateau. Such a disagreement is due to the off-

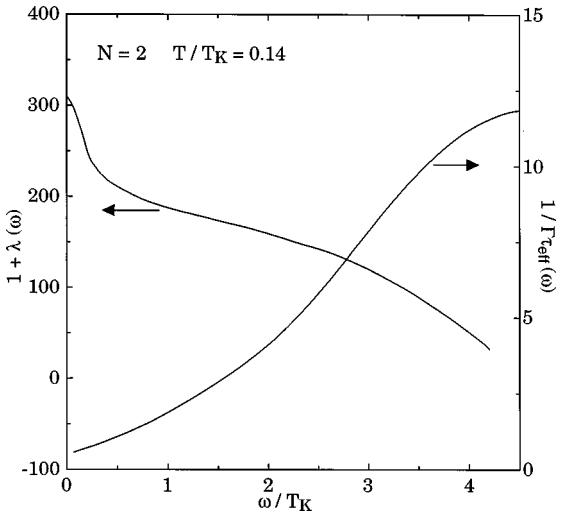

FIG. 13. Effective mass enhancement $[1+\lambda(\omega)]$ and effective relaxation rate for the twofold degenerate Anderson lattice model. Monotonic behavior follows from the greater proximity of the Abrikosov-Suhl-Kondo resonance to the Fermi level. The narrow feature near zero frequency is a numerical artifact (Cox and Grewe, 1988).

Fermi-level position of the Abrikosov-Suhl-Kondo resonance. A remedy to this discrepancy might lie in considering lower orbital degeneracy such as might arise from crystal-field splitting. The calculations of the optical effective mass and scattering rate for the present model with $N=2$ at low temperatures are displayed in Fig. 13 (Cox and Grewe, 1988). As the temperature is raised, the curves fall away from the low-temperature behavior, so that both become rather featureless. At least a qualitative agreement with the experimental data can be now established. In the following discussion of the experimental results, we shall address this issue in more detail.

In conclusion, because of the low-frequency ω^2 dependence of the full Kondo-lattice self-energy, it follows (Cox and Grewe, 1988) that

$$\sigma^{-1}(\omega,T)\sim[\omega^2+(6k_BT)^2], \tag{25}$$

a well-known result in the absence of intersite interactions. Alternatively, we can say that Eq. (25) manifests the Fermi-liquid nature of the Kondo-like ground state (Ashcroft and Mermin, 1976),

$$\frac{1}{\tau}=a(\hbar\omega)^2+b(k_BT)^2, \tag{26}$$

where a and b are temperature- and frequency independent constants, and the ratio b/a is π^2 or $(2\pi)^2$ for quasiparticle (seen in photoemission experiment) or transport (seen in optical experiment) scattering rate, respectively.

The major piece of theoretical work that is left out of these calculations is the inclusion of intersite interactions. It is supposed that the primary effect of these correlations for the present calculations is to renormalize the inelastic scattering but not to produce significant qualitative changes in the results.

Millis and Lee (1987) reached similar results for $\tau(\omega,T)$. In fact, when electron-boson scattering is dominant, the imaginary part of the self-energy Z_c at low frequencies is

$$\mathrm{Im}\,\Sigma_c(\omega,T)=\frac{n_f}{N}\frac{m^*}{m_b}\frac{\omega^2+\pi^2T^2}{\varepsilon_f}. \tag{27}$$

This form for the self-energy agrees with the frequency and temperature-dependent functional form of the scattering rate [Eq. (26)]. Similarly, Riseborough (1983) calculated the frequency dependent scattering due to spin fluctuations. Besides a T^2 contribution to the resistivity, the calculated scattering rate also reduces to Eq. (26) in the low-frequency and low-temperature limit.

Finally, we should like to mention the more recent work by Schweitzer and Czycholl (1991), who calculated the temperature dependence of the electronic transport properties of heavy-electron systems within the self-consistent second-order U-perturbation treatment of the periodic Anderson model. This approach, within which explicit calculations are possible in the limit of a large spatial dimension (d) for correlated lattice electrons, properly fulfills the Luttinger theorem. Such a "dynamical mean-field theory" approach in the $d=\infty$ limit proves to be suitable for the calculation of measurable physical quantities. Schweitzer and Czycholl explicitly calculate transport quantities, which nicely illustrate and reproduce the typical behaviors for nearly the whole temperature regime for various positions of the f level. Therefore the $d=\infty$ approach can be applied not only to the half filled Anderson lattice (corresponding to an insulator, see Sec. IV.E) but also to a metallic mixed-valent regime and it can describe $d=3$ systems as well.

E. Discussion of the excitation spectrum in heavy-electron systems

The general trend of the optical conductivity is rather common in all heavy-electron materials. In fact, at high temperatures we can easily recognize a rather broad metalliclike behavior (i.e., Drude, see below), indicative of a scattering rate (i.e., the width of the Drude term) of the order of 0.1 eV. In contrast, at relatively low temperatures we observe the gradual emergence of a narrow mode centered at zero frequency in $\sigma_1(\omega)$, which merges into the high-temperature $\sigma_1(\omega)$ at far-infrared frequencies (Figs. 5 and 7–9), possibly going through a rather deep minimum in $\sigma_1(\omega)$ (as in UPt_3 at about 3 cm^{-1}; see Fig. 7). This dramatic temperature dependence does, nevertheless, preserve the good agreement between the σ_{dc} values and the $\omega\to0$ limit of $\sigma_1(\omega)$. What will attract our interest below is the low-temperature narrow mode centered at zero frequency which will be associated with the many-body ground state, and the possible evidence of a pseudogaplike feature in the excitation spectrum of heavy-electron systems (Donovan *et al.*, 1997).

1. The phenomenological Drude-Lorentz approach

The classical dispersion theory based on the Drude-Lorentz approach (Wooten, 1972) will allow us to iden-

tify several intrinsic parameters characterizing both the many-body ground state and the so-called normal single impurity phase. The optical conductivity can generally be approximated by a sum of Lorentz harmonic oscillators and of the Drude term. The former contributions arise each time an absorption at finite frequency takes place and they are usually ascribed to vibrational infrared active modes (phonons) or/and to electronic interband transitions. The precise nature and origin of the considered harmonic oscillators will be specified later in the discussion of the different compounds. The Drude term applies for metals and describes the free charge carriers contribution to the electrodynamic response. The general formula for the complex dielectric function is

$$\tilde{\varepsilon}(\omega)=\varepsilon_\infty-\frac{\omega_p^2}{\omega(\omega+i\Gamma)}+\sum_j\frac{\omega_{p,j}^2}{(\omega_j^2-\omega^2)-i\Gamma_j\omega}, \quad (28)$$

where ω_p and $\Gamma\sim 1/\tau$ in the Drude term are the plasma frequency and the damping (i.e., scattering relaxation rate) of the free charge carriers, while ω_j, Γ_j, and ω_{pj} are the resonance frequency, the damping, and the mode strength of the harmonic oscillators, respectively. The high-frequency absorptions above the ultraviolet spectral range are taken into account by ε_∞. This phenomenological fit is a useful approach in order to decouple the various components determining the excitation spectrum and to evaluate several parameters like, the plasma frequency and the scattering relaxation rate, which can be afterwards compared with similar quantities arrived at by other experiments. Alternatively, one can apply a more crude multiband Drude model, as suggested by Sulewski *et al.* (1988), where the total optical conductivity is a sum of several Drude terms. Equation (28) is, however, more general and can better reproduce the complex shape of the optical conductivity in heavy-electron materials (see below).

2. Identification of the various contributions in $\sigma(\omega)$

The goal of this section is to identify and discuss the various components of the dynamics of the charge excitation spectrum with particular emphasis on the excitations at low frequency and temperature. Since our purpose is merely to obtain the plasma frequency associated with the free charge carriers, a set of Lorentzian oscillators is sufficient for a phenomenological description of the high-frequency part (i.e., above the plasma edge) of the excitation spectrum. Subtracting off the Lorentzians (corresponding to the feature between 1 and 8 eV) allows an estimate of the total spectral weight associated with the Drude-like part of the optical conductivity assigned to the free charge carriers. The optical conductivity at high temperatures in heavy-electron compounds is suggestive of a frequency-independent behavior with a relaxation rate of approximately $1/(2\pi\tau)\sim 1000\,\mathrm{cm}^{-1}$. Moreover, the conductivity drops below its dc value at frequencies of the order of $1/\tau$ and is starting to flatten again for $\omega>\omega_h\sim 3000\,\mathrm{cm}^{-1}$, with a Drude-like roll off as ω^{-2}. "Sum-rule" arguments lead to the following integral (Wooten, 1972):

$$I_1=\int_0^{\omega_h}\sigma_1(\omega,T\gg T_{\mathrm{co}})d\omega=\frac{\pi ne^2}{2m_b}=\frac{\omega_p^2}{8}. \quad (29)$$

Equation (29) is, strictly speaking, a partial sum rule, crossing over to the total sum rule for $\omega_h\to\infty$. From Eq. (29), one can thus determine the unscreened optical plasma frequency $\hbar\omega_p\sim 3.5\,\mathrm{eV}$ for $CeAl_3$ (Awasthi *et al.*, 1993) and 2.6 eV for UPt_3 (Sulewski *et al.*, 1988).

At low temperatures (i.e., $T<T_{\mathrm{co}}$), what remains in the conductivity, after the high-frequency interband transitions are removed, is not a simple Drude free-carrier structure. As already pointed out, there is the appearance of a narrow mode centered at zero frequency below the far-infrared spectral range which saturates at higher frequencies (i.e., $\omega>\omega_c$, ω_c being the frequency above which the conductivity at 300 K is indistinguishable, within the experimental error, from that at lower temperatures [Figs. 5 and 7]), merging in a broad absorption. Such a broad absorption extends up to the midinfrared and visible spectral range. The development of the low-frequency narrow mode at $T\ll T_{\mathrm{co}}$ bears a striking similarity with the theoretical prediction of $\sigma_1(\omega)$ (see Figs. 10 and 12).

The narrow low-frequency part of the spectrum at low temperatures is very much reminiscent of a Drude term with renormalized scattering rate. In fact, in the spirit of Eq. (28), one can rewrite the Drude term with the plasma frequency $\omega_p^*=\omega_p/\sqrt{m^*/m_b}$ and the scattering relaxation time $\tau^*=\tau m^*/m_b$, which correspond to the bare quantities ω_p and τ being renormalized by the enhanced effective mass m^* of the heavy quasiparticles at low temperatures. This is actually equivalent to Eq. (10) in the approach by Millis and Lee (1987). Similarly as at 300 K, we can apply sum-rule arguments and calculate the total spectral weight below the narrow "Drude-like" mode. This will allow us to estimate the renormalized plasma frequency ω_p^*:

$$I_2=\int_0^{\omega_c}\sigma_1(\omega,T\ll T_{\mathrm{co}})d\omega=\frac{\pi ne^2}{2m^*}=\frac{(\omega_p^*)^2}{8}, \quad (30)$$

where ω_c is the cutoff frequency, defined above. A comparison of the plasma frequency at 300 K with the renormalized ω_p^* at temperatures lower than T_{co} leads to the expression

$$\left(\frac{\omega_p(300\ \mathrm{K})}{\omega_p^*}\right)=\sqrt{\frac{m^*}{m_b}}\sqrt{\frac{n(300\ \mathrm{K})}{n(T<T_{\mathrm{co}})}}. \quad (31)$$

With the assumption that the total charge-carrier concentration does not change below T_{co} it is possible to directly estimate the enhancement of the effective mass m^*. Table II summarizes the plasma frequencies for various typical heavy-electron systems, obtained by applying either the phenomenological fit [Eq. (28)] or by the sum-rule arguments [Eqs. (29) and (30)]. Both methods give equivalent values to within a few percent. Table

TABLE II. Plasma frequencies ω_p and ω_p^* [from the phenomenological fit with Eq. (28) or from the sum rule with Eqs. (29) and (30)], effective mass m^*/m_b [from Eq. (31)], and m^*/m_e [from Eqs. (2) and (30)] of several heavy-electron systems.

	ω_p (eV)	ω_p^* (eV)	m^*/m_b	m^*/m_e	Ref.
$CeAl_3$	3.5	0.155	510	809	Awashi *et al.*, 1993
UPt_3	2.6	0.323	65	248	Sulewski *et al.*, 1988
$CePd_3$	2.3	0.35	40	36	Webb *et al.*, 1986; Marabelli, 1989; Awasthi *et al.*, 1989
$CeCu_6$	1.84	0.15	150	602	Marabelli, 1989

II also displays the effective mass at low temperatures, obtained through Eq. (31), corresponding to the ratio of I_1/I_2.

It must be observed that the ω_p and ω_p^* plasma frequencies allow the determination of m^* with respect to the band mass m_b, which can be significantly larger than the free-electron mass m_e. For instance, in $CePd_3$ the plasma frequency ω_p suggests a band mass approximately between $1m_e$ and $2m_e$. Consequently, m^*/m_b is expected to be close to m^*/m_e. The conduction band in UPt_3, however, is believed to be heavier (Strange and Gyorffy, 1985; Boring *et al.*, 1985; Oguchi and Freeman, 1985; Wang *et al.*, 1985), and the plasma frequency is indicative of a band mass between 3 and $4m_e$.

The preceding analysis is appealing because the strength of correlation effects was extracted on the basis of the frequency dependent conductivity alone. However, complicated band-structure effects, which determine the unrenormalized plasma frequency and optical relaxation time, have been neglected. An alternative analysis, which compares only parameters which are sensitive to low-energy fluctuations, can be performed by using the Sommerfeld γ value of the specific heat (Table I). By combining the expression for γ of Eq. (2) with ω_p^* given by Eq. (30), two parameters m^*/m_e and n can be extracted. This analysis avoids difficulties associated with a complicated energy dependent density of states since both ω_p^* and γ are determined from experiments that sample the density of states within the same energy range. Note that 5 K corresponds to approximately 100 GHz, and a specific heat measured at this temperature samples a thermal energy range k_BT comparable to the microwave far-infrared frequency range. An important caveat in this alternative analysis is that the thermodynamic and transport enhancements must be determined by the same electrons. The results of this analysis are also included in Table II. The effective-mass m^*/m_e agrees favorably with mass enhancement derived from the low- and high-frequency conductivity data and this suggests that a one-band model is appropriate to account for the various properties of these materials. Nevertheless, we recall that the difference is principally due to the ratio m_b/m_e (as mentioned above) and also to the assumption that the charge-carrier's concentration remains constant. This latter approximation might be too crude and could lead to some correction factors. For instance, the above analysis does not rule out smaller carrier number associated with the coherent state, along with a smaller mass enhancement, because only the ratio n/m^* appears in all expression used and the specific-heat coefficient $\gamma \sim n^{1/3}$ [Eq. (2)] would be only weakly affected by a reduction of the carrier number.

So far, we have focused our attention on the $T \rightarrow 0$ limit of the electrodynamic response. Later in the discussion (Sec. II.E.4) we will address the issue of the temperature dependence of m^*, which incorporates the development of the correlation effects. In fact, the approach based on the ratio I_2/I_1 [Eq. (31)] is not suitable for estimating the temperature dependence of m^*, since the low-frequency resonance becomes increasingly less distinguishable from the frequency independent response at high temperatures, making it harder to estimate the ratio I_2/I_1.

3. The low-temperature far-infrared absorption in $\sigma_1(\omega)$

The overall behavior of the frequency dependent conductivity at low temperatures is in general agreement with the results obtained from various calculations (see Figs. 10 and 12) (Millis and Lee, 1987; Cox and Grewe, 1988; Freytag and Keller, 1990). In the previous section, we have already identified, in the narrow mode at low-temperatures and frequencies, the optical fingerprint associated with the heavy quasiparticles. Another important feature in $\sigma_1(\omega)$ at low temperatures is the roll off of such a narrow Drude mode. Almost all compounds display a saturation of $\sigma_1(\omega)$ (Figs. 5, 7, and 8) to a more or less constant value from far infrared up to the midinfrared and visible spectral range, where the onset of electronic interband transitions takes place. However, Marabelli and coworkers (1986, 1988, 1989, 1990a, 1990b) observed a minimum in $\sigma_1(\omega)$ of $CeCu_6$ (Fig. 9) and UPt_3 single crystals at far infrared frequencies. As stated above in the theoretical section, such a minimum could correspond to the energy range around $\tilde{\omega}_p^*$ [Eq. (11)], where the crossover between the plasma edgelike feature in $R(\omega)$ at $\omega \sim \tilde{\omega}_p^*$ and the onset of the s-$f(d)$ excitation for $\omega > \tilde{\omega}_p^*$ takes place. The broad midinfrared feature, ascribed to s-$f(d)$ excitations, has been named hybridization gap (Wachter, 1994), because it is the di-

rect consequence of the hybridization process between the localized f electron and the broad conduction band.

Nevertheless, the majority of theoretical works do not take hybridization gaps into account, principally because they are intended to describe phenomena occurring only at the lowest temperatures. In fact, besides the theoretical work of Freytag and Keller (1990), where a minimum in $\sigma_1(\omega)$ at $k_B T_K$ is suggested, most of the calculations predict a saturation of $\sigma_1(\omega)$ at frequencies larger than ω_c (see Figs. 10 and 12) (Millis and Lee, 1987; Cox and Grewe, 1988). As already pointed out, the universality of this hybridization gaplike feature is also experimentally a matter of debate, since a saturation of $\sigma_1(\omega)$ at $\omega > \omega_c$ is, instead, mostly seen.

Anyway, the most recent optical experiments (Donovan *et al.*, 1997) on UPt_3 questioned even more seriously the hybridization-gap interpretation. As shown in Fig. 7, there is an important temperature dependence in the spectral range near 7 cm^{-1} (~0.9 meV), which is at much lower frequencies than the feature apparently seen in UPt_3 as well as in $CeCu_6$ by Marabelli *et al.* (1986 and 1988). The absorption is identified by Donovan *et al.* (1997) with a pseudogaplike absorption instead of a hybridization gap. The conductivity at 1.2 K can be decomposed into a Drude part and a high-frequency response. This latter feature appears both in measurements on single crystals and on the polycrystalline specimen. Because the single-crystal measurements probe the response only along one axis, while the polycrystal measurements average over all crystal axes, it is argued that the pseudogap must open up along the entire Fermi surface. The broad maximum observed around 7 cm^{-1} is different from what is observed for a three-dimensional semiconductor [where the conductivity increases as $(\hbar\omega-\Delta)^{1/2}$ above the gap], and is instead reminiscent of what is expected for a spin-density wave (SDW) gap, such as that observed in organic metals like $(TMTSF)_2PF_6$ (Degiorgi, Dressel, Schwartz *et al.*, 1996) and in some heavy-fermion compounds with a magnetic ground state (Degiorgi *et al.*, 1997). Magnetic correlations have been known to be important in UPt_3 (Kjems and Broholm, 1988), and it would be natural to associate the pseudogap with the onset of magnetic correlations below 5 K. The energy scale associated with the gap structure, $\Delta \sim 0.5$ meV, would support such a relation (Donovan *et al.*, 1997).

4. Frequency and temperature dependence of m^* and Γ

Another method of estimating m^*/m_b together with the scattering rate Γ is to consider the low-frequency resonance arising from free carriers undergoing frequency dependent scattering. This means that the optical conductivity may be described by a so-called generalized Drude model (Sulewski *et al.*, 1988; Awasthi *et al.*, 1993). Obviously, the frequency dependence of Γ implies, through the Kramers-Kronig relation between σ_1 and σ_2, that also m^* is frequency dependent. This method is particularly compelling at low frequencies, where no obvious method exists for separating $\sigma_1(\omega)$ into an ordinary Drude contribution and midinfrared modes. It will allow us to reveal a fundamental relationship between the scattering rates derived from either dc transport properties or the optical response in the infrared frequency range. Moreover, the application of the generalized Drude at different temperatures will permit the evaluation of the temperature dependence of m^* and Γ. Therefore the complex conductivity may be written as (Thomas *et al.*, 1988)

$$\sigma(\omega) = \frac{\frac{{\omega_p}^2}{4\pi}}{\Gamma(\omega) - i\omega \frac{m^*(\omega)}{m_b}}, \tag{32}$$

where ω_p is the unscreened optical plasma frequency of Eq. (29). A relationship between σ_1, σ_2, and Γ together with m^*/m_b is then obtained as follows:

$$\Gamma(\omega) = \frac{{\omega_p}^2}{4\pi} \frac{\sigma_1}{|\sigma|^2} \tag{33}$$

and

$$\frac{m^*(\omega)}{m_b} = \frac{\omega_p^2}{4\pi} \frac{\sigma_2}{\omega|\sigma|^2}. \tag{34}$$

When $\omega \ll \Gamma$ and $\omega \to 0$, σ_1 is constant and σ_2 should tend to zero, while both $\Gamma(\omega)$ and $m^*(\omega)$ must assume frequency independent values. Figure 14 (Awasthi *et al.*, 1993) displays $m^*(\omega, T)$ and $\Gamma(\omega, T)$ for $CeAl_3$ at various temperatures.

We first discuss the frequency dependent $m^*(\omega, T)$, shown in Fig. 14(b) for $CeAl_3$. At 10 K and above, the coherent state does not exist as the surface impedance results suggest (Fig. 3), and consequently no mass enhancement is expected. At low temperatures, we expect m^* in Eq. (34) to assume constant values at frequencies below which Γ becomes frequency independent. This crossover frequency [say $\omega_{co}(T)$] is approximately 0.3, 0.9, and 0.7 cm^{-1} at 1.2, 3.0, and 5.0 K, respectively [Fig. 14(a)]. The values of m^*/m_b for $CeAl_3$ at ω_{co}'s are 360, 225, and $160 m_b$, which we believe to be appropriate estimates of the zero frequency effective masses at these temperatures (see Table II). Thus a substantial increase in the effective mass occurs only below 3 K (for $CeAl_3$, $T_K \sim 3$ K!). Similarly, $m^*(\omega, 1.2\text{ K})$ for UPt_3 saturates to an enhanced value of approximately $240 m_e$ (i.e., $m^* \sim 65 m_b$) (Sulewski *et al.*, 1988; Donovan *et al.*, 1997).

In order to highlight the comparison with the thermodynamic results, Fig. 15 shows the effective mass vs temperature, along with the specific-heat (C_p/T) data for $CeAl_3$ (Brodale *et al.*, 1986). The two sets of results were normalized (somewhat arbitrarily) at 5 K for the purpose of comparison. The low- and the high-temperature saturation limits of the electrodynamic mass are associated with the narrow mode in the density of states and the broad underlying band, respectively. At mid temperatures, the effective dynamical mass has intermediate values due to the temperature-dependent Fermi-surface renormalization. Regarding the thermodynamic experiments, C_p/T and χ primarily measure the density of

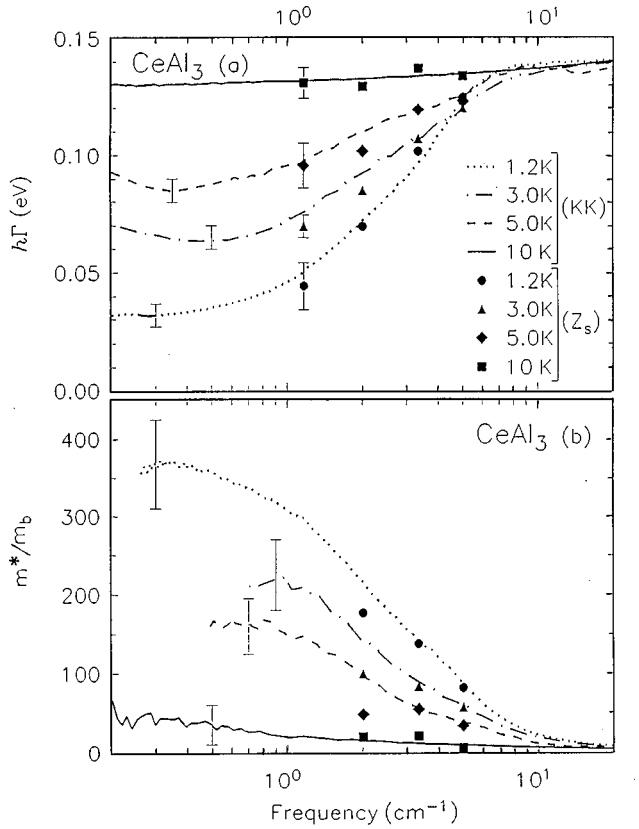

FIG. 14. Scattering rate and effective mass in $CeAl_3$. (a) Frequency-dependent optical scattering rate for $CeAl_3$ at four temperatures from Eq. (33), along with the values obtained using the microwave data. (b) Frequency dependence of m^* obtained from Eq. (34) (Awasthi *et al.*, 1993).

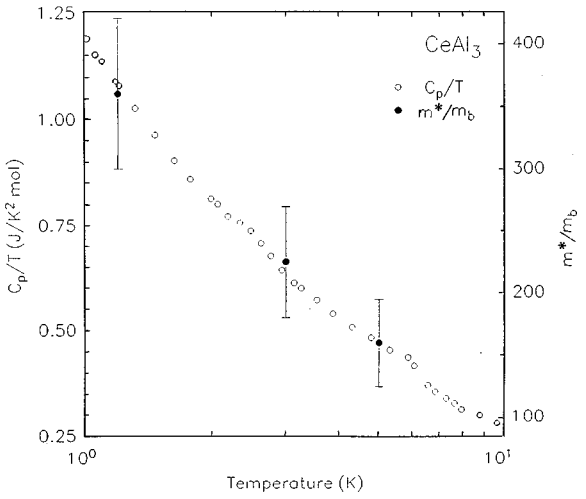

FIG. 15. Temperature dependence of the effective dynamical mass obtained from Fig. 14(b) for $CeAl_3$ (Awasthi *et al.*, 1993). Also shown for comparison is C_p/T (Brodale *et al.*, 1986).

states at the Fermi level (averaged over an energy width k_BT). The decrease of C_p/T and χ with temperature reflects the gradual disappearance of correlation effects, and the contribution of higher-order temperature-corrections. For $T\sim T_K$ (i.e., the many-body resonance width) these higher-order terms (in the Bethe-Sommerfeld expansion) become important. Consequently, C_p/T may not be expected to give the correct temperature dependence of the effective mass directly. Nevertheless, it is remarkable that the thermo- and electrodynamic quantities have comparably similar temperature dependences (Fig. 15).

The analysis of the optical data in terms of the generalized Drude approach [Eq. (32)] also supplies the frequency dependence of the scattering rate $\Gamma(\omega)$. The values of Γ obtained directly from the surface impedance measurements are also shown in Fig. 14(a). There is an excellent agreement with those from the Kramers-Kronig analysis. At each temperature, the error bar on the 35 GHz point also represents the maximum percentage uncertainty in the higher-frequency surface-impedance results. Above approximately 7 cm^{-1}, the temperature dependence of Γ in $CeAl_3$ disappears, while at low frequencies, the scattering rate is only temperature dependent. Interestingly, by 10 K (=7 cm^{-1}), there is little frequency dependence left in Γ, as well! This latter behavior could be considered as an indirect manifestation of the equivalence of temperature and frequency, establishing temperature as the only relevant energy scale of the system.

Moreover, while the frequency dependence of σ_1 is due to a small scattering rate, its roll off to a finite value starts where Γ acquires a significant frequency dependence. This also implies that a simple Drude picture [Eq. (28)] with constant parameters reproduces the narrow $\sigma_1(\omega)$ at low temperatures and frequencies only roughly. Such an oversimplified Drude-like description [Eq. (28)] was nevertheless useful in view of the spectral weight arguments which led to the optical characterization of the "heavy-electron" ground state.

It is worth noting that Fig. 14(a) displays the so-called unrenormalized scattering rate Γ. Sometimes in the literature, one can find an alternative definition in terms of the renormalized scattering rate $\Gamma^*=\Gamma(m_b/m^*)$. For $CeAl_3$ Γ^* in its dc limit, i.e. $\Gamma^*(\omega\rightarrow 0)$, has values of 0.7, 2.5, and 4.5 cm^{-1} at 1.2, 3, and 5 K, respectively. It is interesting to observe that the values roughly correspond to the width of the narrow mode centered at zero frequency in $\sigma_1(\omega)$ (Fig. 5). Also the latest measurements on UPt_3 suggest that, below about 100 GHz, Γ and m^* are only weakly dependent on frequency (Donovan *et al.*, 1997).

Finally, the quantitative estimation of the parameters $m^*(\omega)$ and $\Gamma(\omega)$ is particularly compelling for the issue about the possible Fermi-liquid nature of these "conventional" heavy-electron systems. Several experiments suggest that in a variety of heavy fermion materials, electron-electron interactions lead, upon lowering the temperature, to the development of a coherent state, where the electrodynamics can be described by a renormalized effective mass and relaxation rate. As the frequency approaches zero, the scattering rate must approach the value given by the dc resistivity, as is borne out by the data. At higher frequencies, the absorptivity is again proportional to the root of the frequency, indicating that the scattering rate saturates. At the lowest

temperatures, the resistivity has a T^2 term, possibly arising from electron-electron or electron-spin-fluctuation interactions. This rise with T^2 in the scattering rate should also imply a similar rise with the square of frequency at the lowest frequencies. Such a ω^2-dependent scattering rate is interpreted as arising from the coupling of the itinerant (heavy) electrons to the spin-fluctuation spectrum, which dresses the electrons giving them a large effective mass at low frequencies. At higher energies the (lighter) electrons should be unscreened, revealing the bare optical band mass, and so should scatter from the spin fluctuations. Sulewski *et al.* (1988) analyzed their data on UPt_3 within a phenomenological model [i.e., Eq. (26)], suggesting a Fermi-liquid-like behavior of $\Gamma(\omega)$. The recent work on UPt_3 (Donovan *et al.*, 1997), extending the investigation to even lower frequencies, casts, however, some doubts about the reliability of such an interpretation.

Indeed, the ω^2 dependence of $1/\tau(\omega)$ at low frequencies ($\omega<10\,\mathrm{cm}^{-1}$) and temperatures ($T<T_{co}<T_K$), combined with the low-temperature T^2 dependence of $1/\tau(T)$ inferred from the transport properties, could suggest a Fermi-liquid behavior, but only from a phenomenological point of view; the functional of $1/\tau(\omega,T)$ bears an overall similarity with the Fermi-liquid prediction of Eq. (26), but the available experimental data [e.g., Sulewski *et al.* (1988)] are rather controversial and do not supply a unique ratio b/a [Eq. (26)]. The experimental verification of Eq. (26) is still not yet completed. This is mainly due to the low energy and temperature scales below which a Fermi-liquid ground state manifests. Such low characteristic energy scales necessitate "optical" investigations at very low frequencies and temperatures, making the experiments very challenging from the technical point of view. Moreover, in the specific case of UPt_3 the coherent state gradually evolves, upon further decrease of temperature, into a state with a pseudogap, related most probably to magnetic correlations (Figs. 6 and 7). Whether this scenario is a general characteristic of heavy-electron compounds remains to be seen. It is evident, however, that this description is in clear conflict with conclusions based on the conventional analysis of the specific heat coefficient γ and the coefficient of the T^2 term in the resistivity [Eq. (1)]. Such analysis has been taken as evidence that UPt_3 is a renormalized Fermi liquid at low temperatures (but above the superconducting transition), with an energy-independent density of states. A comprehensive clarification of this issue is left for the future.

III. NON-FERMI-LIQUID KONDO ALLOYS

A. Fermi liquid versus non-Fermi-liquid behavior

During the past two years, there has been a great deal of interest in a narrow class of materials among the highly correlated metals, which exhibit non-Fermi-liquid properties at low temperatures (Maple *et al.*, 1994, 1995; von Löhneysen, 1995; Steglich *et al.*, 1997; von Löhneysen *et al.*, 1997). We shall first start from Landau's Fermi-liquid theory, which is fundamental for our understanding of electron excitations in metals, as it establishes a one-to-one correspondence between the excitations of a free-electron gas and those of interacting conduction electrons in metals. One of the central points of Fermi-liquid theory is the existence of a single energy scale, the Fermi-energy E_F, and for energies $E\ll E_F$ and temperatures $k_BT\ll E_F$ the electronic properties display universal behavior (Ashcroft and Mermin, 1976). For some time it seemed that in no other solids have the predictions of Fermi-liquid theory more strikingly been realized than in the heavy-electron intermetallics [for example, see UPt_3; Ott and Fisk (1987), and Fisk *et al.* (1988)]. In a number of these *f*-electron based compounds, analyses of the low-temperature specific heat, magnetization, electrical resistivity, and dynamical susceptibility display a dependence on a single energy scale consistent with Fermi-liquid theory, although unprecedented mass enhancements of 10^2–10^3 imply strong electronic interactions (Secs. II and V).

More recent experimental work has indicated, however, that several heavy-electron compounds and related alloys display quite remarkable properties, which manifest much less well a "conventional" Fermi-liquid behavior. Deviations from Fermi-liquid predictions have now been observed in several *f*-electron alloys, including $UCu_{5-x}Pd_x$ (where $x=1$ and 1.5) (Andraka and Stewart, 1993; Ott, 1996), $CeCu_{5.9}Au_{0.1}$ (von Löhneysen *et al.*, 1994), $Y_{1-x}U_xPd_3$ (where $x<0.2$) (Andraka and Tsvelik, 1991; Seaman *et al.*, 1991; Ott *et al.*, 1993; Xu *et al.*, 1994) $Th_{1-x}U_xRu_2Si_2$ (where $x<0.07$) (Amitsuka *et al.*, 1993), $U_{1-x}Th_xPd_2Al_3$ (where $x>0.4$) (Maple *et al.*, 1994 and 1995) Ce_7Ni_3 (Umeo *et al.*, 1997), and $Th_{1-x}U_xCu_2Si_2$ (where $x<0.1$) (Lenkewitz *et al.*, 1997).

Typically, the non-Fermi-liquid behavior is observed as a diverging linear coefficient of the specific-heat C for temperature $T\to 0$:

$$C/T\sim(-1/T_0)\ln(T/bT_0), \tag{35}$$

and a strong T dependence of the magnetic susceptibility χ as $T\to 0$:

$$\chi(T)=1-c(T/T_0)^{1/2}, \tag{36}$$

(where b and c are constants of the order of unity) while Fermi-liquid theory predicts $\gamma\sim\chi\sim$constant at $T\to 0$. Furthermore, the electrical resistivity ρ shows a T dependence as

$$\rho(T)=\rho_0-AT^m \tag{37}$$

with usually $A>0$, and often $m=1$, instead of the Fermi-liquid behavior $m=2$ [Eq. (1)] arising from particle-particle interaction. However, we should caution on the validity of Eqs. (35)–(37), since these fits are but one possible interpretation of the data and merely represent the trend encountered in various non-Fermi-liquid Kondo alloys. More precisely, Eqs. (35)–(37) do not have the same validity for all non-Fermi-liquid compounds and sometimes apply over different temperature regimes for different quantities and in some cases over a temperature range less than a decade. Table III summa-

TABLE III. Examples of *f*-electron systems that exhibit characteristic non-Fermi-liquid behavior in the low-temperature specific heat $C(T)$ [Eq. (35)], magnetic susceptibility $\chi(T)$ [Eq. (36)], and electrical resistivity $\rho(T)$ [Eq. (37)], with $m=1$. "Yes" denotes agreement with the non-Fermi-liquid behavior, and in brackets we display the corresponding temperature range of validity for Eqs. (35)–(37). The characteristic temperature T_0 is proportional to T_K and is deduced from $\beta=d(C/T)/d\ln T$, the logarithmic divergence in the specific heat, so that $T_0=0.251\,\mathrm{R}/\beta$.

	$\rho(T)$	$C(T)/T$	$\chi(T)$	T_0 (K)	Ref.
$La_{0.9}Ce_{0.1}Cu_2Si_2$	yes ($1<T<5$ K)	yes ($1.8<T<10$ K)	$-\ln(T/bT_K)$ ($1<T<10$ K)	9	Andraka, 1994b; Maple *et al.*, 1994, 1995
$M_{1-x}U_xPd_3$ (M=Sc,Y)	yes ($T<30$ K)	yes ($0.5<T<10$ K)	yes ($0.6<T<40$ K)	40–220	Seaman *et al.*, 1991; Andraka and Tsvelik, 1991; Ott *et al.*, 1993; Xu *et al.*, 1994 Maple *et al.*, 1994, 1995
$UCu_{3.5}Pd_{1.5}$	yes ($T<30$ K)	yes ($2<T<15$ K)	yes ($2<T<15$ K)	28	Andraka and Stewart, 1993; Maple *et al.*, 1994, 1995; Ott, 1996
$U_{1-x}Th_xPd_2Al_3$	yes ($T<40$ K)	yes ($0.5<T<10$ K)	yes ($T<10$ K)	20	Maple *et al.*, 1994, 1995
$M_{0.1}U_{0.9}Ni_2Al_3$ (M=Pr,Th)		yes ($1.8<T<9$ K)	yes ($1.8<T<9$ K)	200	Kim *et al.*, 1993; Maple *et al.*, 1994, 1995
$Ce_{1-x}Th_xRhSb$		yes ($1<T<10$ K)		33	Andraka *et al.*, 1994a; Maple *et al.*, 1994, 1995
$Th_{1-x}U_xRu_2Si_2$		yes ($4<T<10$ K)	$-\ln(T/bT_K)$ ($0.1<T<10$ K)	11	Amitsuka *et al.*, 1993; Maple *et al.*, 1994, 1995;
$U_{0.9}Th_{0.1}Be_{13}$	yes ($A<0$) $m=1$: $0.23<T<0.7$ K $m=\frac{1}{2}$: $0.7<T<4$ K	yes ($1.7<T<10$ K)	yes ($1.7<T<10$ K)	8	Maple *et al.*, 1994, 1995; Dickey *et al.*, 1997
$U_{0.1}Th_{0.9}Cu_2Si_2$	yes ($A<0$) ($0.1<T<3.5$ K)	yes ($0.4<T<10$ K)			Maple *et al.*, 1994, 1995; Lenkewitz *et al.*, 1997
$CeCu_{5.9}Au_{0.1}$	yes ($A<0$) ($0.1<T<1$ K)	yes ($0.1<T<3$ K)	yes ($0.1<T<3$ K)	3.5	von Löhneysen *et al.*, 1994; Maple *et al.*, 1994, 1995

rizes the characteristic non-Fermi-liquid properties of several Kondo alloys together with the corresponding temperature range where non-Fermi-liquid behavior applies. Note that the characteristic temperature T_0 generally scales with T_K. In the following paragraph we shall discuss in particular the Kondo alloy systems which have also been investigated optically; namely, $Y_{1-x}U_xPd_3$, $U_{1-x}Th_xPd_2Al_3$, and $UCu_{5-x}Pd_x$.

As far as the other systems are concerned, we shall review here just a few peculiarities. The non-Fermi-liquid behavior in $CeCu_{5.9}Au_{0.1}$ was attributed to the proximity to magnetic order in the sense that this system is at the edge of a zero-temperature quantum phase transition (von Löhneysen *et al.*, 1994). This picture is further motivated by the latest neutron-scattering experiment, which enforces a model of three-dimensional conduction electrons coupled to two-dimensional critical ferromagnetic fluctuation near such a quantum critical point (Rosch *et al.*, 1997). It has been, moreover, established that in a large magnetic field ($B>3$ T) Fermi-liquid behavior is recovered (von Löhneysen *et al.*, 1994). Interestingly, the sister compound $CeCu_{5.7}Au_{0.3}$ has an antiferromagnetic phase at $T_N=0.49$ K for pressure $p=0$, which can be continuously tuned to zero with pressure. At the critical pressure $p_c=8.2$ kbar $CeCu_{5.7}Au_{0.3}$ displays the same logarithmically divergent behavior in $C(T)$ as in $CeCu_{5.9}Au_{0.1}$ at zero applied pressure (Bogenberger and von Löhneysen, 1995). This clearly demonstrates that non-Fermi-liquid can be tuned with pressure. This result also represents (apart from alloying experiments) the first tuning experiment of the specific heat in a magnetic-nonmagnetic quantum phase transition in heavy-electron systems, although a number of pressure studies have revealed the interplay between Kondo compensation and magnetic order (Sereni and Kappler, 1994; Bogenberger and von Löhneysen, 1995). Similarly, Ce_7Ni_3 has a $T_N=1.9$ K at $p=0$, which vanishes near $p_c=0.33$ GPa. Non-Fermi-liquid appears for applied pressure between 0.4 and 0.62 GPa. Above 0.62 GPa a Fermi-liquid behavior is recovered (Umeo *et al.*, 1997). Finally, it is worth mentioning that $Th_{1-x}U_xCu_2Si_2$ exhibits non-Fermi-liquid behavior for $x<0.1$, in the neighborhood of ferromagnetism, which develops for alloys with $x>0.15$ (Lenkewitz *et al.*, 1997).

B. A few examples of non-Fermi-liquid Kondo alloys

1. $U_xY_{1-x}Pd_3$

The $U_xY_{1-x}Pd_3$ system exhibits many interesting phenomena including a structural phase transition, spin-

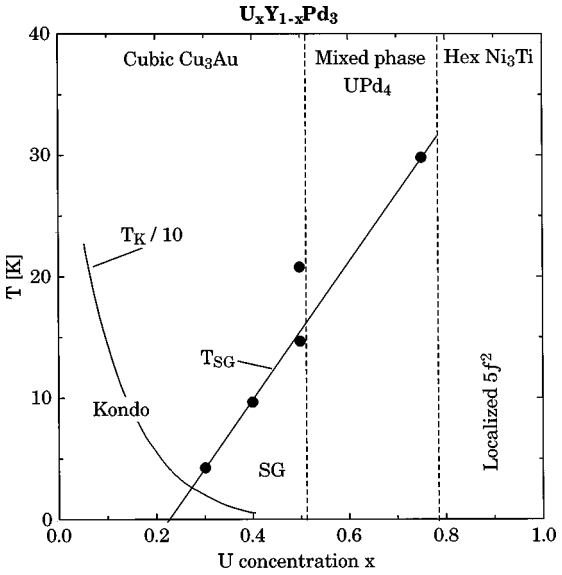

FIG. 16. Low-temperature U concentration phase diagram of $U_xY_{1-x}Pd_3$ (Maple *et al.*, 1994).

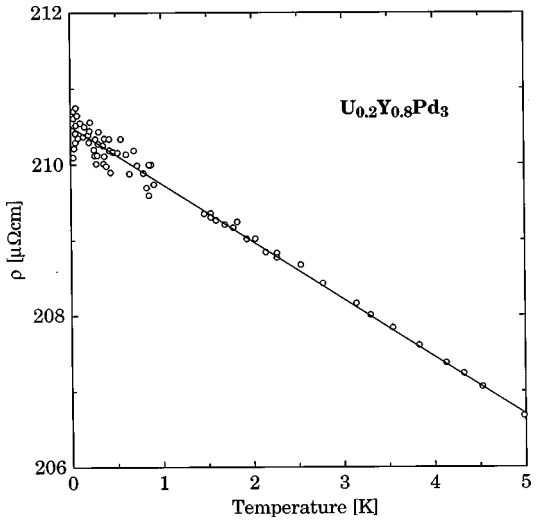

FIG. 17. Temperature dependence of the resistivity $\rho(T)$ in $U_{0.2}Y_{0.8}Pd_3$ at $T<5$ K (Ott *et al.*, 1993).

glass freezing, crystalline electric-field effects, Fermi-level tuning, and unusual Kondo behavior (Seaman *et al.*, 1991; Maple *et al.*, 1994). Of particular interest is the Kondo behavior, which occurs at low U concentration for Y and has low-temperature properties with non-Fermi-liquid characteristics.

Shown in Fig. 16 (Maple *et al.*, 1994) is the temperature-U concentration (T-x) phase diagram of $U_xY_{1-x}Pd_3$, which summarizes the general behavior as a function of x. Besides the mixed phase region for $0.6<x<0.8$, the samples, which form in the hexagonal Ni_3Ti crystal structure ($0.9<x<1$), appear to have nonmagnetic ground state. On the other hand, the intermetallic compound UPd_3 has recently been studied by inelastic neutron scattering (McEwen *et al.*, 1992) and reported to undergo a quadrupolar transition at 6.5 K, followed by a magnetic transition at 4.5 K. UPd_3 is one of the few actinide materials whose properties are all consistent with localized $5f$ electrons. Moreover, sharp crystal-field levels are observed that are indicative of an f^2 nonmagnetic ground state and tetravalent U ions (Maple *et al.*, 1994 and 1995).

The samples with U concentrations $0.3<x<0.5$, which form in the cubic Cu_3Au structure, exhibit spin-glass (SG) freezing below a temperature T_{SG} which increases monotonically with x, as shown in Fig. 16. Such an increase is expected for RKKY interactions whose strength increases as $J^2N(E_F)x$, where J is the exchange interaction parameter (Maple *et al.*, 1994 and 1995). Furthermore, recent muon spin-relaxation measurements on $U_xY_{1-x}Pd_3$ demonstrate that spin-glass order in this system can be understood in the context of induced moments (Wu *et al.*, 1993 and 1994; Amato, 1997).

For $0<x<0.2$, $U_xY_{1-x}Pd_3$ exhibits unusual Kondo behavior with a Kondo temperature T_K that increases with decreasing x, as indicated in Fig. 16. This is consistent with the "Fermi-level tuning" revealed by previous photoemission studies of $U_xY_{1-x}Pd_3$ (Kang *et al.*, 1989), where it was found that the separation between E_F and the $5f$ peak below it, $|E_F-E_{5f}|$, decreases with decreasing x as UPd_3 is diluted with Y. Because $N(E_F)$ is low throughout the series (~1 state/eV cell), the drop in E_F is rather large (~1 eV as x decreases from 1 to 0). The nearly linear decrease in the binding energy with decreasing x should cause a large increase in T_K [Eq. (3)].

The existence of a Kondo effect in $U_xY_{1-x}Pd_3$ system for $x<0.3$ is evident from the electrical resistivity $\rho(T)$, which increases logarithmically with decreasing temperature at high temperatures $T>T_K$. However, at $T \ll T_K$, $\rho(T)$ does not saturate quadratically which is expected for a conventional Kondo effect [Eq. (1)], reflecting the behavior of a Fermi liquid. Rather, the behavior of Eq. (37) with $m=1$ is found for $T<30$ K. Figure 17 (Ott *et al.*, 1993) shows $\rho(T)$ for $U_{0.2}Y_{0.8}Pd_3$, from where the linearity in T of $\rho(T)$ can be recognized. At very low temperatures ($T<0.1$ K), there is a deviation from such a linear behavior (however, the resolution is here not quite good enough) whose origin is yet unknown although it may represent a crossover to a Fermi-liquid behavior.

The specific heat (Ott *et al.*, 1993; Maple *et al.*, 1994, 1995) also displays the characteristic non-Fermi-liquid-like logarithmic divergence [Eq. (35)] over the temperature range $0.7<T<10$ K. Such non-Fermi-liquid behavior is obviously in contrast to a conventional Kondo effect where C/T approaches a constant value. A remarkable aspect of the specific-heat data is that the associated entropy $S(T)$ saturates to a value close to $(R/2)\ln 2$ before continuing to increase due to the higher temperature upturns in $\Delta C/T$. This suggests a finite zero-temperature entropy of the same value, in order that the full degeneracy of the ground doublet be recovered at high temperatures. This entropy is expected to be removed at low but finite temperatures due to any weak interactions which might lift the ground-state degeneracy. Below 0.5 K C/T rises dramatically without

any sign of saturation. Furthermore, Ott *et al.* (1993) reported that the upturn in C/T of $U_{0.2}Y_{0.8}Pd_3$ persists to at least 0.05 K. The deviation away from logarithmic dependence is well described by $\Delta C/T = A T^{-2}$, which is the temperature dependence of a Schottky anomaly in the high-temperature limit. The magnitude of A from the measurements of Ott *et al.* (1993) is too large for a nuclear Schottky anomaly in the high-temperature limit, but for a two-level electronic Schottky anomaly it corresponds to a level splitting of 2.5 mK. It has been suggested previously that this rise may account for the missing entropy of $(R/2)\ln 2$.

The magnetic susceptibility (Maple *et al.*, 1994, 1995) exhibits a Curie-Weiss temperature dependence at high temperatures $T > 150$. At low temperatures $\chi(T)$ increases more rapidly with decreasing temperature than the Curie-Weiss temperature dependence, and continues to increase with positive curvature down to the lowest measured temperature. Such a temperature dependence is again in contrast to the Fermi-liquid behavior of the single channel, $S = \frac{1}{2}$ Kondo effect in which $\chi(T)$ becomes temperature independent for $T \ll T_K$ due to screening of the impurity moments by the conduction electrons. The $\chi(T)$ data are well described by Eq. (36), even though the precise temperature dependence of $\chi(T)$ at the lowest temperatures is masked by the possible presence of magnetic impurities other than U.

2. $U_{1-x}Th_xPd_2Al_3$

The reference system UPd_2Al_3 belongs to the class of materials, characterized by the coexistence of superconductivity and antiferromagnetism. Its large ordered magnetic moment of $0.85\mu_B$ is in contrast to the small ordered moments ($\sim 0.02\mu_B$) observed for URu_2Si_2 and UPt_3, two other heavy-electron compounds in which superconductivity and antiferromagnetism also coexist with $T_c < T_N$. The Th-doped UPd_2Al_3 provides an interesting opportunity to scan a rather complex phase diagram, where the evolution from the coexistence of superconductivity and magnetic order towards non-Fermi-liquid behavior can be studied. Such a phase diagram is shown in Fig. 18, while Fig. 19 displays the temperature dependence of the dc resistivity $\rho(T)$ for various Th concentration (Maple *et al.*, 1994, 1995). The electrical resistivity of this system shows a smooth evolution from Kondo lattice to single-ion Kondo behavior as the U concentration is decreased.

In the Kondo-lattice regime ($x < 0.4$), the Neel temperature T_N for antiferromagnetic ordering of the U ions and the superconducting critical temperature T_c of UPd_2Al_3 decrease somewhat with increasing Th-dopant concentration x and the features associated with the antiferromagnetism and superconductivity are rapidly suppressed and eventually become undetectable. For $x < 0.4$ and at temperatures $T_c < T \ll T_N$, $\rho(T)$ can be fitted by a T^2 dependent term (Dalichaouch *et al.*, 1992; Bakker *et al.*, 1993).

However, in the single-ion Kondo regime for $x > 0.4$, the resistivity increases linearly [Eq. (37)] with decreasing temperature below approximately 50 K and the specific heat diverges logarithmically at low temperatures [Eq. (35)], indicative of non-Fermi-liquid behavior. The fully Th-doped ($x = 1$) material is also rather peculiar since $\rho(T)$ can be fitted by Eq. (37) with $m = 1$ and $A < 0$ over a very large temperature regime from 50 up to 300 K and, furthermore, has a superconducting phase transition at $T_c = 0.2$ K. However, the phase diagram is yet incomplete near $x = 1$ but it is certainly remarkable that UPd_2Al_3 has an isostructural counter part based on a rare-earth or actinide element with an empty or filled *f*-electron shell, which is also superconducting (Maple *et al.*, 1995).

Similarly to $U_{0.2}Y_{0.8}Pd_3$, the resistivity $\rho(T)$ levels off at low temperatures (i.e., $T < 0.5$ K) for $x > 0.4$, suggest-

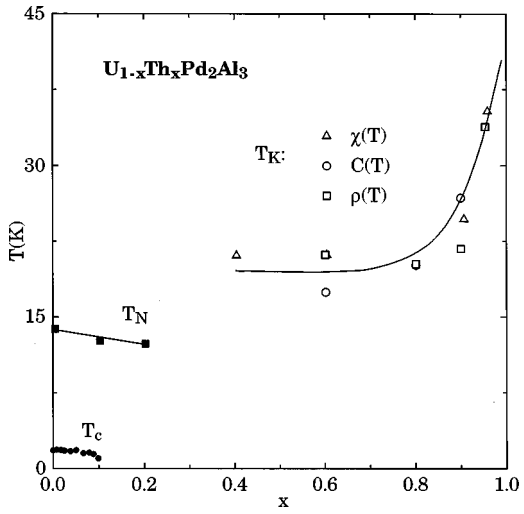

FIG. 18. Low-temperature U concentration phase diagram of $U_{1-x}Th_xPd_2Al_3$ (Maple *et al.*, 1995).

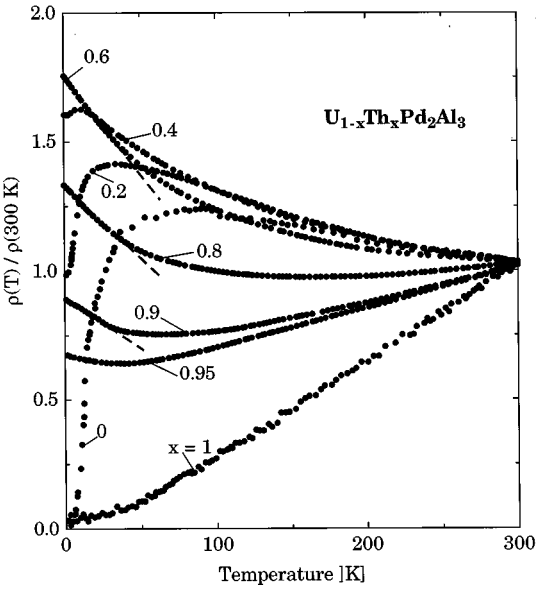

FIG. 19. Temperature dependence of the resistivity $\rho(T)$ in $U_{1-x}Th_xPd_2Al_3$. The dashed lines for $x = 0.6$, 0.8, and 0.9 represent fits to Eq. (37) with $m = 1$, indicative of non-Fermi-liquid behavior (Maple *et al.*, 1995).

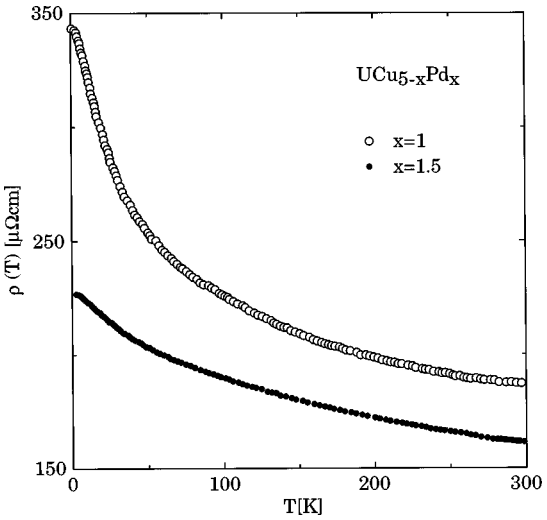

FIG. 20. Temperature dependence of the resistivity $\rho(T)$ in $UCu_{5-x}Pd_x$ ($x=1$ and 1.5) (Ott, 1996).

ing that the degeneracy of the conduction-electron channels or the localized electron spin or charge degrees of freedom have been removed by some type of residual interaction, producing an evolution towards single-channel Fermi-liquid behavior (Maple *et al.*, 1995). Experiments are still in progress in order to determine whether the specific heat exhibits a sharp upturn at low temperatures, deviating from the divergent logarithmic behavior, as it does in the $U_xY_{1-x}Pd_3$ system.

The $\chi(T)$ data for UPd_2Al_3 exhibit a maximum near 40 K and an abrupt drop at T_N. With increasing x, the maximum in $\chi(T)$ is suppressed until it disappears at $x=0.1$ and, below 10 K, is accompanied by an increase in χ with decreasing temperature. For $x>0.4$, $\chi(T)$ merges in a square-root dependence at low temperatures [Eq. (36)], again indicative of non-Fermi-liquid behavior.

3. $UCu_{5-x}Pd_x$

This family of compounds is peculiar among the uranium-based intermetallics known to have non-Fermi-liquid properties as it is a concentrated moment system (the previous two examples can be classified as diluted systems). All $x<2.5$ share the common ABe_5 structure, characterized by a periodic fcc uranium lattice with two inequivalent copper sites. The parent compound UCu_5 is a prototype Kondo-lattice antiferromagnet. Upon substitution of Pd for Cu ($UCu_{5-x}Pd_x$), the antiferromagnetic order is quickly suppressed, vanishing at a Pd concentration x between 0.5 and 1, and a spin-glass regime is observed for $x>2$ (Maple *et al.*, 1994, 1995). The intermediate values $x=1$ and 1.5 display no long-range order of any kind at the lowest temperatures, although thermal and transport measurements at temperatures below ~20 K reveal that both have remarkable temperature and magnetic-field scaling (Andraka and Stewart, 1993). For both UCu_4Pd and $UCu_{3.5}Pd_{1.5}$, the resistivity [shown in Fig. 20, Ott (1996)], the specific heat and the static magnetic susceptibility display typical non-Fermi-liquid behaviors [i.e., Eqs. (35)–(37)]. The leveling off of $\rho(T)$ below approximately 1 K is clearly recognized here.

Moreover, neutron time of flight measurements (Aronson *et al.*, 1995, 1996) performed for energy transfer between 0.5 and 400 MeV at temperatures from 10 to 300 K reveal unusual frequency/temperature scaling properties of the magnetic excitation. The scaling of the magnetic excitations can be expressed in terms of the dynamical susceptibility $\chi''(T)$, which for frequencies $\omega<\omega^*\sim 25$ meV follows the universal scaling relation

$$\chi''(\omega,T)T^{1/3}=(T/\omega)^{1/3}Z(\omega/T) \tag{38}$$

with $Z\sim\tanh(\omega/1.2T)$. Even though this choice may not be unique (Maple *et al.*, 1995; Aronson *et al.*, 1995, 1996), it represents a qualitatively new type of magnetic response for an *f*-electron-based system. Moreover, by adding those low-energy excitations (at $\omega<\omega^*$) with the high-energy localized moment excitations (at $\omega>\omega^*$) one can calculate the static susceptibility $\chi(T)$ through the Kramers-Kronig relation linking $\chi''(T)$ and $\chi(T)$. A good agreement has been found with the measured static susceptibility (Aronson *et al.*, 1996), indicating that relatively little of the magnetic response falls outside the experimental energy window ($1<\omega<200$ meV).

Finally, although both systems display virtually identical temperature dependences in ρ, C, and χ, the nature of the magnetic excitations for $UCu_{3.5}Pd_{1.5}$ and UCu_4Pd are qualitatively different from those of $U_{0.2}Y_{0.8}Pd_3$ (Mook *et al.*, 1993; McEwen *et al.*, 1995). The uranium ions in the latter compound have a nonmagnetic ground state, and a magnetic response consisting of two inelastic crystal-field levels at ~5 and 16 meV. In contrast, a broad, quasielastic magnetic response was found to be virtually identical for UCu_4Pd and $UCu_{3.5}Pd_{1.5}$, indicative of a magnetic ground state for the uranium ions, with no evidence for distinct crystal-field excitations.

C. Optical properties of a few prototype non-Fermi-liquid Kondo alloys

Generally, optical investigations, extending over a broad frequency range and at various temperatures, are an efficient experimental tool for the simultaneous study of the energy and temperature dependence of intrinsic parameters characterizing these systems. Of particular relevance, in connection with the anomalous dc electrical resistivity, is the identification of the energy and temperature dependence of the transport relaxation time τ. When scattering due to phonon modes or impurities is negligible, the scattering rate $\Gamma=1/\tau$ for a conventional Fermi-liquid system has the energy (frequency ω) and temperature dependence of Eq. (26). Consequently, the motivation for the optical work resides in the fact that non-Fermi-liquid behavior is expected to considerably affect both the temperature and frequency dependence of τ, thus leading to distinct deviations from the behavior expressed in Eq. (26).

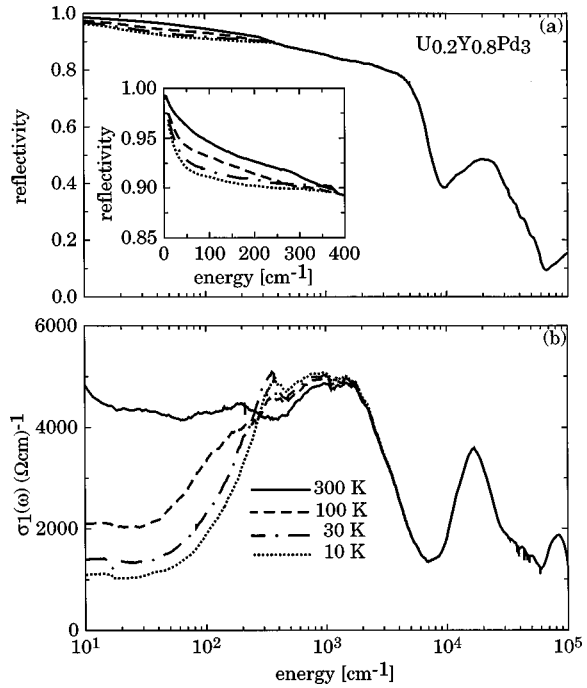

FIG. 21. Optical properties of $U_{0.2}Y_{0.8}Pd_3$. (a) Reflectivity spectra of $U_{0.2}Y_{0.8}Pd_3$ at 300, 100, 30, and 10 K and (b) corresponding optical conductivity (note the logarithmic scale). The inset is an enlargement of the reflectivity in the far-infrared frequency range (linear scale) (Degiorgi, Ott, and Hulliger, 1995).

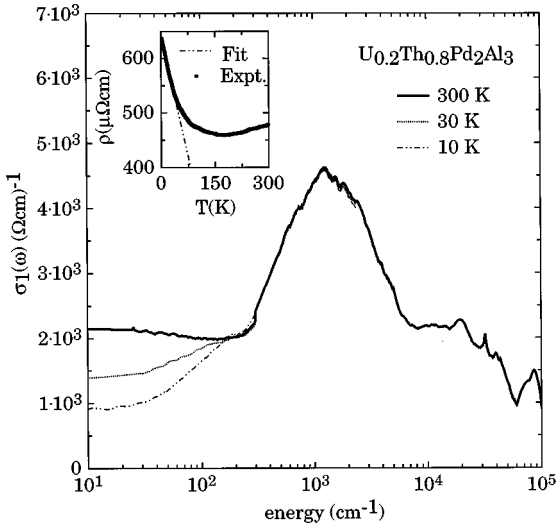

FIG. 22. Optical conductivity at 300, 30, and 10 K for $U_{0.2}Th_{0.8}Pd_2Al_3$ (note the logarithmic energy scale). The inset displays the temperature dependence of the resistivity $\rho(T)$ with the fit using Eq. (43) at $\omega=0$, with $m=1$, and $T_0=217$ K (Degiorgi, Wachter, Maple, *et al.*, 1996).

1. $U_{0.2}Y_{0.8}Pd_3$

Figure 21(a) presents the complete reflectivity spectra at several temperatures, from which the optical conductivities $\sigma_1(\omega)$, displayed in Fig. 21(b), were calculated (Degiorgi, Ott, and Hulliger, 1995). One can note immediately that in the far-infrared spectral range the reflectivity decreases with decreasing temperature, while it is temperature independent at high frequencies. Consequently, the optical conductivity $\sigma_1(\omega)$ in far infrared and its dc (i.e., $\omega\rightarrow 0$) limit drop as well.

A rather broad maximum in $\sigma_1(\omega)$ at about 1600 cm^{-1}, apparent already at 300 K, overlaps a low-frequency Drude component due to free charge carriers. Below 100 K, an additional broad shoulder appears at about 350 cm^{-1} overlapping the midinfrared absorption mentioned above. A very simple phenomenological description of the optical conductivity may be obtained using the classical dispersion theory and associating several harmonic Lorentz oscillators with the absorption maxima at 1.6×10^3, 1.8×10^4, and 8×10^4 cm^{-1}, overlapping the free charge-carrier contribution, described by the Drude model [Eq. (28)]. At temperatures of 100 K and less, it is necessary to introduce an additional harmonic oscillator in order to account for the far-infrared shoulder at 350 cm^{-1}. This phenomenological analysis permits the evaluation of several parameters, like the unscreened plasma frequency (ω_p), the relaxation scattering rate (Γ) of the free charge carriers, and also the mode strength, or spectral weight, associated with the broad absorptions from the far infrared up to the ultraviolet frequency range (Degiorgi, Ott, and Hulliger, 1995).

One can ascribe the high-frequency excitations to electroniclike interband transitions. For a more precise identification of these absorptions, however, one has to await a complete band-structure calculation and the corresponding joint density of states. Somewhat more puzzling is the appearance of the absorption at 350 cm^{-1} at low temperatures. It remains to be seen whether it may be related to excitations between levels of $5f$ electrons split by the crystalline electric field or simply to some phonon modes. Recent neutron-scattering measurements (Mook *et al.*, 1993) indicate, however, crystal-field splittings of distinctly lower energies.

As we shall demonstrate below, the appearance of a far-infrared absorption at energies between 100 and 300 cm^{-1} at low temperatures seems to be a characteristic of all these materials. It should be noted that this additional absorption cannot be reconciled with possible crystal-field excitations since it is not suppressed when such excitations are absent. Therefore it turns out to be an intrinsic feature associated with the onset of the non-Fermi-liquid state. In the discussion, this low-frequency spectral range will be approached from a more comprehensive point of view with the application of the generalized Drude model [Eq. (32)] (Thomas *et al.*, 1988), where the interplay of low-frequency metallic behavior and finite frequency excitation is globally taken into account.

2. $U_{1-x}Th_xPd_2Al_3$

The optical conductivity $\sigma_1(\omega)$ for the $x=0.8$ compound at several temperatures is displayed in Fig. 22 (Degiorgi, Wachter, Maple, *et al.*, 1996). The measurements for $x=0$ are presented in Degiorgi, Dressel, *et al.* (1994) and Degiorgi *et al.* (1997). For $x=0.1$, similar results as for the undoped materials were obtained, while

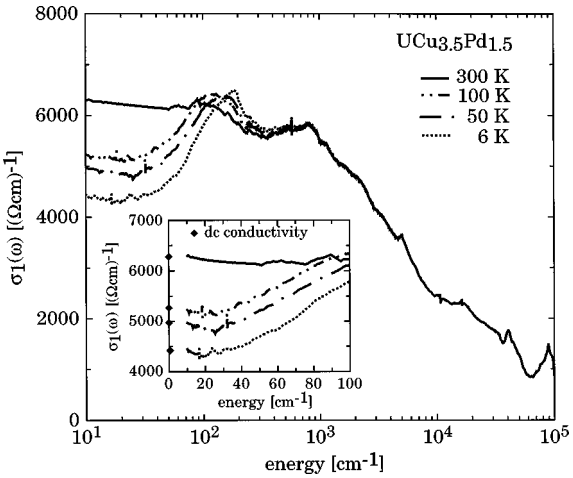

FIG. 23. Optical conductivity of $UCu_{3.5}Pd_{1.5}$ at 300, 100, 50, and 6 K. The inset is an enlargement of the optical conductivity in the far-infrared frequency range (linear scale), showing the good agreement between the $\sigma_1(\omega\rightarrow 0)$ limit and the dc values of the conductivity (Degiorgi and Ott, 1996; Ott, 1996).

the results presented here for the $x=0.8$ compound can be considered as representative of the compounds with $0.4<x<0.9$.

For all investigated compounds there is a fair agreement between the $\omega\rightarrow 0$ limit of the optical conductivity σ_1 at various temperatures and the $\sigma_{dc}=\sigma_1(\omega\rightarrow 0)$ values, obtained from the dc transport investigation (for example, see the inset of Fig. 22 with $\rho(T)$ of the $x=0.8$ compound). The results of Fig. 22 bear a striking similarity to those obtained for $U_{0.2}Y_{0.8}Pd_3$ (see Fig. 21). In fact, there is once again a suppression of Drude weight in far infrared with decreasing temperature. Moreover, such a behavior is somehow upside down with respect to the far-infrared enhancement in $\sigma_1(\omega)$ at low temperatures encountered in the reference undoped UPd_2Al_3 material (Degiorgi, Dressel, *et al.*, 1994; Degiorgi, Ott, Dressel, *et al.*, 1995).

At about 1600 cm^{-1} we observe a rather broad maximum in $\sigma_1(\omega)$, apparent at all temperatures, which overlaps a low-frequency metallic component due to free charge carriers. Below 100 K, there is an additional broad shoulder at about 100 cm^{-1}, overlapped by the low-frequency tail of the midinfrared absorption mentioned above. The high-frequency excitations are associated to electroniclike interband transitions.

3. $UCu_{5-x}Pd_x$

Figure 23 (Degiorgi and Ott, 1996) shows $\sigma_1(\omega)$ at several temperatures for $x=1.5$. Similar results were also obtained for $x=1$. The inset is an expanded plot of $\sigma_1(\omega)$ in the far infrared. We note immediately that in this spectral range $\sigma_1(\omega)$ decreases with decreasing temperature, while it is temperature independent at high frequencies. This is obviously in accordance with the increasing resistivity with decreasing temperature. There is also a fair agreement between the $\omega\rightarrow 0$ limit of the optical conductivity σ_1 at various temperatures and the σ_{dc} values, obtained from the dc transport investigation (see inset of Fig. 23) (Andraka and Stewart, 1993; Ott, 1996). At 300 K $\sigma_1(\omega)$ is basically Drude-like up to the midinfrared spectral range. Overlapping this typical metallic contribution is a broad maximum due to an absorption at approximately 1000 cm^{-1}. Below 100 K, apart from the suppression of $\sigma_1(\omega)$ in the far infrared, there is a displacement of spectral weight leading to a new feature at about 100–200 cm^{-1}. The high-frequency and temperature-independent excitations in the rest of the spectrum are ascribed to electroniclike interband transitions.

Moreover, $\sigma_1(\omega)$ of $UCu_{5-x}Pd_x$ contrasts with the results obtained on the parent compound UCu_5 (Degiorgi, Ott, Dressel, *et al.*, 1994). In UCu_5, $\sigma_1(\omega)$ develops a narrow Drude-like mode in far infrared with decreasing temperature and by crossing the antiferromagnetic phase transition (i.e., $T<T_N$) there is the additional appearance of a new absorption at about 30 cm^{-1}. This latter feature was ascribed to the excitation across a spin-density-wave-like gap, opening at the Fermi surface because of the antiferromagnetic transition.

Summarizing, the peculiar far-infrared temperature dependence of $\sigma_1(\omega)$ (i.e., the suppression of the Drude weight with decreasing temperature) is common to various Kondo alloys with supposed non-Fermi-liquid behavior.

D. Theoretical routes to non-Fermi-liquid behavior in Kondo alloys

The Fermi-liquid theory of Landau has provided a remarkably robust paradigm for describing the properties of interacting fermion systems. The key notion of this theory is that the low-lying excitations of the interacting system possess a 1:1 map to those of the noninteracting system and hence are called ''quasiparticles.'' The existence of such quasiparticles is the defining property of Landau-Fermi-liquid behavior. In the metallic context, one may think of the quasiparticles as propagating electronlike wave packets with renormalized magnetic moment and effective mass reflecting the ''molecular field'' of the surrounding medium. A sharp Fermi surface remains in the electron occupancy function n_k, which measures the number of electrons with a given momentum. For energies ω and temperatures T asymptotically close to the Fermi surface the excitations have a decay rate going as $a(\hbar\omega)^2+b(k_BT)^2$, which is much smaller than the quasiparticle energy, and generally translates at low temperatures into a T^2 contribution to the electrical resistivity $\rho(T)$ [Eq. (1)] and a ω^2 contribution to the scattering relaxation rate $\Gamma(\omega)$ [Eq. (26)]. This theory has proven useful in describing phase transitions within the Fermi liquid, such as superconductivity, which is viewed as a pairing of Landau quasiparticles in conventional metals such as aluminium (Ashcroft and Mermin, 1976).

The Fermi-liquid paradigm appears now to be breaking down empirically in numerous materials, notably the quasi-two-dimensional cuprate superconductors

(Tanner and Timusk, 1992) and a number of fully three-dimensional heavy-electron alloys and compounds (Maple *et al.*, 1994, 1995). In these systems such anomalies as a conductivity with linear dependence on ω (see below) and T, and logarithmically divergent linear specific-heat coefficients are often observed. If the quasiparticle paradigm indeed breaks down, this may require completely new concepts to understand these materials. While the Luttinger-liquid theory provides an elegant way to achieve non-Fermi-liquid behavior in one dimension (with, for example, no jump discontinuity in n_k and separation or unbinding of spin and charge quantum numbers), this results from the special point character of the Fermi surface (Schultz, 1991). Whether the essential spin-charge separation may ''bootstrap'' into higher dimensions remains unclear. Among the remaining theories explaining experiments are those based upon proximity to a zero-temperature quantum critical point (Hertz, 1976; Continentino, 1993; Millis, 1993; Tsvelik and Reizer, 1993; Sachdev *et al.*, 1995; Sengupta and Georges, 1995; Zülicke and Millis, 1995; Sachdev, 1997a), those based upon disorder induced distribution of Kondo scales in local-moment systems (Dobrosavljevic *et al.*, 1992; Bernal *et al.*, 1995; Miranda *et al.*, 1997a, 1997b), and those which hope to explain the physics from impurity to lattice-crossover effects in the multichannel Kondo model (Cox, 1987, 1993; Sacramento and Schlottmann, 1989; Schlottmann and Sacramento, 1993; Cox and Jarrell, 1996).

1. *n*-channel Kondo model

The n-channel Kondo model for an impurity spin S and an arbitrary number of orbital conduction-electron channels is given by (Schlottmann and Sacramento, 1993)

$$H_K=\sum_{km\sigma}\varepsilon_k a^*_{km\sigma}a_{km\sigma}+J\sum_{kk'm\sigma\sigma'}Sa^*_{km\sigma}s_{\sigma\sigma'}a_{k'm\sigma'}, \tag{39}$$

where S are the spin operators describing the magnetic impurity, J is the antiferromagnetic coupling constant, s are the Pauli matrices and m labels the orbital channels. In general, the number of channels n and the impurity spin S can be considered as independent model parameters. Three qualitatively different situations have to be distinguished:

(i) If $n=2S$ the number of conduction-electron channels is exactly sufficient to compensate the impurity spin into a singlet, giving rise to Fermi-liquid behavior.

(ii) If $n<2S$ the impurity spin is only partially compensated (undercompensated spin), since there are not enough conduction-electron channels to yield a singlet ground state. This leaves an effective degeneracy (in zero field) at low temperatures of $(2S+1-n)$.

(iii) If $n>2S$ the number of conduction-electron channels is larger than required to compensate the impurity spin. The impurity is said to be overcompensated and critical behavior is obtained as the temperature and the external field tend to zero.

The multichannel Kondo (impurity) model, first considered by Nozieres and Blandin (1980) in an attempt to describe the physics of realistic dilute alloy systems in which the impurity and/or the conduction band can have various finite degeneracies, has been solved exactly using the Bethe Ansatz and, very recently, by conformal field theory (Schlottmann and Sacramento, 1993). A special but widely used application of the n-channel Kondo model is the two-channel model, which consists of two identical species of noninteracting electrons antiferromagnetically coupled to a spin-$\frac{1}{2}$ impurity. Non-Fermi-liquid behavior results because of the inability to screen out the impurity spin: it is energetically favorable for both conduction-electron bands to couple to the impurity which gives a spin-$\frac{1}{2}$ complex on all length scales. As a result, the ground state is degenerate and the model produces a local marginal Fermi-liquid excitation spectrum, with logarithmically divergent $\Delta C/T$ and $\chi(T)$, a resistivity which exhibits a $\sqrt{T}$ dependence as $T\rightarrow 0$, and a residual ground-state entropy of $(R/2)\ln 2$. These latter theoretical results are partially in agreement with experiments (see Secs. III.A and III.B, and Table III). However, the prediction for $\rho(T)$ is in disagreement with the experimental results, which indicate a linear behavior as $T\rightarrow 0$. In contrast, the single-channel Kondo model has a singlet ground state with the impurity spin screened out, and a Fermi-liquid excitation spectrum corresponding to the removal of one conduction state from the system.

So far, the magnetic two-channel Kondo effect has been considered. However, in the case of vanishing magnetic dipole matrix elements but nonvanishing electric quadrupole matrix elements, one considers the local quadrupolar degrees of freedom described by an effective isotropic spin $\frac{1}{2}$ (pseudospin). The orbital motion of conduction states couples ''antiferromagnetically'' to this local quadrupolar ''spin'' to quenched it. The orbital quadrupolar moments are invariant under time reversal, so that two channels of conduction quadrupolar pseudospin couple to the f site (Cox, 1987). In other words, one can then map the problem into the so-called two-channel quadrupolar Kondo effect, which leads to the same results as for the magnetic two-channel Kondo model. Obviously, for such a two-channel quadrupolar Kondo effect, it is the electric quadrupolar susceptibility (which can be extracted from ultrasound measurement) that diverges logarithmically. The quadrupolar two-channel Kondo model was first introduced on symmetry ground in order to understand the physics of the heavy-electron superconductor UBe_{13} (see conclusion) (Cox, 1987; Cox and Zawadowski, 1998).

Jarrell and coworkers (1996, 1997) extended the two-channel Kondo approach to the lattice limit. One might anticipate that, ignoring the renormalization of the environment around each spin, the array of single-channel model singlets would renormalize the potential scattering but the array of many-body doublets in the two-channel case would give rise, in contrast, to a dynamical spin disorder scattering. In the absence of any cooperative transition, inducing coherence to the spin array, a

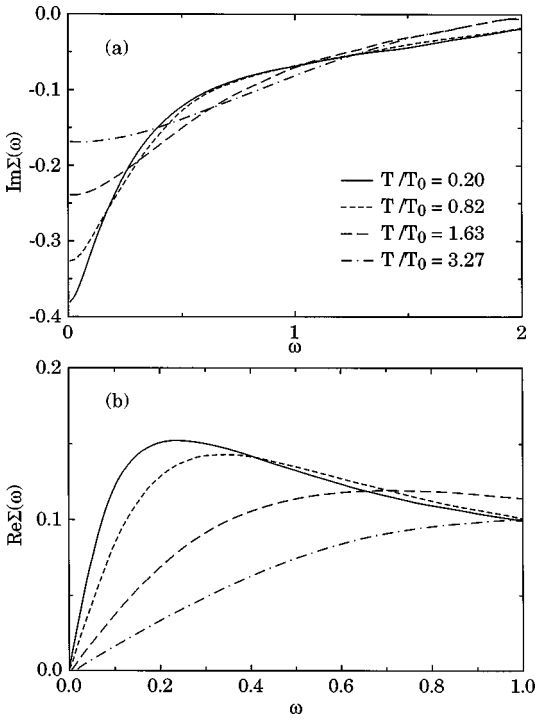

FIG. 24. Two-channel Kondo lattice self-energy: (a) imaginary and (b) real part. As the temperature is lowered an anomalous behavior, different from the Fermi-liquid expectation, develops (Jarrell *et al.*, 1996, 1997).

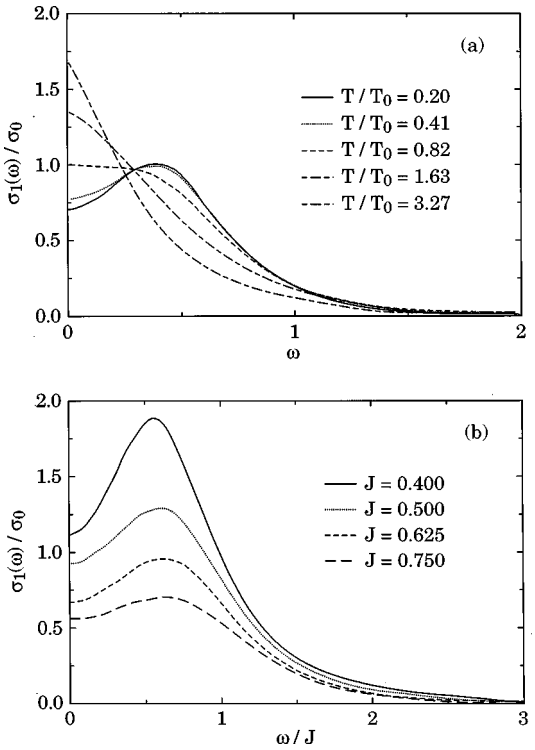

FIG. 25. Optical conductivity of the two-channel Kondo lattice. (a) Optical conductivity when $J=0.625$. As the temperature is lowered $T<T_0$, the optical conductivity develops a pseudogap at low frequencies with a vanishing Drude weight. (b) Optical conductivity vs ω/J when $T=0.0156$ for various values of J. $\sigma_1(\omega)$ displays a finite-frequency peak at roughly $\omega\sim 0.6J$ (Jarrell *et al.*, 1996, 1997).

non-Fermi-liquid behavior can be expected. The Hamiltonian for the two-channel Kondo lattice is (Jarrell *et al.*, 1996)

$$H=J\sum_{i\alpha}\mathbf{S}_i\mathbf{s}_{i\alpha}-\frac{t^*}{2\sqrt{d}}\sum_{\langle ij\rangle\alpha\sigma}(c^*_{i\alpha\sigma}c_{j\alpha\sigma}+\text{H.c.})$$

$$-\mu\sum_{i\alpha\sigma}c^*_{i\alpha\sigma}c_{i\alpha\sigma}, \tag{40}$$

where $c^*_{i\alpha\sigma}$ ($c_{i\alpha\sigma}$) creates (destroys) an electron on site i in channel $\alpha=1,2$ of spin s, $\mathbf{S}_i$ is the Kondo spin on site i, $\mathbf{s}_{i\alpha}$ are the conduction-electron spin operators for site i and channel α, and t^* is the hopping integral. Jarrell and coworkers (1996 and 1997) also presented the first rigorous solution for the dynamics of the two-channel Kondo-lattice model in infinite spatial dimension ($d=\infty$). They found that below

$$T_0\sim 0.85J\exp(-1.01t^*/J)$$

(defining a so-called Kondo scale) the single-particle properties of the model have a non-Fermi-liquid behavior. For example, the imaginary part of the one-electron self-energy [Fig. 24(a)] appears to approach [away from the origin of the complex plane where the function $\Sigma(\omega)$ is not analytic]

$$\text{Im}\,\Sigma(\omega)\sim -c+|\omega|, \tag{41}$$

instead of the Fermi-liquid form represented by Eq. (27). Similarly, the real part of $\Sigma(\omega)$ [Fig. 24(b)] is anomalous since its initial slope is positive indicating a quasiparticle renormalization factor that is greater than one. Moreover, at low temperatures the numerical calculation of the resistivity can be fitted by Eq. (37) with $m\sim 1.03$. Such an almost linear T dependence of $\rho(T)$ suggests a rather good agreement with the experimental findings (see Figs. 17, 19, and 20).

The computed optical conductivity (Fig. 25) displays a progressive suppression of the Drude weight at low temperatures together with a finite frequency peak at $\omega\sim 0.6J$. Both these features again support an interpretation in terms of a new kind of non-Fermi-liquid metallic state (Jarrell *et al.*, 1996, 1997). The peculiar frequency dependence of $\Sigma(\omega)$ and of $\sigma_1(\omega)$ will be of relevance later by the discussion of the experimental optical properties in terms of $\Gamma(\omega)$ and $m^*(\omega)$. Generally, and as partially anticipated before, there are strong reasons to argue for the applicability of the two-channel Kondo model to the alloys $U_xY_{1-x}Pd_3$ and $U_xTh_{1-x}Ru_2Si_2$, and, in its lattice version, to the concentrated heavy-electron system UBe_{13}.

2. Disordered driven non-Fermi-liquid behavior

Another possible explanation for non-Fermi-liquid behavior in Kondo alloys is the presence of disorder for sufficiently dirty metals (Dobrosavljevic *et al.*, 1992; Bernal *et al.*, 1995; Miranda *et al.*, 1997a, 1997b). In this model, the presence of random disorder results in a distribution of Kondo temperature values which could be

singular enough to produce diverging C/T and χ at $T=0$, again a strongly non-Fermi-liquid behavior.

In a recent study (Bernal *et al.*, 1995) the strong inhomogeneous broadening of the copper nuclear-magnetic-resonance line of $UCu_{5-x}Pd_x$ ($x=1$ and 1.5) has been used as an indication of the essential role played by disorder in at least one of these compounds. The presence of strong spatial fluctuations in the characteristic Kondo temperature T_K of the local moments was assumed. By using a model distribution function $P(T_K)$ that was fitted to experiments and well-known single-impurity results, Bernal *et al.* (1995) were then able to quantitatively describe the low-temperature thermodynamic properties (specific heat and magnetic susceptibility) which were independently measured. The proposed picture implicitly assumes independent local moments, which is well known to be sufficient for understanding the thermodynamics of most heavy-electron compounds. Of course, in the context of transport in concentrated Kondo systems, such an assumption appears to be unjustified, since it cannot be reconciled with the well-established coherence effects at low temperatures (Miranda *et al.*, 1997a, 1997b).

Miranda and coworkers (1997a, 1997b) addressed the problem with $d=\infty$ approximation to see whether disorder effects can explain not only the thermodynamics, but also the transport anomalies in these systems. Their theoretical approach is based on the central idea that moderate bare disorder in a lattice model of localized moments is magnified due to the strong local correlations between the moments and the conduction electrons. In particular a broad distribution of energy scales is generated (i.e., a distribution of Kondo-temperature T_K). As a result, the low-temperature properties can be viewed as resulting from a dilute gas of localized elementary excitations—those Kondo spins that become incoherent. Miranda *et al.* (1997a, 1997b) were able to prove that in sufficiently disordered Kondo alloys, such that $P(T_K)\sim$const at low temperatures, the resistivity decreases linearly with temperature. In other words, the effect of disorder [e.g., on $\rho(T)$] can be understood as follows. Suppose one is measuring some property at temperature T. As seen in Fig. 26 (Miranda *et al.*, 1997a, 1997b), there are always a few f sites with $T_K \ll T$. While the remainder of sites will have undergone quenching and effectively fallen out of the problem, these low-T_K spins remain unquenched and dominate the low-temperature behavior. As T is lowered, their number decreases and it is their gradual screening which is ultimately responsible for the non-Fermi-liquid behavior. Therefore it is the presence of low-T_K spins, unquenched even at low temperatures, which give rise to anomalous scattering. Moreover, an immediate consequence of the physical origin of the anomalous scattering in this disorder model is a negative magnetoresistance at low temperatures. Much like the temperature, a magnetic field acts to destroy low-T_K Kondo singlets and thus to suppress their effectiveness as source of disorder (Miranda *et al.*, 1996). It must be stressed that $P(T=0)\neq 0$ is essential, otherwise with $P(T=0)=0$ a Fermi-liquid behavior is recovered, since all spins freeze out at some finite temperature. Essentially, disorder fluctuations lead to the absence of a characteristic energy scale, which is associated with a conventional Fermi liquid.

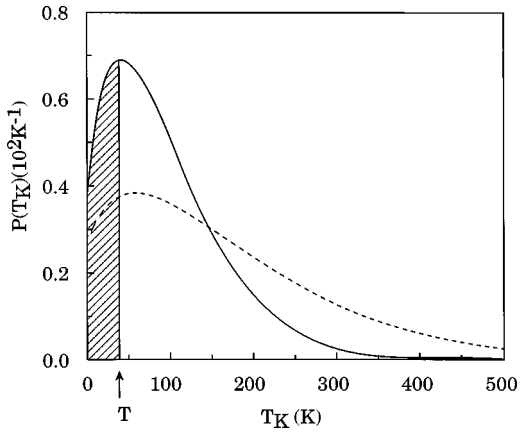

FIG. 26. Kondo temperature distributions $P(T_K)$ determined experimentally for $UCu_{5-x}Pd_x$ (Miranda *et al.*, 1997a, 1997b).

Recently, Chattopadhyay and Jarrell (1997) calculated the dynamical quantities such as the optical conductivity and the self-energy within the phenomenological framework introduced by Dobrosavljevic *et al.* (1992), again for $d=\infty$. They chose three different distributions $P(T_K)$, corresponding to very strong, very weak and a phenomenological disorder. The latter approaches (weak and phenomenological) were motivated by Miranda *et al.*'s argument (1997a, 1997b), that the $P(T_K)$ should be relatively constant at low temperatures. Also consistent with Miranda *et al.* (1997a, 1997b) they considered the distribution of Kondo scales as arising from a distribution of couplings between the conduction and the f electrons.

The nature of the disorder gives rise to very different physics in each case. For a very weakly disordered system, $\mathrm{Im}\,\Sigma(\omega)$ goes as the square of the frequency [i.e., as in Eq. (27) with ω^2 for $\omega\to 0$], suggesting the formation of a local Fermi liquid with a resistivity $\rho(T)\sim T^2$ [Eq. (1)]. For the case of very strong disorder, $P(T_K)$ is divergent at low T_K and even though on the metallic side, having a large number of spins with a very low Kondo temperature, a non-Fermi-liquid ground state develops. For this scenario,

$$\mathrm{Im}\,\Sigma(\omega)\sim -c+\omega^{1/4} \text{ at low } \omega. \tag{42}$$

If the distribution of Kondo scales is intermediate between these two cases, Eq. (41) for $\mathrm{Im}\,\Sigma(\omega)$ is recovered. Moreover, averaging the energy ω over a region of width k_BT near the Fermi surface results in a linear in T resistivity. The calculated optical conductivity of the phenomenologically disordered system is shown in Fig. 27 (Chattopadhyay and Jarrell, 1997). The progressive suppression of the Drude peak with decreasing temperature and a low-frequency pseudogap in the real part of the optical conductivity, a negative low-temperature optical mass, and a linear in frequency optical dynamical scattering rate at low temperature are found. However,

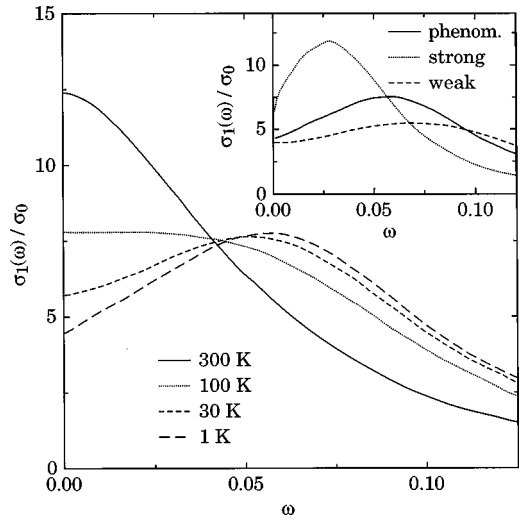

FIG. 27. Optical conductivity for the phenomenological distribution of Kondo scales at various temperatures. At low temperatures a finite number of unquenched spins prevent the formation of a Fermi liquid. The interesting feature is the development of a Drude peak as one goes from temperatures much below the bulk Kondo value ($T_K \sim 100$ K) to those much above it. The inset shows the conductivity for three different $P(T_K)$ when $T=0$. The one corresponding to weak disorder has a ω^2 behavior as $\omega \to 0$, suggesting the formation of a local Fermi liquid (Chattopadhyay and Jarrell, 1997).

the results for the disorder model depend quite sensitively on the details of $P(T_K)$ for low T_K, which was adjusted in such a way to fit the experiments. It was already pointed out that the disorder driven model has some relevance to the non-Fermi-liquid physics of $UCu_{5-x}Pd_x$ at low temperatures (i.e., $T<10$ K). Nevertheless, in the intermediate temperature regime, Aronson *et al.* (1996) emphasized that a quite different power-law behavior than Eqs. (36) and (37) for $\chi(T)$ and $\rho(T)$, respectively, holds, thus favoring an unconventional single-impurity scaling.

It is important to stress once again that Kondo disorder is not the sole possible explanation of non-Fermi-liquid behavior in these systems. In fact, the two-channel Kondo-lattice model (Jarrell *et al.*, 1996, 1997) displays remarkably similar optical properties (see above). On the other hand, the linear behavior of $\rho(T)$ in the two-channel Kondo model is merely an empirical observation based on numerical results. Moreover, it remains to be seen if an appropriate two-channel Kondo model can accurately describe the transport and optical properties of dilute systems.

3. Scaling behavior due to fluctuations in the vicinity of a critical point

Andraka and Tsvelik (1991) have raised several objections to the multichannel Kondo interpretation of the non-Fermi-liquid behavior in $U_xY_{1-x}Pd_3$ and other *f*-electron systems. One of these objections is based on specific-heat measurements on $U_{0.2}Y_{0.8}Pd_3$ where they find that the specific heat scales as $C(H,T)/T - C(0,T)/T = -f(H/T^\beta)$ with $\beta = 1.3 \pm 0.1$. They argue that a scaling dimension β greater than one precludes a single-site interpretation of this phenomenon. Moreover, it has been noted that scaling of the magnetic field for a two-channel spin-$\frac{1}{2}$ Kondo effect has predicted scaling dimensions of $\frac{1}{2}$ for the magnetic case and $\frac{1}{4}$ for the nonmagnetic (quadrupolar) case well outside the experimental uncertainty of β. A phenomenological theory for the non-Fermi-liquid behavior of *f*-electron systems such as $U_{0.2}Y_{0.8}Pd_3$ and $UCu_{3.5}Pd_{1.5}$ has been proposed by Tsvelik and Reizer (1993). According to this theory, the alloys have a critical point at $T=0$ K so that their low-temperature thermodynamics is determined by collective modes corresponding to fluctuations in the order parameter in the vicinity of a critical point, rather than single-particle fermion excitations, as in a Fermi liquid. This scenario would also seem to be applicable to the $CeCu_{5.9}Au_{0.1}$ system in addition to those mentioned before. Nonetheless, we caution that the scaling exponents deduced from experiment so far lack internal consistency with the context of this particular theory.

The approach by Tsvelik and Reizer (1993) must be seen in a much broader context of models, where non-Fermi-liquid behavior is due to the proximity to a zero-temperature critical point. In fact, besides critical point occurring in models of isolated impurity (Cox, 1987), another class of proposed critical points would separate a $T=0$ magnetically ordered phase from a phase with no long-range order (Hertz, 1976; Continentino, 1993; Millis, 1993; Tsvelik and Reizer, 1993; Sachdev *et al.*, 1995; Sengupta and Georges, 1995; Zülicke and Millis, 1995; Sachdev, 1997a). For these latter models, there is not to date any calculation of the dynamics of the charge excitation spectrum. Therefore in the following, we shall only sketch a few essential aspects, referring the reader to the literature for a more ample discussion. Inspired by or based on the pioneering analysis of quantum critical phenomena by Hertz (1976), Millis (1993) and Zülicke and Millis (1995) provide quantitative expressions for the universal contributions to the specific heat of a three-dimensional metal near $T=0$ magnetic-nonmagnetic phase transition. In two companion papers, Sachdev *et al.* (1995) and Sengupta and Georges (1995) investigated the Kondo metal for the case of a transition into a spin-glass phase. Within a mean-field approach, it was found that in the quantum critical regime nonanalytic corrections to the Fermi-liquid behavior for the specific heat and uniform static susceptibility develops, while the resistivity ($\delta\rho \sim T^{3/2}$ instead of $\rho(T) \sim T^2$ for Fermi liquid) and nuclear-magnetic-resonance relaxation rate ($1/TT_1 \sim 1/T^{3/4}$, instead of $1/TT_1 \sim$ const for Fermi-liquid Korringa behavior) have a non-Fermi-liquid dependence on temperature (Sachdev *et al.*, 1995; Sachdev, 1997a). The reported experimental behavior [mainly following the trend envisaged by Eqs. (35)–(37)] is not in good agreement with these mean-field results. This raises theoretical questions associated with the fluctuations beyond mean field. Moreover, the non-Fermi-liquid behavior in systems such as $U_xY_{1-x}Pd_3$ and $U_{1-x}Th_xPd_2Al_3$, which definitely do exhibit Kondo-like

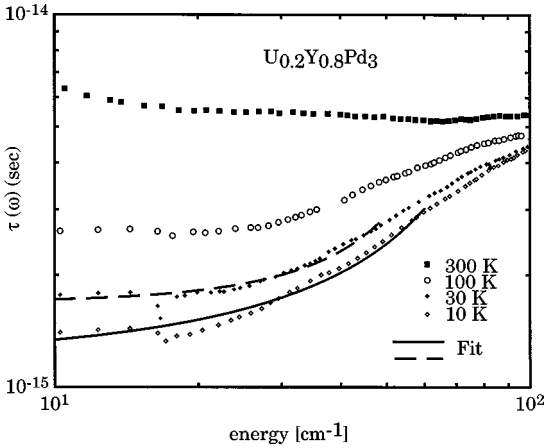

FIG. 28. Frequency dependence of the scattering relaxation time at various temperatures for $U_{0.2}Y_{0.8}Pd_3$ with the corresponding fits [Eq. (43)] at 10 and 30 K, using the parameters given in Table IV (Degiorgi, Ott, and Hulliger, 1995).

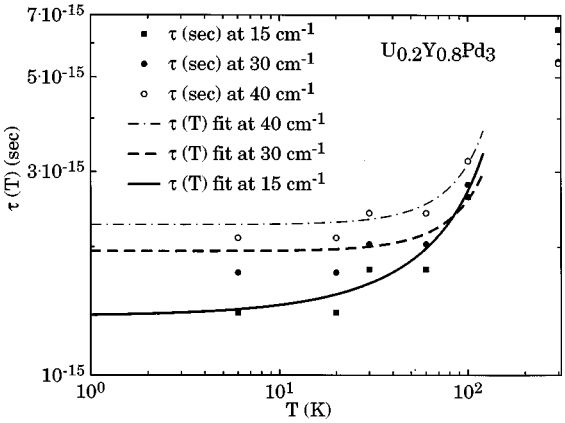

FIG. 29. Temperature dependence of the scattering relaxation time of $U_{0.2}Y_{0.8}Pd_3$ read at different frequencies (Fig. 28) and with the corresponding fits using Eq. (43), with the parameters given in Table IV (Degiorgi, Ott, and Hulliger, 1995).

features in $\rho(T)$ and $\chi(T)$ at high temperatures $T < T_K$, persists into the dilute-U concentration limit, suggesting that a single-site mechanism as a multichannel Kondo effect might be operative (Cox, 1987).

Finally, it should be stressed that Kondo-disorder and spin-glass quantum critical-point models are not mutually exclusive. Sachdev (1997b) pointed out that these mechanisms are really better viewed as different limiting regimes of the same underlying physics and that no material is strictly in one or the other regime. In other words, the Kondo disorder model is in many ways a precursor effect of the transition into a metallic spin glass. This is more or less the approach taken in the recent work by Castro-Neto *et al.* (1998), who study the interplay among disorder, the RKKY, and Kondo interactions, arguing that non-Fermi-liquid behavior is due to the existence of a Griffiths phase close to a quantum critical point.

E. Optical evidence of non-Fermi-liquid behavior

The frequency dependence of the scattering rate as well as of the effective mass can be in principle determined by using the generalized Drude model of Eq. (32). Considering such an approach as a general transformation, one can invert the complex optical conductivity obtained from the Kramers-Kronig transformation. Figures 28 and 29 (Degiorgi, Ott, and Hulliger, 1995) present the frequency dependence of the scattering time τ at various temperatures and the corresponding temperature dependence of τ at some representative frequencies for $U_{0.2}Y_{0.8}Pd_3$, respectively. For $U_{1-x}Th_xPd_2Al_3$, $\tau(\omega)$ of the $x=0.8$ compound for several temperatures is displayed in Fig. 30(a), while Fig. 30(b) shows $\Gamma=1/\tau$ at low temperatures for various Th dopings (Degiorgi, Wachter, Maple, *et al.*, 1996). Finally, Fig. 31 (Degiorgi and Ott, 1996) shows $\Gamma=1/\tau$ at various temperatures evaluated from the $UCu_{3.5}Pd_{1.5}$ data.

For all investigated compounds, similar features and behaviors have been found, which can be summarized as follows. At 300 K, $\tau(\omega)$ is almost constant, while at lower temperatures a quite significant frequency dependence develops (Figs. 28–31). We point out that we consider the frequency dependence of $\tau(\omega)$ for $\omega<100\,\mathrm{cm}^{-1}$, i.e., well below the frequency range dominated by the mid-infrared absorptions between 1000 and 2000 cm^{-1}.

Since the temperature variation of the dc resistivity at moderately low temperatures ($1<T<20$ K) is found to vary like $1-(T/T_0)^m$, with m approximately equal to one, one is tempted to generalize this temperature dependence by including a frequency dependence for the scattering relaxation rate of the charge carriers in the form

$$\Gamma=\frac{1}{\tau}=\frac{1}{\tau_0}\left[1-\left(\frac{T}{T_0}\right)^m-\left(\frac{\omega}{\omega_0}\right)^m\right], \tag{43}$$

where ω_0 and T_0 play the role of a cutoff frequency and temperature, respectively, and τ_0 is a constant.

At temperatures below 30 K (see, for example, the data obtained at 6 or 10 K, Figs. 28–31) one finds a good fit to $\Gamma(\omega,T)$ with $m\sim1$, and values of T_0 and $\hbar\omega_0$ summarized in Table IV. With these parameters it is possible to fit the frequency range in $\Gamma(\omega)$ extending from dc up to approximately 80 cm^{-1}. The ω-linear dependence seems to be the unique characteristic of these materials in their non-Fermi-liquid regime and it represents a clear deviation from the Fermi-liquid predictions of Eq. (26). It is, moreover, remarkable that the values of m and T_0 are quite close to those obtained by independently fitting the dc resistivity (see, for example, inset of Fig. 22). However, the cutoff temperature T_0 of Eq. (43) does not always agree with the estimation of the similar quantity from the specific heat (Table III). The similarity of the T and ω dependence (see Fig. 29 at various ω) implies the near equivalence of temperature and frequency or energy, establishing the temperature itself as the only relevant energy scale of the system well below the characteristic energies represented by the quantities T_0 and ω_0. However, what kind of relationship or scaling between ω_0 and T_0 might be established remains an open issue. So far, it seems that the fitted cutoff energy

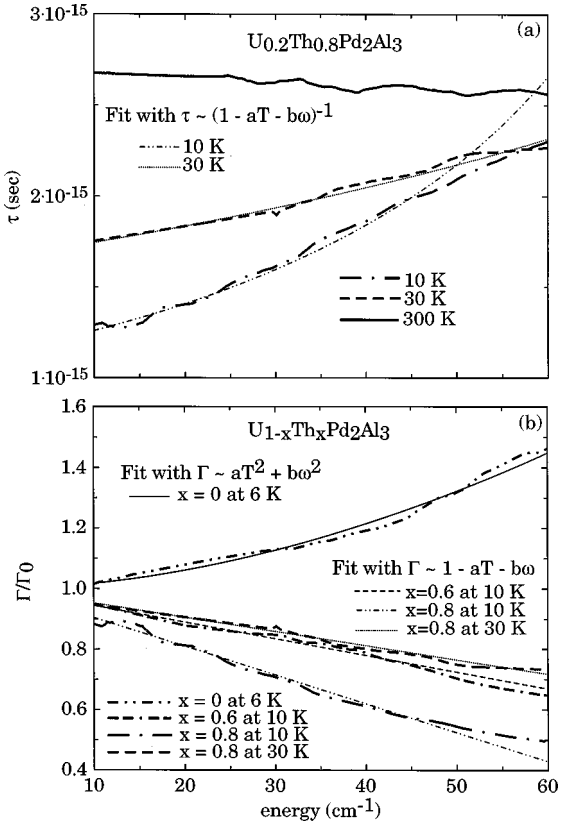

FIG. 30. Scattering rate in $U_{1-x}Th_xPd_2Al_3$. (a) Frequency dependence of the transport relaxation time τ of $U_{1-x}Th_xPd_2Al_3$ for $x=0.8$ at various temperatures with the corresponding fits [Eq. (43)] at 10 and 30 K, using the parameters given in Table IV. (b) Frequency dependence of the scattering relaxation rate $\Gamma=1/\tau$ at low temperatures for different Th dopings together with the fits using Eqs. (26) and (43). The data have been normalized by $\Gamma_0=\Gamma(\omega=0)$, in order to eliminate the dependence from ω_p (Degiorgi, Wachter, Maple, *et al.*, 1996).

and temperature scales are somehow independent. Above 90 cm^{-1}, additional scattering mechanisms start to be important and the frequency dependence of $\Gamma(\omega)$ is more and more influenced by the infrared (at 100 cm^{-1}) and midinfrared (at 1000 cm^{-1}) absorptions. This also means that the limitation of the frequency range, in which the behavior of Eq. (43) is valid, implies that only a very small part of the infrared spectral weight below approximately 2000 cm^{-1} can be assigned to the carriers involved in the non-Fermi-liquid behavior. On the other hand, for $T>30$ K, the exponent m tends to increase, and the tendency of $\Gamma(\omega)$ to saturate to a constant value is clearly manifested in the far-infrared spectral range.

Figure 30(b), which depicts the low-temperature $\Gamma(\omega)$ for the Th-doped UPd_2Al_3 system, well incorporates the main conclusions of this analysis. In the $\Gamma(\omega)/\Gamma_0$ representation, one can, first of all, better appreciate the ω-linear dependence for Th doping with $x>0.4$. For clarity, the presentation is limited to the $x=0.8$ compound at 10 and 30 K, and to the $x=0.6$ one at 10 K. Second, Fig. 30(b) demonstrates the capability of optical investigation to discriminate between different frequency dependences; namely, a crossover upon Th doping from a Fermi-liquid-like to a non-Fermi-liquid behavior. Indeed, it is rather compelling that for low Th doping ($x<0.2$), for which the representative $x=0$ case is shown, a more conventional Fermi-liquid-like behavior [Eq. (26)] is recovered. Nevertheless, we must caution that the Fermi-liquid behavior in the frequency dependence of τ for $x<0.2$ might be only apparent and could be considerably influenced by the analysis of the data in the spectral range below far infrared (Dressel *et al.*, 1998). In fact, it is quite remarkable that a ω^2 dependence extends up to relatively high far-infrared frequencies (of the order of 60 cm^{-1}), even though the corresponding T^2 dependence of the transport scattering relaxation rate applies only for temperatures smaller than 15 K. More detailed optical investigations in the mm and microwave spectral range would be important in order to clarify the apparent crossover to a Fermi-liquid behavior for small Th doping.

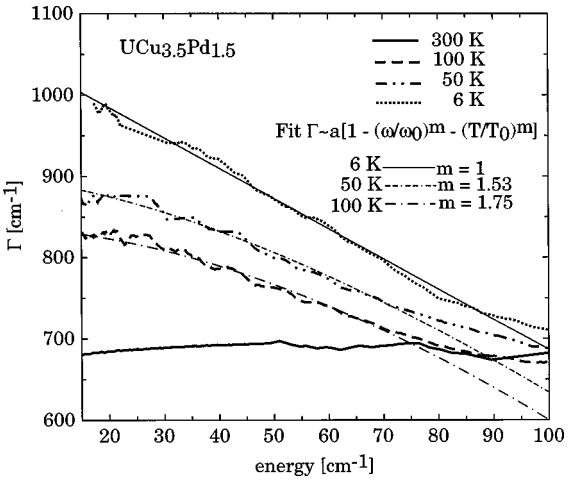

FIG. 31. Frequency dependence of the transport relaxation rate Γ of $UCu_{3.5}Pd_{1.5}$ at various temperatures with the corresponding fits [Eq. (43)] (Degiorgi and Ott, 1996).

Another quantity, which can be extracted from $\sigma(\omega)$, is the enhancement of the effective mass. Figure 32 (Degiorgi and Ott, 1996) displays such a quantity for the case of $UCu_{8.5}Pd_{1.5}$. Similar results were also obtained for the other optically investigated compounds. The remarkable feature is that $m^*(\omega)$ is frequency dependent and negative (see below).

F. Comparison with theory

It is now of relevance to compare the experimental findings with the theoretical models. We limit here our

TABLE IV. Fit parameters of Eq. (43) for a few non-Fermi-liquid Kondo alloys.

	$\hbar\omega_0$ (cm^{-1})	T_0 (K)	m
$U_{0.2}Y_{0.8}Pd_3$	106	260	0.93
UCu_4Pd	948	71	1
$UCu_{3.5}Pd_{1.5}$	308	78	1
$U_{0.4}Th_{0.6}Pd_2Al_3$	173	251	1
$U_{0.2}Th_{0.8}Pd_2Al_3$	110	189	1

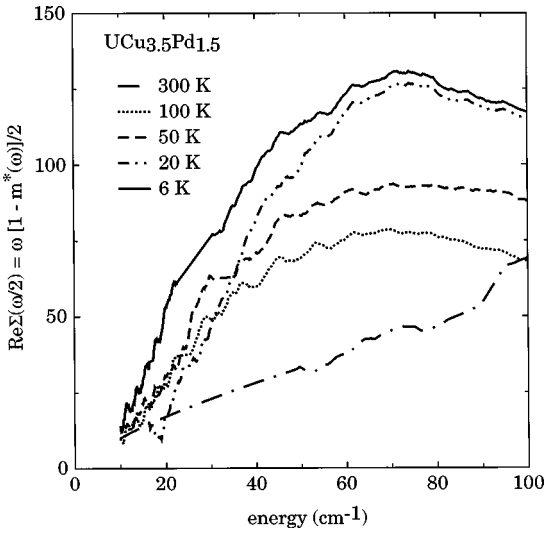

FIG. 32. Enhancement of the effective mass of $UCu_{3.5}Pd_{1.5}$, expressed in terms of $\mathrm{Re}\,\Sigma(\omega)$ [see Eq. (44)] (Degiorgi and Ott, 1996).

attention to the two-channel Kondo approach and the disordered-driven non-Fermi-liquid model, for which to date the optical properties have been calculated (Jarrell *et al.*, 1996, 1997; Chattopadhyay and Jarrell, 1997). Both models suggest a breakdown of the quasiparticle concept, where one-electron excitations are ill defined on approach to the Fermi surface. In terms of $\sigma_1(\omega)$, the predictions (Figs. 25 and 27) of these two theoretical approaches are in very good agreement with the optical data (Figs. 21–23). The relevant feature consists of the suppression of the Drude weight and the apparent pseudogaplike behavior of $\sigma_1(\omega)$ at low temperatures.

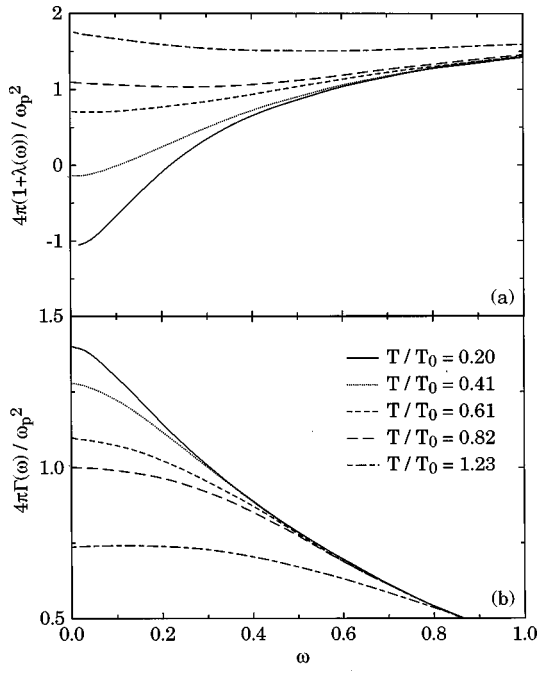

FIG. 33. Mass enhancement $[1+\lambda(\omega)]$ (a) and optical scattering rate $\Gamma(\omega)$ (b) obtained from the optical conductivity shown in Fig. 25 (Jarrell *et al.*, 1996, 1997).

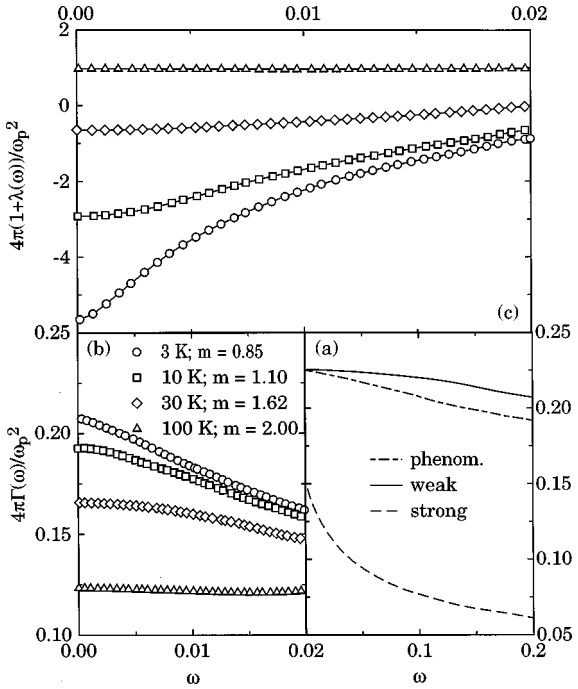

FIG. 34. Theoretical scattering rate and effective mass. (a) Frequency dependence of the scattering relaxation rate Γ at $T=0$ for the three different $P(T_K)$ (see text). (b) $\Gamma(\omega)$ for $P_{\mathrm{ph}}(T_K)$ (ph stands for phenomenological model, see Figs. 26 and 27) at different temperatures, and finally, (c) optical mass enhancement for $P_{\mathrm{ph}}(T_K)$ at different temperatures. At low temperatures $1+\lambda(\omega)<0$ is indicative of a non-Fermi-liquid behavior. The parameter m in (b) corresponds to the exponent in Eq. (43), obtained by fitting the numerical results (Chattopadhyay and Jarrell, 1997).

An alternative and possibly more precise way to reveal the non-Fermi-liquid nature of these Kondo alloys is to evaluate the frequency dependence of m^* and Γ (see Sec. III.E), and to look for possible deviations with respect to the Landau-Fermi-liquid framework (see Sec. II). Such a procedure and a comparison with the theory can be performed, in general, through the self-energy $\Sigma(\omega)$. Even though the quasiparticles do not exist one can try to establish a relationship between the components of the complex self-energy $\Sigma(\omega)$, and $m^*(\omega)$ and $\Gamma(\omega)$ evaluated from the generalized Drude model [Eq. (32)]. For a Fermi liquid (i.e., for quasiparticles) one expects

$$m^*(\omega)=[1+\lambda(\omega)]m_b=1-(2/\omega)\,\mathrm{Re}\,\Sigma(\omega/2) \qquad (44)$$

and

$$\Gamma(\omega)=-2\,\mathrm{Im}\,\Sigma(\omega/2). \qquad (45)$$

From the strict theoretical point of view, there is a difference between $\mathrm{Im}\,\Sigma(\omega)$ and $\Gamma(\omega)$: the first is a true one-particle relaxation rate, the second reflects the two-particle nature of the energy absorption process associated with electrical charge transport. Generally, $\Gamma(\omega)$ and $\mathrm{Im}\,\Sigma(\omega)$ are equivalent [Eq. (45)] (only for a Fermi liquid at very low temperatures and frequencies.

Figures 33 and 34 (Jarrell *et al.*, 1996, 1997; Chattopadhyay and Jarrell, 1997) display $m^*(\omega)$ and $\Gamma(\omega)$ ob-

tained by inverting the calculated $\sigma(\omega)$ for both the two-channel and disordered-driven Kondo models, respectively. One can immediately appreciate the qualitative good agreement between theory and experiments in both cases, and also the good correspondence [through Eqs. (44) and (45)] between $\Gamma(\omega)$ and $m^*(\omega)$, and $\mathrm{Re}\,\Sigma(\omega)$ and $\mathrm{Im}\,\Sigma(\omega)$; see, for example, Figs. 24 and 32. This latter agreement indicates that the optical and quasiparticle scattering rates are consistent, even though strictly speaking quasiparticles do not exist.

As already pointed out, optical results alone cannot distinguish between the different theoretical approaches, a situation which is common to other experimental quantities [$\rho(T)$, $C(T)$, and $\chi(T)$], as well. However, for the two-channel Kondo model m^* will be again positive for large enough J. Thus the negative mass enhancement should be viewed as a sufficient but not necessary condition identifying feature of a non-Fermi liquid. On the other hand, the tuning of disorder (i.e., by changing the alloying) will not affect the two-channel Kondo lattice model unless it is sufficient to change the average J, but affect quite considerably the position of the peak in $\sigma_1(\omega)$ (see inset of Fig. 27) in the disorder-driven non-Fermi-liquid model. This aspect might be used in order to discriminate between the two approaches. A systematic optical work on systems, where the doping is precisely tunable, would be of great importance, and in the perspective of the results arrived at by other methods should lead to a comprehensive and possibly unique understanding of this class of highly correlated materials.

IV. KONDO INSULATORS

In heavy-electron compounds, the high-temperature state is believed to consist of a lattice of uncorrelated $4f$ ions, each independently scattering conduction electrons by the Kondo mechanism. On the other hand at low temperatures, correlations exist, and two types of a coherent state can occur. As we have already discussed, in the vast majority of cases the ground state is metallic with a large variety of possibilities (paramagnetic, antiferromagnetic, or superconducting). In a very limited number of cases the ground state is insulating with a small energy gap. Table V summarizes the members of this class of Kondo-like materials with a small semiconducting gap, as determined by the activated behavior of the transport properties (Aeppli and Fisk, 1992). This gap is believed to arise in a lattice of Kondo impurities from hybridization of the f and conduction electrons, and hence is called a hybridization gap (Wachter, 1994). Since the Kondo-lattice Hamiltonian is applied, the term "Kondo insulator" has been coined. The Kondo semiconductors are, with one exception, cubic, and their lattice parameters indicate mixed-valence character for the f element in all cases, which also led to the definition of intermediate-valent semiconductor (Wachter, 1994).

In this review, we shall limit our attention to three prototype Kondo semiconductors: $Ce_3Bi_4Pt_3$, SmB_6, and FeSi, for which a rather extensive optical work has been performed. FeSi is of particular interest because this cubic compound shares certain similarities in physical properties with the various rare-earth hybridization-gap semiconductors. Of course, this possibility is of high current interest because it would make FeSi particularly suitable for investigating aspects of the electronic properties of a d-transition-metal system that might be related with features of correlation effects in f-electron materials.

TABLE V. Examples of so-called Kondo insulators or semiconductors, with their crystallographic structure and activation gap evaluated from the transport measurements (Aeppli and Fisk, 1992).

	Structure	Δ (K)
CeNiSn	ε-TiNiSn	3
$Ce_3Bi_4Pt_3$	$Y_3Sb_4Au_3$	42
SmB_6	CaB_6	27
SmS	NaCl	300–3000
TmTe	NaCl	3500
YbB_{12}	UB_{12}	62
UNiSn	MgAgAs	700
FeSi	FeSi	300

A. Some relevant properties

1. $Ce_3Bi_4Pt_3$

The reference compound $La_3Bi_4Pt_3$ is metallic at all temperatures, while the isostructural $Ce_3Bi_4Pt_3$ is semiconducting, its resistance, shown in Fig. 35 (Hundley *et al.*, 1990), rising some two orders of magnitude on cooling from 300 to 4 K. The transport gap Δ is approximately 50 K (Table V), and the low-temperature resistance levels off at a value that is quite sample dependent, but is generally of order 1 Ω cm. The Hall constant shows activated behavior with activation barrier $\Delta \sim 40$ K ($\sim$3.5 MeV). Inelastic neutron scattering on powders (Severing *et al.*, 1991) yield a magnetic gap without substructure of 12 meV. The high-temperature magnetic susceptibility is Curie-Weiss, with effective moment slightly reduced from the full $4f^1$ Hund's rule ground-state moment of $2.54\mu_B$. The magnetic susceptibility $\chi(T)$ goes through a maximum at 80 K, falling by about half at low temperature before rising in a sample-dependent Curie tail at lowest T. This tail is almost certainly due to extrinsic dirt, an interpretation confirmed by the neutron measurements (Aeppli and Fisk, 1992). Substituting La for Ce or Au for Pt decreases the resistance significantly (Fig. 35), and large ($x=0.3$) dopings eliminate the semiconducting characteristic in the resistivity completely and lead to a large electronic specific heat $\gamma\sim$150 mJ/mol-x K^2. Pure $Ce_3Bi_4Pt_3$ has $\gamma\sim$3 mJ/mol-Ce K^2, a sample-dependent value that is larger in samples with larger Curie tails. This γ is less than the 9 mJ/mol-La K^2 of pure $La_3Bi_4Pt_3$.

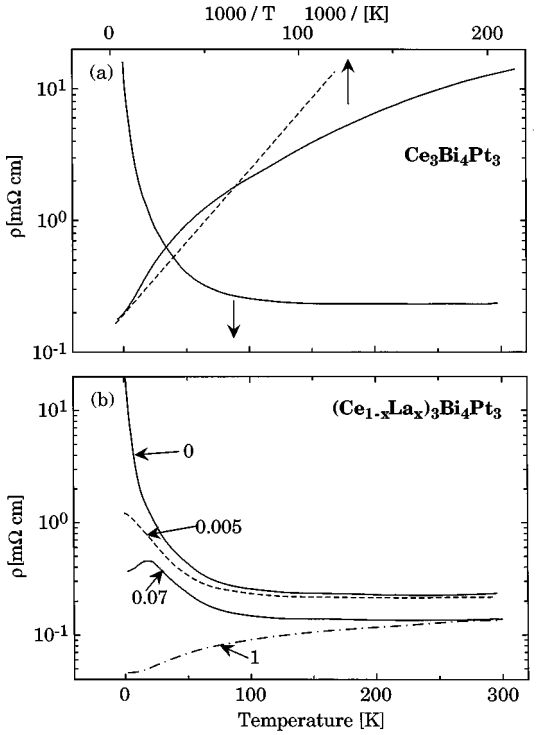

FIG. 35. Transport properties of $(Ce_{1-x}La_x)Bi_4Pt_3$. (a) The logarithm of the resistivity of $Ce_3Bi_4Pt_3$ vs temperature T and inverse temperature $1000/T$. The dashed line represents activated behavior. (b) Resistivity vs temperature for $(Ce_{1-x}La_x)_3Bi_4Pt_3$ for several values of x given in the figure. The resistivity for $x=0.07$ is typical of a moderately disordered valence-fluctuation metal (Hundley *et al.*, 1990).

All these features, together with a large negative magnetoresistance at low T and an increasing semiconducting gap with hydrostatic pressure, suggest a scenario of a nonmagnetic semiconductor at low T with a gap of roughly 50 K, and local moment behavior at $T>100$ K, with strong scattering of carriers, reminiscent of Kondo metals. Moreover, the most recent measurement of the pressure dependence of $\rho(T)$ (Cooley *et al.*, 1997) shows that the transport at high temperatures is dominated by excitations across a small activation gap, which increases rapidly with pressure. The low-temperature transport involves variable range hopping between extrinsic states in the gap.

2. SmB_6

SmB_6 is another prototypical member of the class of narrow-gap semiconductors. The most recent electrical resistivity measurement as a function of temperature for pressure ranging from 1 bar to 66 kbar on SmB_6 single crystal is displayed in Fig. 36 (Cooley *et al.*, 1995). The measured resistivity is well described at 45 kbar and below by a parallel combination of an activated term, dominant above 5 K, and a constant residual term ρ_0, accounting for the temperature-independent resistivity found below ~3.5 K. The activation gap Δ is suppressed linearly ~0.5 K/kbar from its ambient pressure value of 41 K. Above 45 kbar, the resistivity is metallic and it is

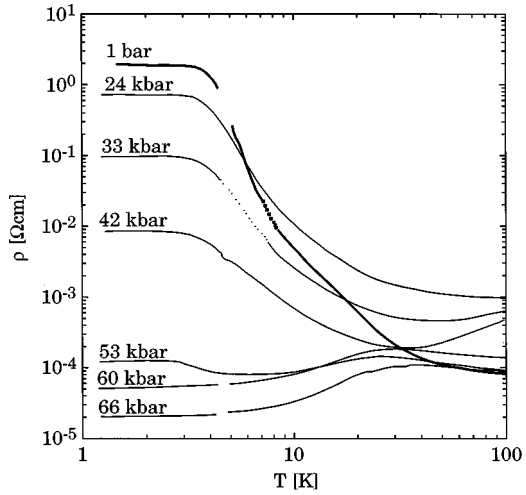

FIG. 36. Pressure dependence of the electrical resistivity ρ of SmB_6 as a function of temperature (Cooley *et al.*, 1995).

no longer possible to extract an activation gap. The measurements indicate a gap instability at a critical pressure P_c between 45 and 53 kbar, in disagreement with the conclusions of previous workers (Beille *et al.*, 1983; Berman *et al.*, 1983), who found that Δ vanished continuously near 60 kbar. In the study reported by Beille *et al.* (1983) the sample was of demonstrably lower quality than the specimen used by Cooley *et al.* (1995), with a significantly smaller ambient pressure gap $\Delta=33$ K and a much smaller $\rho_0\sim 10\,\mathrm{m}\,\Omega\,\mathrm{cm}$, both symptomatic of Sm vacancies or defects introduced in powdering.

From the thermodynamic point of view, it is worth noting that the measurements of the thermal expansion and of the specific heat are also well described by a semiconducting gap model (Mandrus *et al.*, 1994). Such a model consists of two narrow bands with width of the order of 100 K. From these latter investigations, it is also believed that such a gap of about 140 K is the single energy scale relevant for driving the thermodynamic properties.

3. FeSi

Nearly 25 years ago FeSi was recognized as a material with puzzling physical properties (Wolfe *et al.*, 1965; Jaccarino *et al.*, 1967), but only recently has a comprehensive series of low-temperature thermal, magnetic, and transport measurements been presented (Hunt *et al.*, 1994; Chernikov *et al.*, 1997; Paschen *et al.*, 1997). The magnetic susceptibility $\chi(T)$ of FeSi rises rapidly with increasing temperature above 100 K, goes through a maximum at around 500 K, and obeys a Curie-Weiss law at higher temperatures. Neutron diffraction, Fe^{57} Mössbauer (Watanabe *et al.*, 1963), and Si^{29} nuclear-magnetic-resonance (Wertheim *et al.*, 1965) studies exclude, however, the onset of an antiferromagnetic behavior below 500 K. An anomalous behavior was also observed for the specific heat (Paschen *et al.*, 1997). Its electronic component was reported to have a broad

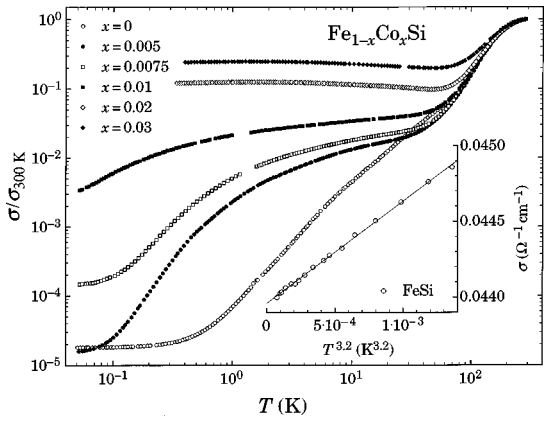

FIG. 37. Temperature variation of the electrical conductivity σ of $Fe_{1-x}Co_xSi$. The inset shows $\sigma(T)$ of nominally pure FeSi plotted as a function of $T^{3.2}$, below 0.17 K (Chernikov *et al.*, 1997).

peak at around 200 K, which is roughly the temperature where the magnetic susceptibility increases most steeply with temperature.

Figure 37 (Chernikov *et al.*, 1997) shows the electrical conductivity $\sigma(T)$ of the polycrystalline sample FeSi, measured in the temperature range between 0.05 and 300 K. We note that although $\sigma(T)$ was measured on a polycrystalline sample, the general features are very close to those revealed in experiments using single crystals. Below 300 K, there is a monotonic drop in conductivity by almost five orders of magnitude to the lowest measured temperature of 0.05 K. Between 200 and 300 K, $\sigma(T)$ suggests that the material enters the electronically degenerate regime. Furthermore, it is not possible to identify a regime of thermally activated conductivity over any extended range of temperature because the temperature variation of σ is, strictly speaking, characterized by a temperature-dependent slope.

Similarly to SmB_6, it has been shown (Mandrus *et al.*, 1995) that above 100 K the behavior of σ of pure FeSi is consistent with that of a hybridization-gap semiconductor, i.e., a system with a strong renormalization of the noninteracting bands and their widths that leads to an enhanced electronic density of states at the gap edges (see below). In the low-temperature regime (i.e., between 2.5 and 40 K), $\sigma(T)$ of pure FeSi can be described with a variable-range hopping behavior (Mott and Davis, 1971; Takagi *et al.*, 1981; Chernikov *et al.*, 1997; Paschen *et al.*, 1997), while at the lowest temperatures below 0.18 K, the conductivity σ is well described by T^{α} with $\alpha \sim 3.2$ (see Fig. 37).

Taken together, the $\sigma(T)$ behavior of FeSi is consistent with that of impure hybridization-gap semiconductors, for which in the intrinsic regime at high temperatures, the $\sigma(T)$ curves are expected to depend only slightly on doping. On the other hand, a strong concentration dependence of $\sigma(T)$ is expected in the regime of extrinsic conductance at low temperatures. This trend is also confirmed by recent investigation on Co-doped FeSi (Chernikov *et al.*, 1997). The high-temperature intrinsic semiconductor description finds its extension to lower

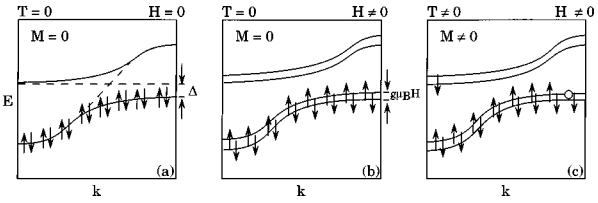

FIG. 38. Schematic band structure and magnetic-field dependence of a Kondo insulator (Aeppli and Fisk, 1992).

temperatures in the assumption of approximately $10^{18}\,cm^{-3}$ donor levels situated less than 1 meV below the conduction-band edge, and of a slightly lower acceptor concentration. These "impurities" could be identified with coordinational defects in the perfect FeSi structure that might be related to a slight Si deficiency (Chernikov *et al.*, 1997; Paschen *et al.*, 1997).

Moreover, the saturation of the electrical conductivity below about 5 K suggests a "metallic" ground state (Hunt *et al.*, 1994), with a density of itinerant charge carriers of the order of only $10^{22}\,cm^{-3}$. A possible origin of this metallic behavior is an impurity band formed out of the donor states, with a spectacularly narrow bandwidth. Thus itinerant and localized states would have to coexist at low temperatures so that the Fermi level would have to lie at or very close to the mobility edge, the energy which separates the localized from the extended states (Mott and Davis, 1971).

B. A phenomenological description: the hybridization-gap model

A simple model that captures most of the properties in Kondo insulators is that of a flat f band hybridizing with a broad conduction band, with exactly two electrons per unit cell. At $T=0$ these two electrons fill the lower hybridized band [Fig. 38(a)]. Furthermore, for applied magnetic fields small compared to the hybridization gap [Fig. 38(b)], the magnetic response χ vanishes because the numbers of up- and down-spin electrons remain equal. As T grows from 0 K, however, the filling of the lower and upper bands deviates from unity and zero, respectively, and a thermally activated Pauli-like term dominates $\chi(T)$ [Fig. 38(c)]. Analogously, the transport properties at low T are those of a semiconductor, while, at T of order of the gap and above, the resistivity should resemble that of a metal. This scenario is supported by a large variety of experimental results (see Sec. IV.A). For instance such a hybridization-gap-semiconductor approach to FeSi seems to consistently describe magnetic, thermodynamic, and transport properties of this material at temperatures exceeding 100 K (Sales *et al.*, 1994; Mandrus *et al.*, 1995; Chernikov *et al.*, 1997; Paschen *et al.*, 1997). In addition, high-resolution photoemission studies of FeSi (Park *et al.*, 1995; Saitoh *et al.*, 1995) have shown the development of a band with spectacularly sharp features near the edge of the valence band, which strongly supports a picture involving two narrow bands at the edges of a narrow gap. The estimated gap was,

however, very small. More recent high-resolution photoemission experiments (Breuer *et al.*, 1997) on poly- and single-crystal specimens with an ordered surface established an incomplete opening of a gap (pseudogap) with similar size to that measured by other techniques (see below).

Nevertheless, this model has been questioned in some cases. Even though the mean-field solution of the Kondo-lattice model neglects long-range magnetic interactions, it has been proposed that these correlations may drive first-order transitions with magnetic field, temperature, or pressure from a Kondo-compensated insulator to magnetically ordered metal (Millis, 1992). Charge degrees of freedom may also play an important role in gap formation, and are essentially ignored in the Kondo-lattice model. Alternatively and in analogy to Mott-Hubbard insulators, the insulating state may have a similar intrinsic instability, like a Mott insulator-to-metal transition involving f electrons, as external variables (i.e., pressure, magnetic field) modify the band structure and correlations. Unlike the continuous insulator-metal transition envisaged in the hybridization-gap scenario, all three of these alternatives encompass a discontinuous vanishing of the gap with pressure, magnetic field, or even temperature. For instance, a recent high-pressure resistivity measurement on SmB_6 (Cooley *et al.*, 1995), briefly mentioned above, indicates that the semiconducting gap cannot be the result of simple Kondo hybridization, since its discontinuous vanishing is not accompanied by a reduction in crystal symmetry. Various experimental evidences, as the absence of magnetic order in the high-pressure metallic state or the magnetic-field independence of the activation gap, led to the suggestion that SmB_6 could be a manifestation of a "classic" Mott-Hubbard system. Nevertheless, a theoretical basis, connecting the systems with typical Kondo features to the disparate Mott-Hubbard ones, remains a challenging task.

C. The excitation spectrum of Kondo insulators

Even though local density-functional band-structure calculations (Mattheiss and Hamann, 1993; Fu *et al.*, 1994) yield a semiconducting gap of roughly the correct size (e.g., ~0.1 eV for FeSi), spin-fluctuation effects are claimed to play an important role, as in FeSi in view of the large magnitude of $\chi(T)$ (Tajima *et al.*, 1988). This would be indicative of substantial discrepancies with conventional band theory and would also hint to a possible difference for the gaps in the charge and spin excitation channels. A relevant issue is then to see whether such discrepancies also arise from the charge fluctuations point of view. In this regard, optical investigations, addressing the charge dynamics, are a suitable experimental tool. The target of the optical work is therefore the crucial issue about the nature of the narrow (hybridizationlike) semiconducting gap.

Another topic of debate concerns the spectral weight transfer that accompanies the opening of the semiconducting optical gap. In fact, in a band insulator, development of a gap is expected to redistribute the spectral weight just above the gap, but large spectral weight transfers are not excluded in the context of strongly correlated electron system. Within a single-impurity Anderson model, the Kondo resonance in the f-spectral function is formed at T_K by transferring spectral weight from much higher energies of order $\pm U$ above and below the Fermi energy (Coleman, 1995). It would be intriguing by itself, if the reversed transfer (i.e., at high energies) would develop in Kondo semiconductors.

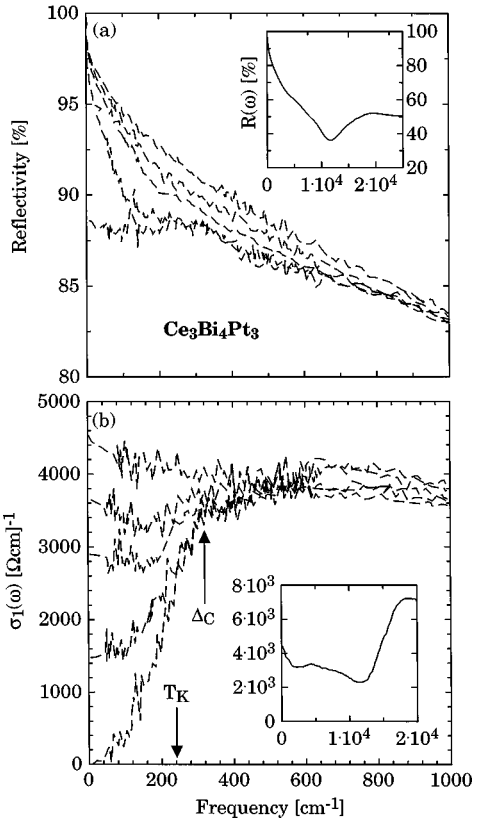

FIG. 39. Optical properties of $Ce_3Bi_4Pt_3$. (a) Far-infrared reflectivity of $Ce_3Bi_4Pt_3$ at several temperatures: from bottom to top, 25, 50, 75, 100, and 300 K. (b) Corresponding real part of the optical conductivity $\sigma_1(\omega)$ at the same temperatures as in (a) (from bottom to top). A gap is opening at Δ_c, which seems to be temperature independent. The insets show the high-frequency spectral range (Bucher *et al.*, 1994).

1. $Ce_3Bi_4Pt_3$

In Fig. 39(a) (Bucher *et al.*, 1994) the infrared reflectivity for $Ce_3Bi_4Pt_3$ is shown for selected temperatures. In the high-temperature region (100 and 300 K) the reflectivity resembles that of a low conducting metal, and does not show much temperature dependence. Below 100 K the reflectivity begins to show strong temperature dependence, and exhibits characteristics of a gap development at low frequencies. In Fig. 39(b), the real part of the optical conductivity $\sigma_1(\omega)$ is shown as a function of frequency for several temperatures. Between 100 and 300 K the conductivity is nearly constant as a function of frequency in the far infrared. Changes of the conductiv-

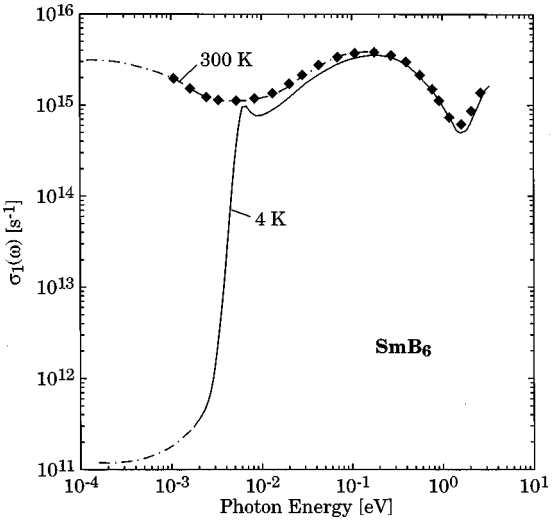

FIG. 40. Real part (σ_1) of the optical conductivity of SmB_6 at 300 and 4 K. The dot-dashed lines are the $\omega \rightarrow 0$ extrapolation (Travaglini and Wachter, 1984).

ity are modest above 100 K. Below this temperature, however, spectral weight begins to disappear from the low-frequency region signifying the development of a charge gap or pseudogap.

2. SmB_6

Similar to $Ce_3Bi_4Pt_3$, the reflectivity of SmB_6 at 300 K is metallic with a small shoulder at 0.1 eV and a screened plasma edge at 1.75 eV (Travaglini and Wachter, 1984). Interesting is once again the reflectivity behavior at low temperatures. $R(\omega)$ is reduced by 10% in the far-infrared region and a new maximum appears at about 5.5 meV, far below any observed optical-phonon frequency (Mörke *et al.*, 1981), and reaches a constant value for $\omega \rightarrow 0$. Consequently, the corresponding real part of the optical conductivity, shown in Fig. 40 (Travaglini and Wachter, 1984), displays the typical features reminiscent of a gap opening in the charge excitation spectrum, i.e., a suppression of spectral weight in the far infrared at low temperatures. Similar optical results over different spectral ranges were also obtained by Nanba *et al.* (1993) and Kimura *et al.* (1992, 1994).

3. FeSi

Figure 41 (Chernikov *et al.*, 1997) presents the optical conductivity of $Fe_{1-x}Co_xSi$ ($0<x<3$) polycrystals at some significant temperatures. The spectra for $x=0$ satisfactorily compare, at least as far as the qualitative shape of $\sigma_1(\omega)$ and its relative temperature dependence are concerned, with several optical results obtained by various groups (Schlesinger *et al.*, 1993; Degiorgi, Hunt, *et al.*, 1994; Ohta *et al.*, 1994; Bauer *et al.*, 1997; Damascelli, Schulte, van der Marel, *et al.*, 1997; Damascelli, Schulte, van der Marel, and Menovsky, 1997), which made use of different types of specimens (i.e., a single crystal grown in vapor transport, or in antimony flux as

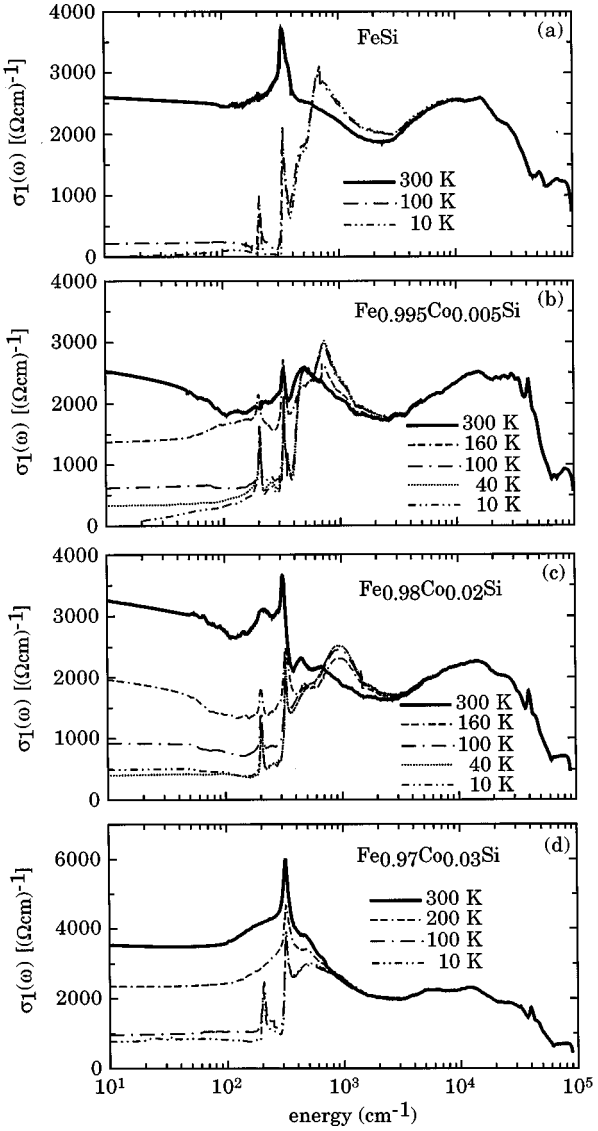

FIG. 41. Optical conductivity as a function of temperature of $Fe_{1-x}Co_xSi$ with $x=0$, 0.5%, 2%, and 3% (Chernikov *et al.*, 1997).

well as polycrystals). This is particularly compelling for FeSi, since it is not a line compound.

The most striking feature is, once again, the strong temperature dependence of $\sigma_1(\omega)$ in the far-infrared. As can be seen in Fig. 41(a), the Drude component in $\sigma_1(\omega)$, ascribed to itinerant charge carriers, is progressively quenched down to 100 K and disappears below 40 K. Even though $\rho(T)$ still increases by orders of magnitude below 40 K, it was not possible to detect any temperature dependence of $\sigma_1(\omega)$ in the far infrared range, this part of the spectrum being characterized by an optical conductivity typical of insulators. The excitation spectrum in far infrared is weakly influenced by doping. In fact, the electrodynamic response of Co-doped FeSi is qualitatively similar to the undoped FeSi. Figures 41(b)–41(d) present $\sigma_1(\omega)$ at several selected temperatures for $Fe_{1-x}Co_xSi$ with $x=0.5$, 2, and 3%. As in FeSi [Fig. 41(a)], there is the progressive opening of a gap, which leads to the suppression of spectral weight in the far-

infrared mid-infrared range. The dc limit of $\sigma_1(\omega)$ at each temperature is consistent with the measured dc conductivity (Fig. 37). At low temperatures, by $x=2$ and 3% one can still observe a (residual) metallic contribution to $\sigma_1(\omega)$, which manifests with a constant $\sigma_1(\omega \rightarrow 0) \neq 0$ behavior below the far-infrared spectral range. This contrasts with the behavior of $\sigma_1(\omega)$ for $x=0$ and 0.5%, where the metallic component is completely suppressed at low temperatures. It is also clearly demonstrated by these data that the suppressed spectral weight due to the opening of the gap piles up at the gap absorption. This is, however, a controversial issue, since Schlesinger *et al.* (1993) for FeSi and Bucher *et al.* (1994) for $Ce_3Bi_4Pt_3$, as well, found missing spectral weight up to very high frequencies (i.e., $\omega > 10\Delta$). The magnitude of the energy gap of FeSi that follows from the optical data is in fair agreement with the transport results (see below) and also with the results of other experiments (i.e., tunneling, Raman etc.) probing the width of the gap in the electronic excitation spectrum (Sarrao *et al.*, 1994; Aarts and Volodin, 1995; Mandrus *et al.*, 1995; Nyhus, Cooper, and Fisk, 1995). The sharp peaks in the far infrared and the absorptions in the visible-ultraviolet spectral range were found to generally agree with the expected vibrational modes (phonons) (Bauer *et al.*, 1997; Damascelli, Schulte, van der Marel, *et al.*, 1997; Damascelli, Schulte, van der Marel, and Menovsky, 1997) and electronic interband transitions (Ohta *et al.*, 1994), respectively.

Moreover, from the residual metallic component below the gap absorption [see Fig. 41(c) and 41(d)] at $T < 10\,\mathrm{K}$ for $x=2$ and 3%, described with a Drude term, one can estimate the effective mass (m^*) and the carrier concentration (n) of the itinerant charges. One can compare the corresponding plasma frequency ω_p, inferred from the phenomenological fit [Eq. (28)], with the Sommerfeld $\gamma(T \rightarrow 0)$ value of the electronic contribution to the specific heat. With $\omega_p = 1832$ and 2652 cm^{-1} and $\gamma = 5.7$ and 7.6 $\mathrm{mJ/mol\,K^2}$ one obtains $m^* \sim 30$, and $n = 9.95 \times 10^{26}$ and $2.14 \times 10^{27}\,\mathrm{m}^{-3}$ for $x=2$ and 3%, respectively. For $x=0$ and 0.5%, only a rough estimation is possible since at low temperatures (i.e., $T < 40\,\mathrm{K}$) the Drude component disappears completely. However, a simple linear extrapolation of ω_p for alloys with $x < 2\%$ and taking into account the corresponding γ values results again in mass enhancement of the order of 30. Such a mass enhancement is surprisingly high for $3d$ transition metal alloys. Thus the low-temperature state of FeSi is that of a strongly correlated metal with a very low concentration of itinerant charge carriers, a rather unusual feature for a $3d$ transition metal compound (Chernikov *et al.*, 1997).

Finally, it is worth noting that the optical investigation on FeSi were also extended over a very broad frequency range, well beyond the far infrared spectrum: namely, in the millimeter-wave and microwave spectral range (Degiorgi, Hunt, *et al.*, 1994), and even lower between 20 Hz and 1 GHz (Lunkenheimer *et al.*, 1995). These results were found to be compatible at low frequencies and temperatures (i.e., in the extrinsic regime) with impuritylike localized states, in agreement with the transport data.

D. The narrow-semiconducting-gap problem

The relevant feature in the electrodynamic response of these Kondo semiconductors is the mid-infrared absorption, which is associated with a semiconductor-type gap, and which will be the focus of the present discussion.

Historically, SmB_6 was the first intermediate-valent system investigated with optical methods. The origin of the semiconducting gap at 5.5 meV was ascribed to the hybridization-gap model (Wachter, 1994), which was found to be in agreement with conclusions drawn from transport, Hall effect (Allen *et al.*, 1979), and tunneling (Batlogg *et al.*, 1981) as well as point-contact spectroscopy (Frankowski and Wachter, 1982) results. However, the pressure-dependent transport measurements in SmB_6 do not fully support this hybridization-gap scenario (see Secs. IV.A and IV.B). Nanba *et al.* (1993) also questioned the d-f hybridization-gap picture for SmB_6. In such a model the gap occurs between the bonding and antibonding states of the d-f mixing band, then sharp peaks of the density of states are expected at both edges of the gap (Fig. 38). The gap excitation is, however, not an allowed dipole transition, from the stand point of a momentum conservation rule. An indirect transition would be possible but with a very small transition probability. It was alternatively proposed (Kasuya *et al.*, 1979; Nanba *et al.*, 1993) that the gap excitation could be the consequence of a weak Wigner crystallization which gives indeed a direct gap. Moreover, the latest Raman investigations questioned again the validity of a simple hybridization-gap model (Nyhus, Cooper, Fisk, and Sarrao, 1995; Nyhus *et al.*, 1997). These latter investigations suggest a gap of about $\Delta_c \sim 290\,\mathrm{cm}^{-1}$ substantially larger than previously found by transport and optical measurements. Furthermore, the opening of the gap is characterized by a suppression of electrons scattering over an energy scale Δ_c that is much larger than the characteristic temperature $T^* \sim 50\,\mathrm{K}$ for the gap development, i.e., $\Delta_c \sim 8 k_B T^*$. The development of the gap in SmB_6 renormalizes electronic states over a wider energy range. This might be not primarily influenced by f-d hybridization but rather by strong Coulomb correlations in the d band, because of the low carrier densities.

Bucher *et al.* (1994) pointed out for $Ce_3Bi_4Pt_3$ an alternative interpretation of 2Δ as the energy needed to excite a bound charge out from a local Kondo singlet and this should set the value for the Kondo energy $k_B T_K$. Moreover, they found that this charge excitation is different from the spin excitation. Indeed, for the spin excitation of the singlet a local triplet is predicted with an additional energy needed to delocalize the charge: $\Delta_c > \Delta_s$. It was established that the ratio $\Delta_c/\Delta_s \sim 1.8$ points to the strong coupling Kondo limit with the predicted ratio $\Delta_c/\Delta_s \sim 2$.

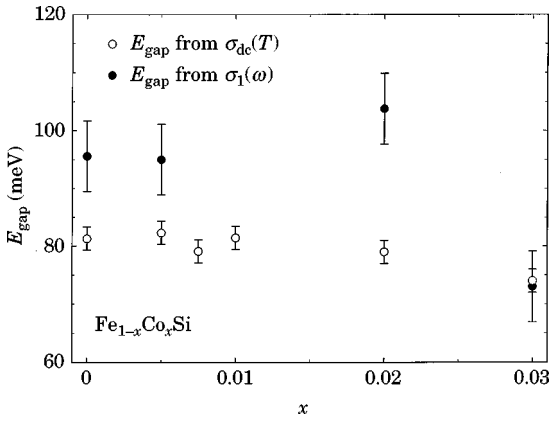

FIG. 42. The optical gap value vs the doping x in $Fe_{1-x}Co_xSi$, evaluated from transport and optical measurements (Chernikov *et al.*, 1997).

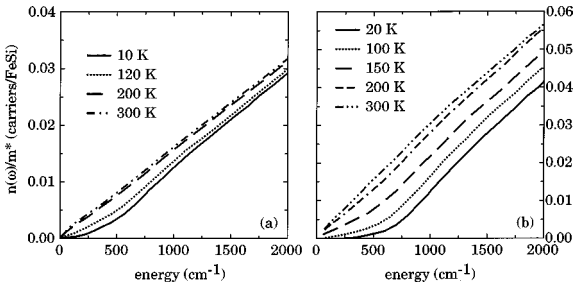

FIG. 43. Frequency dependence of the spectral weight sum rule, defined as the ratio between the effective charge carrier concentration up to ω and the effective mass, at various temperatures, calculated using Eq. (46) from the data of (a) Degiorgi, Hunt, *et al.* (1994) in Fig. 41(a) and (b) Schlesinger *et al.* (1993).

As far as FeSi is concerned, the optical gap seems to be in qualitatively fair agreement with results of band-structure calculations, even though its magnitude is smaller than the predicted gap. The systematic optical study on Co-doped FeSi permits to establish the precise doping dependence of the optical gap. This is performed by analyzing $\sigma_1(\omega)$ within the Lorentz-Drude approach [Eq. (28)], which permits to better decouple the various contributions in the excitation spectrum. Figure 42 (Chernikov *et al.*, 1997) shows the gap value vs the doping x in $Fe_{1-x}Co_xSi$. The comparison with the value extracted from the transport properties demonstrates that the gap is doping independent for $x<2\%$ and seems to undergo a 10–20% reduction by $x=3\%$ (particularly from the optical point of view).

A general conclusion with respect to the gap issue as inferred from the optical data could be that such an excitation is consistent with the great majority of experimental findings, even though its origins (also with respect of various theoretical suggestions) is difficult to establish on the basis of optical investigation alone.

Another important issue concerns the redistribution of the missing spectral weight below the gap. For the present results of Fig. 41, the spectral weight of FeSi is essentially recovered at a frequency $\omega_c \sim 8\Delta$, where $2\Delta = 770$ cm^{-1} is the gap excitation frequency. A similar conclusion for SmB_6 (Fig. 40) is in order, as well. The spectral-weight function is defined as [see also Eq. (29)]

$$\frac{n(\omega)}{m^*} = \frac{2}{\pi}\int_0^{\omega} \sigma_1(\omega')d\omega', \tag{46}$$

which is displayed in Fig. 43(a) for FeSi after the data of Degiorgi, Hunt, *et al.* (1994). Equivalent evaluations were also obtained for similar data by Chernikov *et al.* (1997) and Paschen *et al.* (1997). It may be seen that the spectral weight that disappeared below the gap is indeed redistributed for this set of data in a limited frequency range, and that above 3000 cm^{-1} there is almost no temperature dependence (i.e., all the curves in Fig. 43(a) merge together). This means that there should be no need for an integration of $\sigma_1(\omega)$ to very high frequencies in order to satisfy the spectral weight sum rule.

Nevertheless, the redistribution of the spectral weight still remains a puzzling and controversial experimental issue. In fact, the result of Fig. 43(a) contrasts with other reported optical results on FeSi, even though the spectra in terms of $\sigma_1(\omega)$ look qualitatively similar. As anticipated before, Schlesinger *et al.* (1993) and Bucher *et al.* (1994) claimed that the Kondo narrow gap semiconductors FeSi and $Ce_3Bi_4Pt_3$ recover the spectral weight, which is missing below the gap, at much larger energies than the gap itself. Figure 43(b) shows the spectral-weight analysis of Schlesinger *et al.* (1993) for FeSi and shall point out such a spectral weight controversy. The absence of a full compensation of spectral intensity due to the (pseudo)gap opening was also established in recent photoemission experiments (Breuer *et al.*, 1997).

On the other hand, Raman-scattering studies of FeSi (Nyhus, Cooper, and Fisk, 1995) reveal below $T<250$ K an abrupt suppression of low-frequency electronic Raman scattering, and a hardening of the characteristic energy for transitions above the charge gap. Even though this might be more consistent with correlation gap models than with a conventional band-gap description, the electronic spectral weight suppressed at low frequencies by the charge gap is primarily recovered within the energy range $\omega<6\Delta$. Analogous conclusions can be reached from Raman data on SmB_6 (Nyhus, Cooper, Fisk, and Sarrao, 1995; Nyhus *et al.*, 1997). Nevertheless, this similarity between the conclusions inferred from the optical data of Figs. 40 and 41 and the Raman spectra should be considered with caution, since both experiments as well as the photoemission one are not equivalent with respect to the spectral weight sum rule. If the redistribution of the spectral weight would take place around the gap, one could consider FeSi at low temperatures as a classical band insulator.

On a more general ground, it is worthwhile to quote the recent work by Di Tusa *et al.* (1997), where a heavy fermion metal emerges upon doping with Al at the Si site the strongly correlated insulator FeSi. The resulting metals and associated insulator-metal transition bear an extraordinary and even quantitative resemblance to those near the classic metal-insulator transition in the more conventional insulator Si. The strong Coulomb ef-

fects present in insulating FeSi serve only to renormalize the critical concentration and effective carrier masses (see Sec. IV.C) in the metallic phase.

E. The transfer of spectral weight in correlated electron systems: the theoretical point of view

The important issue associated with the redistribution and transfer of spectral weight in spectroscopies (like photoemission and optics) of strongly correlated electron systems was recently studied by Rozenberg *et al.* (1996). They started from the consideration that traditional methods used in the strong correlation problem—exact diagonalization of small clusters (van Veenendaal and Sawatzky, 1993, 1994), slave boson approaches (Millis, 1992), and perturbative calculations—have not been very successful in describing the interesting transfer of optical weight that takes place as a function of temperature in the strong correlation regime. Recently, much progress has been achieved by mapping lattice models into impurity models embedded in an effective medium. This technique, the local impurity self-consistent approximation (LISA) (Georges *et al.*, 1996), is a dynamical mean-field theory that becomes exact in the limit of a large number of spatial dimension (Metzner and Vollhardt, 1989). For instance, the Hubbard and Anderson lattice models can both be mapped onto the Anderson impurity model subject to different self-consistency conditions for the conduction-electron bath (Georges and Kotliar, 1992; Georges, Kotliar, and Si, 1992). These resulting self-consistent impurity problems can be analyzed by a variety of numerical techniques (Georges and Krauth, 1992; Jarrell, 1992; Rozenberg *et al.*, 1992).

First of all, it is important to recall the definition of the optical conductivity for a given system (Rozenberg *et al.*, 1996):

$$\sigma(\omega)=\frac{1}{V\omega}\,\mathrm{Im}\int_0^\infty(\langle[J(t),J(0)]\rangle)e^{i\omega t}\,dt, \tag{47}$$

where V is the volume, J is the current operator, and $\langle\,\rangle$ indicates an average over a finite temperature ensemble or over the ground state at zero temperature. In general, $\sigma(\omega)$ obeys a version of the f sum rule (Kohn, 1964; Maldague, 1977):

$$\int_0^\infty\sigma(\omega)d\omega=\frac{\pi}{V}\mathrm{Im}\langle[P,J]\rangle, \tag{48}$$

where P is a polarization operator obeying $dP/dt=J$.

In a model which includes *all electrons and all bands*, the current operator J is given by

$$J=\frac{e}{m}\sum_i p_i\delta(r-r_i), \tag{49}$$

where p_i is the momentum and r_i the position of the ith electron, and e and m denote its charge and bare mass. P is given by

$$P=e\sum_i r_i\delta(r-r_i). \tag{50}$$

Thus $(1/V)\langle[P,J]\rangle=ine^2/m$, where n is the density of electrons, and the sum rule becomes

$$\int_0^\infty\sigma(\omega)d\omega=\frac{\pi ne^2}{2m}, \tag{51}$$

equivalent to Eqs. (29) and (46) for the upper integration limit tending to infinity. This result is clearly temperature independent, and does not depend on the strength of the interactions (Rozenberg *et al.*, 1996).

When dealing with strongly correlated electron systems, in a frequency range where few of the bands are believed to be important, it is customary to work with an effective model with one or two bands, such as the Hubbard or periodic Anderson model. The current operator is thus projected onto the low-energy sector. In this case the expectation value $\langle[P,J]\rangle$ is no longer $\sim ne^2/2m$ [Eq. (51)], but is proportional to the expectation value of the kinetic energy $\langle K\rangle$ of the conduction electrons in the case of nearest-neighbor hopping (Maldague, 1977; Baeriswyl *et al.*, 1987). In general, $\langle K\rangle$ depends on the temperature and strength of interactions; therefore, for these few-band models, the optical weight sum rule will depend on them as well. If the projection onto a few-band model is valid, this result also implicity indicates that a portion of the optical spectral weight (the weight not exhausted by $\langle K\rangle$) is transferred to much higher energies; that is, to bands that were excluded by the projection to low energies (Rozenberg *et al.*, 1996).

As it was anticipated, the kinetic energy is related to the conductivity by the sum rule

$$\int_0^\infty\sigma(\omega)d\omega=-\frac{\pi e^2a^2}{2d\hbar^2\nu}\langle K\rangle=\frac{\omega_p^2}{8\pi}. \tag{52}$$

An important result is the notable dependence of the plasma frequency ω_p on temperature. This feature emerges because correlation effects generate small energy scales (e.g., the ''Kondo temperature'' of the associated impurity). It is the competition between the small scales and the temperature that gives rise to an unusual temperature dependence to the integrated optical spectral weight.

In the present review, we limit our attention to the discussion of the periodic Anderson model (PAM), following the treatment of Rozenberg *et al.* (1996). In a pedagogical and intuitive manner, the physical content of the periodic Anderson model within the dynamical mean-field theory can be seen in the following way. There are two different types of electrons; c electrons, which form a band, and f electrons with localized orbitals. In the noninteracting particle-hole symmetric case, the hybridization amplitude V opens a gap in the c-electron density of states $\Delta_{\mathrm{ind}}\sim V^2/D$ ($D=2t$ is the half band width with t the hopping amplitude). On the other hand, the original δ-function peak of the localized f electrons broadens by hybridizing with the conduction electrons and also opens a gap Δ_{ind}.

When the effect of the interaction term is considered, as the local repulsive U is increased, one finds that for low frequencies the noninteracting picture which was

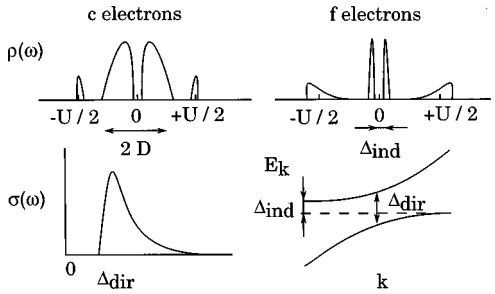

FIG. 44. Schematic DOS (half-filling) for c and f electrons in the periodic Anderson model (top). The corresponding schematic optical spectra at $T=0$ (bottom left) and the schematic band structure with the direct and indirect gaps (bottom right) (Rozenberg *et al.*, 1996).

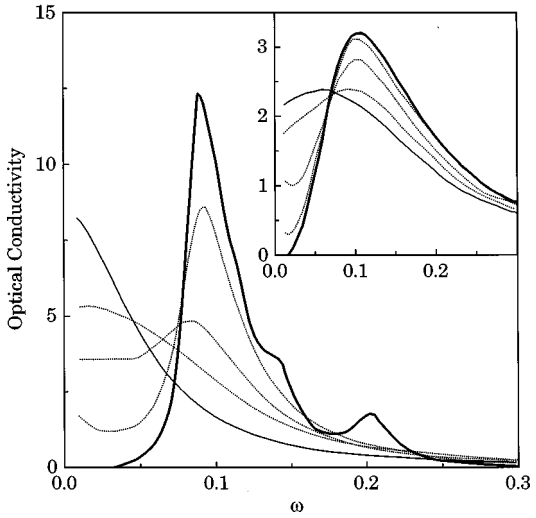

FIG. 45. The optical conductivity of the Anderson model at $T=0.001$ (bold), 0.005, 0.01, 0.02 (dotted), and 0.03 (thin). The interaction $U=3$ and $V=0.25$. Inset: the same quantity at $T=0.001$ (bold), 0.005, 0.01, 0.02 (dotted), and 0.03 (thin) with Lorentzian random site disorder of width $\Gamma=0.05$ (Rozenberg *et al.*, 1996).

just described still holds; though with the bare hybridization V being renormalized to a smaller value V^*. Thus one can say that there is a hybridization band insulator with the hybridization amplitude renormalized by interactions. This can also be interpreted by considering that the interacting f electrons form a band of "Kondo-like" quasiparticles, allowing the definition of a coherence temperature T^*. This coherent band further opens a gap due to the periodicity of the lattice. This is the well-known scenario that is borne out from slave-boson mean-field theory and variational calculations (Coleman, 1984; Rice and Ueda, 1986; Rozenberg *et al.*, 1996). On the other hand, the present dynamical mean-field theory also captures the high-energy part of the f-electron density of states that develops incoherent satellite peaks at frequencies $\pm U/2$ with a spectral weight that is transferred from low frequencies. Consequently, the c-electron density of states is mainly made of a central broadband of half-width $D=2t$ and a gap at the center that narrows as $V\rightarrow V^*$. Also, it develops some small high-frequency structures, that result from the hybridization with the f electrons. Figure 44 (Rozenberg *et al.*, 1996) schematically presents the density of states for the c and f electrons. Since the f sites are localized orbitals, only the c electrons contribute to the optical response of this system. At $T=0$, following the previous interpretation in terms of a renormalized noninteracting hybridization band insulator one expects to find an optical conductivity spectra with a gap $\Delta_{\rm dir}$, which decreases as the interaction is increased. One also expects that $\Delta_{\rm ind}\ll\Delta_{\rm dir}$, as the first corresponds to the indirect gap from the density of states $\Delta_{\rm ind}\sim V^{*2}/D$, while the second is the direct gap $\Delta_{\rm dir}\sim V^*$ that is defined as the minimum energy for interband transitions at a given k (see Fig. 44).

This model should be appropriate for the Kondo insulators, which are expected to display anomalous temperature dependence induced by correlations. Indeed, while the most qualitative physics of these systems is well understood, several features remain puzzling (Aeppli and Fisk, 1992). The charge gap Δ_c, measured in optical conductivity is larger than the spin gap Δ_s, measured in neutron scattering (Bucher *et al.*, 1994). Also, the transport gap Δ_t obtained from the activation energy in dc transport measurements is smaller than Δ_c (see, for example Fig. 42). From the optical experiments on SmB_6, $Ce_3Bi_4Pt_3$, and FeSi presented above (Secs. IV.C and IV.D), one can distinguish some common features regarding the energy scales associated with the formation of the optical gap. The gap Δ_c, begins to open at a characteristic temperature $T^*\sim\Delta/5$ and becomes fully developed at a much smaller temperature of the order of $T^*/5$. Also, the gap is temperature independent below T^*. Just as example, in $Ce_3Bi_4Pt_3$, it is found that $\Delta_c\sim 450$ K, $\Delta_s\sim 250$ K, and $T^*\sim 100$ K, and the optical gap is completely depleted only below 25 K. Qualitatively similar results were reported for FeSi, with $\Delta_c\sim 1000$ K, and $T^*\sim 200$ K, and the gap becomes depleted between 20 and 100 K.

The mean-field theory accounts for all these observations. Figure 45 (Rozenberg *et al.*, 1996) shows the optical conductivity for different temperatures with the parameters $U=3$ and $V=0.25$ fixed. The gap is essentially temperature independent. It begins to form at $T^*\sim 0.02\sim\Delta_c/5$, and is fully depleted only at temperatures of the order of $T^*/5$. The mean-field theory is able to capture the qualitative aspect of the experimental results. This basically consists in the individualization of three different energy scales: a large one which corresponds to the gap of the optical spectra $\Delta_c\sim\Delta_{\rm dir}$, an intermediate scale $T^*\sim\Delta_c/5$ where this gap starts to form and quasiparticle features start to appear in the density of states, and a third and smaller scale $\Delta_{\rm ind}\sim T^*/5$, which corresponds to the temperature where the optical gap is completely depleted.

In order to make a meaningful comparison with the experimental data, one has to add the effects of disorder by putting a Lorentzian distributed random site energy on the conduction-electron band with width $\Gamma=0.05$. The results are displayed in the inset of Fig. 45, showing

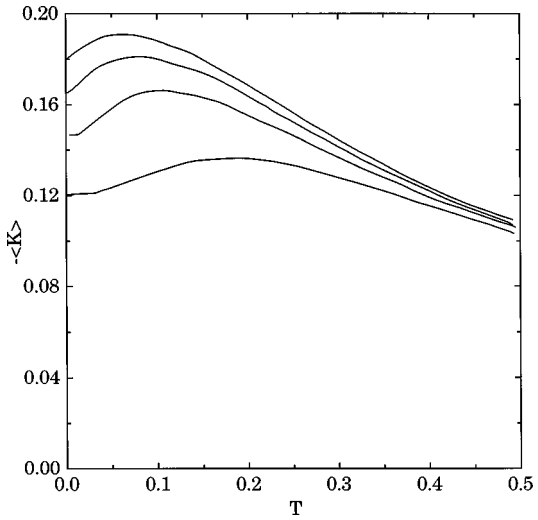

FIG. 46. Expectation value minus the kinetic energy $\langle K \rangle$ as a function of the temperature for $U=0,2,3,4$, and $V=0.4$ (bottom to top) as obtained from iteration perturbation theory. This quantity is directly related to the optical conductivity sum rule. It predicts a notable decrease in the total optical spectral weight as the temperature is decreased in the range below the maxima (Rozenberg *et al.*, 1996).

that the introduction of disorder places the overall shape of the spectra in closer agreement with the experimental results. This latter theoretical result also bears a similarity, at least qualitative, with $\sigma_1(\omega)$ calculated with a self-consistent augmented spherical wave method by Fu *et al.* (1994). They incorporated in the calculation simple finite-temperature effects, given by electron-phonon scattering of intrinsic carriers. The rough features, encountered in the experimental data, are reproduced. However, the number of intrinsic carriers is low compared to experimental observations, even with an *ad hoc* renormalization of the gap, and a strong scattering mechanism with attendant disordering of the band structure is required, as well.

In the following, we briefly address the question of the integrated spectral weight from the theoretical point of view. Rozenberg *et al.* (1996) suggested that, in order to contribute to the proper interpretation of the experimental data, it is important to compute the kinetic energy of the model at finite temperature, which is directly related to the sum rule of Eq. (52). The results are presented in Fig. 46 (Rozenberg *et al.*, 1996), which shows the notable dependence of the kinetic energy with temperature and interaction strength [the negative of $\langle K \rangle$ is plotted which is the quantity that enters Eq. (52)]. The strong correlation effects that renders $\langle K \rangle$ a function of the temperature implies that if the periodic Anderson model is the relevant model for the systems at low energies, then the results predict the behavior of the integrated optical weight within the low-frequency range. The behavior of $\langle K(T) \rangle$ in Fig. 46 is nonmonotonic. As the temperature is increased from zero, one can observe initially that the kinetic energy decreases. This is a consequence of electron delocalization, since the system becomes a metal as the small gap in the density of states is filled. The kinetic energy then goes through a minimum and starts to increase as the temperature is further increased. This is due simply to the thermal excitation of electrons within the single conduction band. Correlations now play an irrelevant role, as the temperature is higher then the coherence temperature T^*.

In regard to the experimental situation in the Kondo insulators, which indicate the apparent violation of the optical sum rule in some cases, these results could give, in principal, a plausible explanation for the observed behavior. In fact, for experimental data obtained at temperatures smaller than the size of the gap Δ_c and restricted to a finite low-frequency range, the model predicts the apparent "disappearance" of spectral weight as the temperature is decreased. However, the experimental state of the art on this issue is not unanimous. Moreover, it might well be that a small percent of the total spectral weight, which is missing at relatively high energies with respect to the gap energy, is beyond the resolution of the experiment.

In conclusion, one should point out that although this simple model (Rozenberg *et al.*, 1996) accounts, rather successfully, for the various energy scales, it fails to provide an accurate reproduction of the detailed experimental line shape of $\sigma_1(\omega)$ and, similarly, to the work of Fu *et al.* (1994), cannot account for the large scattering rate measured in these materials, if one does not include the effects of disorder in the model. It also remains to be seen if the sensitivity of the model at low energies is still compatible with a quantity [Eq. (52)] obtained by integrating over the whole frequency range. Moreover, questions are raised about the role of the bands, which are excluded by the projection to low energies in the calculation of $\langle K \rangle$. One might argue that at high frequencies such bands might lead to important contribution in the optical sum rules. Furthermore, this approach leaves open the main controversy in the experimental results; namely, up to which frequency range one can recover the missing spectral weight due to the opening of the gap.

V. CONCLUSION

A. Systematics

The complete electrodynamic response of a series of heavy-electron systems in the correlated state (i.e., at temperatures below T_{co}) displays the typical behavior expected for the excitation spectrum of heavy quasiparticles (see Sec. II.D). In fact, at $T<T_{co}$ there is the progressive development of a narrow mode centered at frequency zero, which is fully established at very low temperatures. The renormalized Drude-like nature of such a narrow mode suggests excitations of the heavy quasiparticles as its origin. It is, moreover, possible to extract several intrinsic parameters characterizing the coherent many-body state, e.g., the enhancement of the effective mass of the heavy electrons.

At this point, it is very tempting to introduce a kind of systematics in order to summarize the major results.

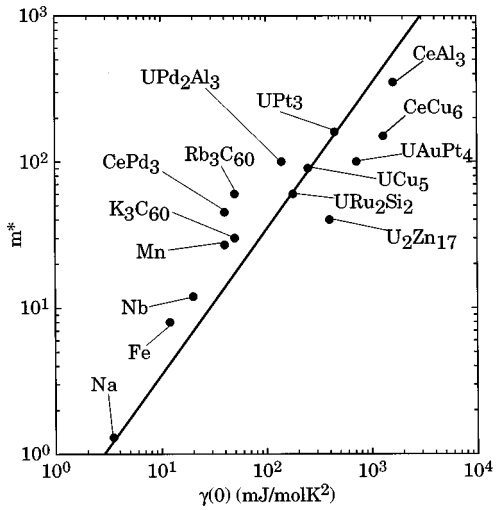

FIG. 47. Specific-heat γ values vs effective mass m^*, evaluated from the optical data using spectral-weight arguments (Degiorgi *et al.*, 1997).

There are several ways to describe in a comprehensive fashion the general trends encountered in these materials. Hill (1970) first suggested a simple and attractive idea: there is a clear dichotomy between magnetic, nonbonding electronic states and nonmagnetic, bonding ones. f orbitals are supposed to bond most easily with other f orbitals, hence a plot of magnetic behavior (such as magnetic-ordering temperature) versus f atom interatomic separations should give a clear border between the magnetic and nonmagnetic intermetallic compounds, the so-called Hill limit (~3.4 Å). It turns out that the Hill limit gives a necessary, but not sufficient, condition for the minimum f-f spacing above which magnetic ordering can occur (Ott and Fisk, 1987).

Another well-recognized striking fact about heavy-electron systems is that $\chi(T\rightarrow 0)$ nearly scales with $\gamma(T\rightarrow 0)$ (Ott and Fisk, 1987; von Löhneysen, 1995). This is somewhat surprising considering the underlying angular momentum of the appropriate f states. Such a scaling between χ and γ is also incorporated by the so-called Wilson ratio, which is of the order of 1 (i.e., 1 for free electrons, while for the heavy electron it is between 2 and 5). Therefore even though the Wilson ratio for the heavy electron can be greater than 1, the free-electron relation between χ and γ approximately and qualitatively holds.

Here, we are mainly interested in a systematic representation, relating quantities inferred from both dynamical (optics) and thermodynamic or transport investigations. Figure 47 (Degiorgi *et al.*, 1997) shows the specific heat $\gamma(T\rightarrow 0)$ values (Ott *et al.*, 1984, 1985; Ott and Fisk, 1987; Fisk *et al.*, 1988; Grewe and Steglich, 1991; Geibel, Schank *et al.*, 1991; Ott, 1992a, 1992b; Caspary *et al.*, 1993; Bernasconi *et al.*, 1994) versus the effective mass m^* of the heavy quasiparticles extracted from the optical data with the spectral-weight analysis [Eq. (30)]. The γ vs m^* representation is, indeed, alternative to γ vs the $T=0$ magnetic susceptibility $\chi(0)$ or vs the coefficient A of the T^2 behavior in the resistivity $\rho(T)$, which are mostly used. This choice (Fig. 47) allows us to compare magnetic with nonmagnetic systems in the same framework. It clearly appears that the conventional as well as the moderate heavy-electron materials undergoing magnetic ordering have γ values nearly scaling with m^*. Such a scaling does not seem to be affected by the onset of magnetic ordering and indicates a kind of universal behavior, and represents the realization of the quasiparticle concept within the Landau-Fermi liquid theory in the prototype heavy-electron systems. The deviations from $\gamma\sim m^*$ (which are not systematic) might be explained by the fact that one compares the outcome of different experimental techniques applied to specimens of different origin.

B. Heavy-electron superconductors

The onset of superconductivity in heavy-electron materials as well as the observation that superconductivity involves the heavy quasiparticles are another fascinating topic of high current interest. Since superconductivity was so unexpected in this kind of material, it did not take long for arguments to be brought forward suggesting that unconventional mechanisms are responsible for this superconductivity. Various experimental facts, to be briefly noted below, make it quite possible that these heavy-electron superconductors are the first in which the pairing of the electrons is not due to phonon exchange, but rather due to electron-electron interactions. In this case the resulting superconducting state is characterized by nonspherical symmetry, opposite to what is accepted for ordinary superconductors (Anderson, 1984; Varma, 1984). Heuristic arguments supporting this possibility are:

(1) the characteristic temperature of the heavy-electron subsystem (the renormalized Fermi temperature) is equal or smaller than the Debye temperature which characterizes the lattice-vibration spectrum.

(2) magnetic interactions (possibly spin fluctuations) dominate the low-temperature physical properties for example, the electrical resistivity or the specific heat. Such interactions are known to be harmful to ordinary superconductivity.

Actual calculations demonstrating a superconducting transition induced by electron-electron interactions in these materials is, of course, a very formidable task, if one considers that such a calculation would also have to predict the transition temperature. Predictions of transition temperatures are known to be quite difficult even in conventional superconductors and also for superfluid ^{3}He. In this case, additional complications due to the peculiarities of the electronic energy spectrum and strong spin-orbit interactions make calculations using known techniques and approximations even less meaningful (Ott and Fisk, 1987).

UPt_3 and UBe_{13} are the two most known superconducting heavy-electron materials, on which a large amount of experimental data has been collected. With respect to the superconducting state properties, some general trends can be recognized (Ott and Fisk, 1987;

Fisk *et al.*, 1988). First of all, one usually finds that the entropy balance between the hypothetical normal and the superconducting state is never quite zero. It is not clear whether this imbalance is due to an as yet unknown feature of the hypothetical normal state as $T \rightarrow 0$ K. Second, a comparison of $C_p(T)$ with the universal BCS prediction (Tinkham, 1975) shows considerable deviations both at $T \sim T_c$ and $T \ll T_c$. The temperature variation of C_p is fairly well approximated by a power law T^n, where $n = 2.85-2.9$, hence close to 3 (contrary to the BCS exponential decay of C_p at $T < T_c$). There is evidence that the superconducting energy gap is anisotropic and has nodes at certain points of the Fermi surface, as is possible for nonsinglet-type pairing of electrons in unconventional superconductors. Third, there is indication from both the thermal conductivity and the specific heat that a considerable contribution linear in T is found, again indicating the possible presence of normal electrons well below T_c. Furthermore, nonclassical behavior was also found for the temperature dependence of the magnetic-field penetration depth λ. From Bardeen-Cooper-Schrieffer theory (Tinkham, 1975) the penetration depth $\lambda(T)$ is expected to be close to the law $[1-(T/T_c)^4]^{-1/2}$ (i.e., the empirical "two-fluid" approximation), while in UBe_{13} is rather proportional to $(T/T_c)^2$ (Ott and Fisk, 1987).

Clearly, all these results indicate that for both UBe_{13} and UPt_3 the superconducting energy gap is not nonzero over the entire Fermi surface. This gap anisotropy, including gap zeros, is particularly intriguing for the cubic compound UBe_{13}. Also for UPt_3 any crystal-structure induced anisotropy should not necessarily lead to gap zeros. These gap anisotropies are used to argue that the superconducting state of UBe_{13} and UPt_3 is characterized by $l \neq 0$ pairing of the electrons, which would then imply that the essential pairing mechanism is not due to the usual electron-phonon interaction (Ott and Fisk, 1987; Fisk *et al.*, 1988).

In previous sections, we pointed out that small amounts of impurities often drastically change the low-temperature physical properties of heavy-electron compounds with respect to their magnetic phase transition. The same is true for the superconducting state of UBe_{13} and UPt_3. The superconductivity of UPt_3 is extremely sensitive to impurities and defects. Powdered UPt_3 obtained by grinding superconducting single crystals is reported to have lost the superconducting properties down to temperatures of a few milli-Kelvin. Small amounts of Pd substituted for Pt have the same devastating effect (Ott and Fisk, 1987).

Generally, the interplay between magnetism and (unconventional) superconductivity is one of the main topics in the physics of strongly correlated electron system (Aeppli and Broholm, 1994). The most important issue for heavy fermion superconductors such as $CeCu_2Si_2$, UPt_3, URu_2Si_2, UPd_2Al_3, and UNi_2Al_3 is that superconductivity is realized in the antiferromagnetic state. Furthermore, the mechanism of the pairing as well as the nature of the small magnetic moment (particularly for UPt_3 and URu_2Si_2) are still open questions and could be also addressed from the perspective of both the local and itinerant characters of the f electrons.

From the optical point of view, the superconductivity in the heavy electron has been less studied, however. The relatively low critical temperature T_c together with the intrinsically low characteristic energy scales (i.e., T_K or $1/\tau^*$) make optical investigation of the superconducting ground state technically very challenging, since extremely low temperatures and energies are required. Nevertheless, there is a lot of interesting problems on which optical methods might add relevant information. For instance, the comparison of the normal and superconducting state optical conductivity could allow the estimation of the penetration depth $\lambda(T)$ from spectral weight arguments. As far as the penetration depth is concerned, one can alternatively extract its temperature dependence from the imaginary part of the surface impedance. Besides $\lambda(T)$, optical investigations would also be helpful in order to disregard or confirm scenarios about the symmetry of the superconducting ground state. This can be achieved by analyzing the nature of the superconducting gap or through the analysis of the coherence factor effect (i.e., Hebel-Slichter coherence peak) in the optical conductivity (Tinkham, 1975). Moreover, the spectral weight argument would allow to establish whether the renormalized (ω_p^*) or the unrenormalized (ω_p) plasma frequency play the major role for superconductivity. This could confirm that the heavy charge carriers are, indeed, involved in the Cooper pairs. Furthermore, it remains to pin down whether superconductivity develops in the clean or dirty limit, a question which can be addressed optically.

C. Non-Fermi-liquid behavior: the UBe_{13} case

The crossover from a Fermi-liquid towards a non-Fermi-liquid ground state among the highly correlated systems raised a lot of interest.[2] The Fermi-liquid theory is very successful even for the description of complex systems like the heavy-electron ones, as also pointed out above (Fig. 47). In some special cases this description is not enough. Anomalous screening of the magnetic impurity or vicinity to a magnetic instability are two possible scenarios for the development of non-Fermi-liquid behavior. Those scenarios also represent two different points of view: namely, a local single-electron effects vs a more collective one.

Besides the transport and thermodynamic investigations, optical data reveal interesting behavior. In fact, the mapping of the complete electrodynamic response of the so-called Kondo alloys (see Sec. III) leads to frequency and temperature dependences of the scattering relaxation rate which deviate remarkably from the Fermi-liquid-prediction of Eq. (26). The optical data

[2]For the most recent developments see: *Proceedings of Conference on Non-Fermi Liquid Behavior*, 1996, J. Phys.: Condens. Matter **8**, edited by P. Coleman, M. B. Maple, and A. J. Millis.

demonstrate that it is possible to monitor the different ground states of the non-Fermi-liquid Kondo alloys by investigating the frequency dependence of an intrinsic parameter, such as the transport relaxation rate $\Gamma(\omega)$. This latter quantity displays a linear temperature or frequency dependence at low frequencies and temperatures, respectively, which is considered to be a clear manifestation of a non-Fermi-liquid-like behavior.

At this point, it would seem important to explore the frequency spectral range extending far below the far infrared. It is expected that at such low frequencies, the low-temperature behavior of $\Gamma(\omega)$ uncovered so far in the far-infrared spectral range will be further emphasized. Moreover, at these low frequencies and temperatures it should be possible to obtain additional information concerning the significance of the deviations from the power law or logarithmic divergences in $\rho(T)$ and $C(T)$ for $T<0.3$ K (Seaman *et al.*, 1991; Ott *et al.*, 1993; Maple *et al.*, 1994). It also remains to be seen what kind of relation may be established between the experimental optical data and the predictions of models based on the occurrence of the quantum phase transition. The combination of optical methods with magnetic-field dependence should, moreover, shed light on the interplay and coupling of charge and magnetic degree of freedom in the non-Fermi-liquid Kondo alloys.

As future outlook, we would like to briefly discuss the superconducting heavy-electron compound UBe_{13}, which is also characterized by a non-Fermi-liquid behavior in γ, and moreover possesses a very large residual resistivity ($\sim$100 $\mu\Omega$ cm) at the superconducting transition even in high-quality samples (as determined by a large T_c) (Ott and Fisk, 1987; Fisk *et al.*, 1988). UBe_{13} is a prototype ''ordered'' non-Fermi-liquid system, where the non-Fermi-liquid behavior may be possible from a two-channel Kondo model description (Cox, 1987, 1993; Ludwig and Affleck, 1991; Kim and Cox, 1994). Based on symmetry grounds, the model predicts that the electrical quadrupole moments of the twofold nonmagnetic Γ_3 ground state of the U ion are screened by orbital motion of the conduction electrons. Because the magnetic moment of the electrons is a spectator to this process, there are two screening channels (see also Sec. III). In the perspective of the previous Sec. (V.B), UBe_{13} is also of compelling importance, because superconductivity arises in a normal state which is clearly not described as Fermi liquid. The other way around, it has been speculated that such a non-Fermi-liquid normal phase corresponds to the manifestation of fluctuations effects due to the vicinity of a superconducting state.

Anders and coworkers (1997) recently presented a solution of one particle properties of the two-channel Anderson lattice model in infinite spatial dimensions. This calculation was performed for UBe_{13} but, in view of the similarity with the model described in Sec. III (particularly the two-channel Kondo lattice), it is suggested to be applicable also for the Kondo alloys. In fact, because of the incoherent normal metal phase, little qualitative difference between the more dilute alloys and the lattice is expected.

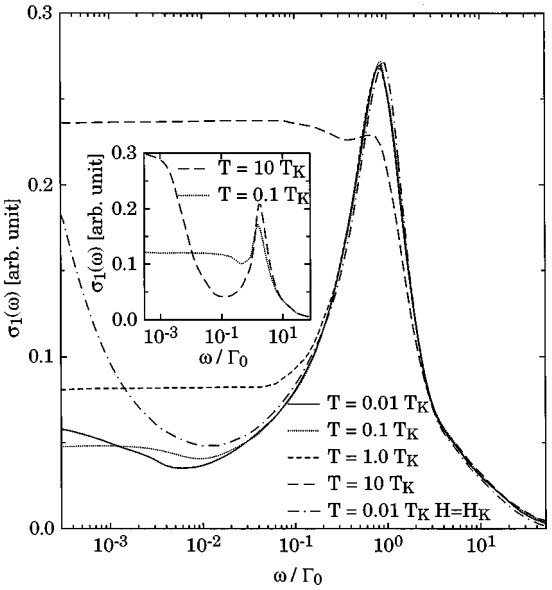

FIG. 48. Optical conductivity in arbitrary units vs frequency over three decades in temperatures. In the inset the corresponding curves for the single-channel periodic Anderson model for two high temperatures are shown (see also Figs. 10 and 12). The dashed-dotted line in the main figure is calculated with $H=H_K$ (Anders *et al.*, 1997).

Besides the calculation of the magnetoresistance, Anders and coworkers (1997) focused their attention on the optical conductivity, displayed in Fig. 48. The large peak at $\sim 0.9\Gamma_0$ results from high-energy charge excitations. With decreasing temperatures the optical conductivity develops a pseudogaplike feature. This is a characteristic feature, encountered also by other similar models for non-Fermi-liquid behavior (see Sec. III). A shift of a small amount of spectral weight to higher frequencies can be seen clearly in the figure by comparing the $T=10T_K$ and the $T=T_K$ curve (note that the logarithmic plot overemphasizes the area of the gap). At low temperatures a small increase in $\sigma(\omega)$ can be observed when $\omega\rightarrow 0$. Nevertheless, no clear Drude peak is seen even for $T=0.01T_K$, one decade lower than the observed maximum in $\rho(T)$. However, in a magnetic field of $H=H_K$ a low-frequency (renormalized) ''Drude'' peak develops again, consistent with the return to Fermi-liquid behavior suggested in $\rho(T,H)$ by the strong negative magnetoresistivity at temperatures below the resistivity maximum in an applied magnetic field (Willis *et al.*, 1987; Anders *et al.*, 1997).

The $\sigma(\omega,T)$ calculations are very compatible with the available yet incomplete optical data for UBe_{13} (Klassen *et al.*, 1987; Eklund *et al.*, 1987; Bonn, Klassen *et al.*, 1988; Bommeli *et al.*, 1997). Figure 49 (Bommeli *et al.*, 1997) shows the most recent data over a broad frequency range on a single crystal. There is a striking agreement with the theory. In fact, a suppression of $\sigma_1(\omega)$ in far infrared, similar to a pseudogap opening, and no clear Drude peaks are seen and the rescaling of the frequency axis suggests a $T_K\sim 10$ K. The differences between experiment and calculation at high frequencies

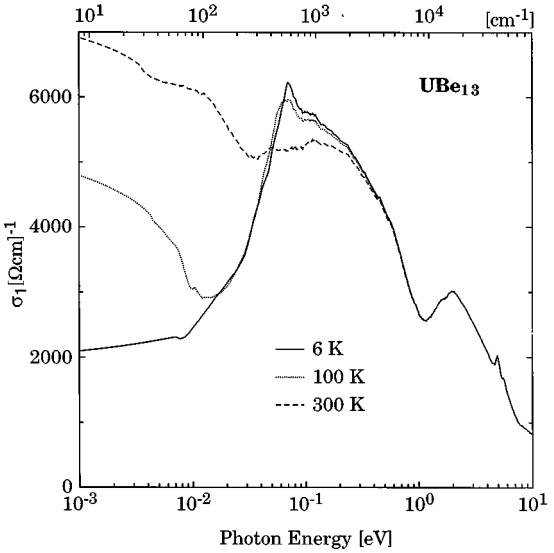

FIG. 49. Optical conductivity of UBe_{13} at 300, 100, and 6 K (Bommeli *et al.*, 1997).

are due to the fact that the calculation neglects the excitations associated with the crystal field splitting or interband transitions. The trend established by the far infrared optical conductivity for $1<T<10$ K is also supported by earlier surface resistance $R_s\sim(\rho_{dc})^{1/2}$ measurements at 100 and 150 GHz (Beyermann *et al.*, 1988).

Obviously, detailed measurements of both R_s and X_s in the microwave spectral range as well as far-infrared reflectivity investigations at $T<6$ K are desired for a more precise evaluation of the temperature dependence of the electrodynamic response. Moreover, it would be useful to have detailed $\sigma(\omega,T)$ data for UBe_{13} in a magnetic field. If a quadrupolar Kondo picture applies here, a *c*-axis magnetic field will split the channels, inducing a narrow Drude-like mode in $\sigma_1(\omega)$ and consequently the crossover to a Fermi-liquid state (Anders *et al.*, 1997). Such a magnetic-field-dependent investigation will permit a more compelling comparison with the calculation.

D. Kondo insulators and low-carrier Kondo systems

Heavy-electron phenomena were originally observed in metallic systems like $CeAl_3$, $CeCu_2Si_2$, UBe_{13}, UPt_3, etc., but more recently they have been also found in semimetals or even in insulators. In this review, we have addressed the topic of the electrodynamic response of the so-called Kondo semiconductors or insulators (Sec. IV). Another class of materials, which is often associated with the Kondo insulators and which was not treated here, corresponds to the low-carrier Kondo systems, like Yb_4As_3 and CeNiSn. This class of materials is presently attracting a lot of interest both theoretically and experimentally (Fulde, 1997). A particularly fascinating member is Yb_4As_3, which undergoes a trigonal distortion at $T_s=300$ K by a weak first-order phase transition. Measurements of the Hall constant reveal a dramatic increase below T_s implying a sharp drop in the charge-carrier density. At low T only one carrier per 10^3 Yb ions remains. With decreasing temperature the resistivity increases to a maximum of approximately 10 mΩ cm, while at low T it is of the form of Eq. (1) as for a Fermi-liquid. The linear specific-heat coefficient γ is found to be $\sim$200 mJ/mol K^2. The spin susceptibility χ_s is Pauli-like and equally enhanced with a Wilson ratio of order unity. No indication of magnetic order is found down to $T=0.045$ K. The above experimental findings strongly suggest heavy-electron behavior which is further confirmed by the observation that A/γ^ν ($\nu\sim2$) is similar to that of other heavy-electron systems. In Yb_4As_3, the low-energy scale (which defines the onset of the heavy-electron behavior) is due to the band width of the spin-density like excitations in chains of Yb^{3+} ions. The few charge carriers (one per 10^3 Yb ion) are not important for the low-temperature specific heat which is governed exclusively by the spin excitations. Therefore this system presents an almost perfect separation between spin and charge degrees of freedom. In other words, the increasing interest on this class of materials resides in the fact that, contrary to metallic heavy-electron systems, not only the effective mass but also the effective charge is strongly renormalized, because the system is a semimetallic one. Consequently, it is more appropriate and less misleading to speak of a neutral heavy-electron instead of a charged heavy-electron (Fulde, 1997).

A systematic optical investigation is right now in progress. For instance, the first optical results on Yb_4As_3 are characterized by an absorption band at 0.4 eV which is strongly temperature dependent. From sum-rule argument, such an absorption seems to be linked to the change of the dc conductivity, and it is ascribed to the mixing of Yb^{3+}-4*f* and Yb-5*d* bands (Kimura *et al.*, 1996, 1997). Further studies will be obviously of relevance for a comprehensive understanding of the dynamics of the charge excitation spectrum and of the anomalous physical properties of this class of materials.

Closing this review, we can generally state that the qualitative picture of heavy-electron materials is quite simple. At high temperatures these compounds show behavior usually associated with Kondo impurity systems. This single-site viewpoint becomes inadequate in a smooth manner on cooling to low temperature, where these systems approach a ground state possessing some of the characteristics of a Fermi liquid. The Fermi-liquid state in the sense of Landau is, however, only established at very low temperatures. As pointed out, this low-temperature state is adopted without a distinct phase transition, but it may itself be unstable against phase transitions that often occur before the Landau-Fermi-liquid state is fully developed and might lead to a non-Fermi-liquid state.

However, various issues remain to be fully understood (see above). For instance, very little is known about how parameters describing the high-temperature regime can be used to describe the low-temperature behavior. So far, only model calculations have been able to reproduce the salient features of experimental quantities. Moreover, there is little predictive capability as to which ma-

terials will develop heavy-electron behavior and even less success with predicting possible phase transitions.

It is fair to claim that heavy-electron physics will continuously lead to a better understanding of possible states and processes in solids in general. The development of theoretical techniques for treating many-body effects among electrons in metals, and the experimental verification of these results, will still attract the interest of the community in the future.

ACKNOWLEDGMENTS

First of all, I would like to thank P. Wachter for his continuous support and for many useful and stimulating discussions. I am also very much indebted to H. R. Ott, G. Grüner, and M. B. Maple for stimulating my interest in these topics and for providing important and valuable criticisms and suggestions. I would like to thank F. Bommeli, B. Ruzicka, F. Salghetti-Drioli, and V. Vescoli for their great help and for carefully reading the manuscript. I also benefited from many discussions with F. Anders, B. Andraka, M. Aronson, A. Castro-Neto, A. Chattopadhyay, P. Coleman, D. L. Cox, S. Donovan, M. Dressel, M. Jarrell, E. Miranda, R. Monnier, T. M. Rice, A. E. Rückenstein, F. Steglich, D. B. Tanner, A. M. Tsvelik, and H. von Löhneysen. I am particularly grateful to J. Müller and H. P. Staub for their technical help. Finally, I would like to acknowledge the important financial support of the Swiss National Foundation for Scientific Research and the ETH Research Council.

REFERENCES

Aarts, J., and A. P. Volodin, 1995, Physica B **206-207**, 43.

Aeppli, G., and C. Broholm, 1994, in *Handbook on the Physics and Chemistry of Rare Earth*, edited by K. A. Gschneider, Jr., L. Eyring, G. L. Lander, and G. R. Choppin (Elsevier, Amsterdam), Vol. 19, p. 123.

Aeppli, G., and Z. Fisk, 1992, Comments Condens. Matter Phys. **16**, 155.

Allen, J. W., B. Batlogg, and P. Wachter, 1979, Phys. Rev. B **20**, 4807.

Amato, A., 1997, Rev. Mod. Phys. **69**, 1119.

Amitsuka, H., T. Hidano, T. Honmo, H. Mitamura, and T. Sakakihara, 1993, Physica B **186-188**, 337.

Anders, F. B., M. Jarrell, and D. L. Cox, 1997, Phys. Rev. Lett. **78**, 2000.

Anderson, P. W., 1984, Phys. Rev. B **30**, 1549.

Andraka, B., 1994a, Phys. Rev. B **49**, 348.

Andraka, B., 1994b, Phys. Rev. B **49**, 3589.

Andraka, B., and G. P. Stewart, 1993, Phys. Rev. B **47**, 3208.

Andraka, B., and A. M. Tsvelik, 1991, Phys. Rev. Lett. **67**, 2886.

Andres, K., J. E. Graebner, and H. R. Ott, 1975, Phys. Rev. Lett. **35**, 1779.

Aronson, M. C., M. B. Maple, R. Chau, A. Georges, A. M. Tsvelik, and R. Osborn, 1996, J. Phys.: Condens. Matter **8**, 9815.

Aronson, M. C., R. Obsorn, R. A. Robinson, J. W. Lynn, R. Chau, C. L. Seaman, and M. B. Maple, 1995, Physica B **206-207**, 108.

Ashcroft, N. W., and N. D. Mermin, 1976, in *Solid State Physics* (Holt-Saunders, Philadelphia).

Awasthi, A. M., W. P. Beyermann, J. P. Carini, and G. Grüner, 1989, Phys. Rev. B **39**, 2377.

Awasthi, A. M., L. Degiorgi, G. Grüner, Y. Dalichaouch, and M. B. Maple, 1993, Phys. Rev. B **48**, 10692.

Baeriswyl, D., C. Gros, and T. M. Rice, 1987, Phys. Rev. B **35**, 8391.

Bakker, K., A. de Visser, L. T. Tai, A. A. Menovsky, and J. J. M. Franse, 1993, Solid State Commun. **86**, 497.

Batlogg, B., P. H. Schmidt, and J. W. Rowell, 1981, in *Valence Fluctuations*, edited by L. M. Falicov, W. Hanke, and M. B. Maple (North-Holland, Amsterdam), p. 267.

Bauer, E., S. Bocelli, R. Hauser, F. Marabelli, and R. Spolenak, 1997, Physica B **230-232**, 794.

Beille, J., M. B. Maple, J. Wittig, Z. Fisk, and L. E. Delong, 1983, Phys. Rev. B **28**, 7397.

Berman, I. V., N. B. Brandt, V. V. Moschalkov, S. N. Pashkevich, V. I. Sidorov, E. S. Konovalova, and Yu. B. Paderno, 1983, JETP Lett. **38**, 477.

Bernal, O. O., D. E. MacLaughlin, H. G. Lukefahr, and B. Andraka, 1995, Phys. Rev. Lett. **75**, 2023.

Bernasconi, A., M. Mombelli, Z. Fisk, and H. R. Ott, 1994, Z. Phys. B **94**, 423.

Beyermann, W. P., A. M. Awasthi, J. P. Carini, and G. Gruner, 1988, J. Magn. Magn. Mater. **76-77**, 207.

Beyermann, W. P., and G. Grüner, 1989, Phys. Rev. Lett. **63**, 2001.

Bogenberger, B., and H. v. Löhneysen, 1995, Phys. Rev. Lett. **74**, 1016.

Bommeli, F., L. Degiorgi, P. Wachter, F. B. Anders, and A. V. Mitin, 1997, Phys. Rev. B **56**, 10001.

Bonn, D. A., R. J. Klassen, J. D. Garrett, T. Timusk, J. L. Smith, and Z. Fisk, 1988, Physica C **153-155**, 453.

Boring, A. M., R. C. Albers, F. M. Mueller, and D. D. Koelling, 1985, Physica B & C **130**, 1711.

Brandt, N. B., and V. V. Moshchalkov, 1984, Adv. Phys. **33**, 373.

Breuer, K., S. Messerli, D. Purdie, M. Garnier, M. Heugsberger, Y. Baer, and M. Mihalik, 1997, Phys. Rev. B **56**, R7061.

Brodale, G. E., R. A. Fisher, and N. E. Phillips, 1986, Phys. Rev. Lett. **56**, 390.

Bucher, B., Z. Schlesinger, P. C. Canfield, and Z. Fisk, 1994, Phys. Rev. Lett. **72**, 522.

Buranov, L. I., and I. F. Shchegolev, 1971, Prib. Tekh. Eksp. **2**, 171.

Caspary, R., P. Hellmann, M. Keller, G. Sparn, C. Wassilew, R. Koehler, C. Geibel, C. Schank, F. Steglich, and N. E. Phillips, 1993, Phys. Rev. Lett. **71**, 2146.

Castro-Neto, A. H., G. Castilla, and B. A. Jones, 1998, Phys. Rev. Lett. **81**, 3531.

Chattopadhyay, A., and M. Jarrell, 1997, Phys. Rev. B **56**, R2920.

Chernikov, M. A., L. Degiorgi, E. Felder, S. Paschen, A. D. Bianchi, and H. R. Ott, 1997, Phys. Rev. B **56**, 1366.

Coleman, P., 1984, Phys. Rev. B **29**, 3055.

Coleman, P., 1995, Phys. Rev. B **206-207**, 872.

Continentino, M. A., 1993, Phys. Rev. B **47**, 11581.

Cooley, J. C., M. C. Aronson, and P. C. Canfield, 1997, Phys. Rev. B **55**, 7533.

Cooley, J. C., M. C. Aronson, Z. Fisk, and P. C. Canfield, 1995, Phys. Rev. Lett. **74**, 1629.

Cox, D. L., 1987, Phys. Rev. Lett. **59**, 1240.
Cox, D. L., 1993, Physica B **186-188**, 312.
Cox, D. L., and N. Grewe, 1988, Z. Phys. B **71**, 321.
Cox, D. L., and M. Jarrell, 1996, J. Phys.: Condens. Matter **8**, 9825.
Cox, D. L., and A. Zawadowski, 1998, Adv. Phys. **47**, 599.
Dalichaouch, Y., M. C. de Andrade, and M. B. Maple, 1992, Phys. Rev. B **46**, 8671.
Damascelli, A., K. Schulte, D. van der Marel, M. Fäth, and A. A. Menovsky, 1997, Physica B **230-232**, 787.
Damascelli, A., K. Schulte, D. van der Marel, and A. A. Menovsky, 1997, Phys. Rev. B **55**, R4863.
Degiorgi, L., 1995, Lecture delivered at ETH-Zurich on Optical Properties of Solids (unpublished).
Degiorgi, L., M. Dressel, G. Grüner, P. Wachter, N. Sato, and T. Komatsubara, 1994, Europhys. Lett. **25**, 311.
Degiorgi, L., M. Dressel, A. Schwartz, B. Alavi, and G. Grüner, 1996, Phys. Rev. Lett. **76**, 3838.
Degiorgi, L., M. B. Hunt, H. R. Ott, M. Dressel, B. J. Feenstra, G. Grüner, Z. Fisk, and P. C. Canfield, 1994, Europhys. Lett. **28**, 341.
Degiorgi, L., and H. R. Ott, 1996, J. Phys.: Condens. Matter **8**, 9901.
Degiorgi, L., H. R. Ott, M. Dressel, G. Grüner, and Z. Fisk, 1994, Europhys. Lett. **26**, 221.
Degiorgi, L., H. R. Ott, M. Dressel, G. Grüner, C. Geibel, F. Steglich, and Z. Fisk, 1995, Physica B **206-207**, 441.
Degiorgi, L., H. R. Ott, and F. Hulliger, 1995, Phys. Rev. B **52**, 42.
Degiorgi, L., St. Thieme, H. R. Ott, M. Dressel, G. Grüner, Y. Dalichaouch, M. B. Maple, Z. Fisk, C. Geibel, and F. Steglich, 1997, Z. Phys. B **102**, 367.
Degiorgi, L., P. Wachter, M. B. Maple, M. C. de Andrade, and J. Herrmann, 1996, Phys. Rev. B **54**, 6065.
de Visser, A., J. J. M. Franse, and A. Menovsky, 1984, J. Magn. Magn. Mater. **43**, 43.
Dickey, R. P., M. C. de Andrade, J. Hermann, M. B. Maple, F. G. Aliev, and R. Villar, 1997, Phys. Rev. B **56**, 11169.
DiTusa, J. F., K. Friemelt, E. Bucher, G. Aeppli, and A. P. Ramirez, 1997, Phys. Rev. Lett. **78**, 2831.
Dobrosavljevic, V., T. R. Kirkpatrick, and G. Kotliar, 1992, Phys. Rev. Lett. **69**, 1113.
Doniach, S., 1977, Physica B & C **91**, 231.
Doniach, S., and S. Engelsberg, 1966, Phys. Rev. Lett. **17**, 750.
Donovan, S., O. Klein, M. Dressel, K. Holczer, and G. Grüner, 1993, Int. J. Infrared Millim. Waves **14**, 2459.
Donovan, S., A. Schwartz, and G. Grüner, 1997, Phys. Rev. Lett. **79**, 1401.
Dressel, M., B. P. Gorshunov, A. V. Pronin, A. A. Mukhin, F. Mayr, A. Seeger, P. Lunkenheimer, A. Loidl, M. Jourdan, M. Huth, and H. Adrian, 1998, Physica B **244**, 125.
Dressel, M., O. Klein, S. Donovan, and G. Gruner, 1993, Int. J. Infrared Millim. Waves **14**, 2489.
Eklund, P. C., D. M. Hoffman, L. E. Delong, E. T. Arakawa, J. L. Smith, and Z. Fisk, 1987, Phys. Rev. B **35**, 4250.
Fisk, Z., D. W. Hess, C. J. Pethick, D. Pines, J. L. Smith, J. D. Thompson, and J. O. Willis, 1988, Science **239**, 33.
Frankowski, I., and P. Wachter, 1982, Solid State Commun. **41**, 577.
Freytag, R., and J. Keller, 1990, Z. Phys. B **80**, 241.
Fu, C., M. P. C. Krijn, and S. Doniach, 1994, Phys. Rev. B **49**, 2219.
Fukuyama, H., 1985, in *Proceedings of the 8th Taniguchi Symposium on the Theory of the Valence Fluctuating State*, Springer Series in Solid State Science, edited by T. Kasuya and T. Saso (Springer, New York).
Fulde, P., 1988, J. Phys. F **18**, 601.
Fulde, P., 1997, Physica B **230-232**, 1 and references therein.
Geibel, C., C. Schank, S. Thies, H. Kitazawa, C. D. Bredl, A. Boehm, M. Rau, A. Grauel, R. Caspary, R. Helfrich, U. Ahlheim, G. Weber, and F. Steglich, 1991, Z. Phys. B **84**, 1.
Geibel, C., S. Thies, D. Kaczorowski, A. Mehner, A. Grauel, B. Seidel, U. Ahlheim, R. Helfrich, K. Petersen, C. D. Bredl, and F. Steglich, 1991, Z. Phys. B **83**, 305.
Georges, A., and G. Kotliar, 1992, Phys. Rev. B **45**, 6479.
Georges, A., G. Kotliar, W. Krauth, and M. J. Rozenberg, 1996 Rev. Mod. Phys. **68**, 13.
Georges, A., G. Kotliar, and Q. Si, 1992, Int. J. Mod. Phys. B **6**, 705.
Georges, A., and W. Krauth, 1992, Phys. Rev. Lett. **69**, 1240.
Grewe, N., and F. Steglich, 1991, in *Handbook on the Physics and Chemistry of Rare Earth*, edited by K. A. Gschneider, Jr., and L. Eyring (Elsevier, Amsterdam), Vol. 14.
Grüner, G., 1974, Adv. Phys. **23**, 941.
Grüner, G., and A. Zawadowski, 1972, Solid State Commun. **11**, 663.
Hertz, J., 1976, Phys. Rev. B **14**, 1165.
Hill, H. H., 1970, in *Plutonium 1970 and Other Actinides*, edited by W. N. Miner (The Metallurgical Society of the AIME, New York), p. 2.
Hundley, M. F., P. C. Canfield, J. D. Thompson, Z. Fisk, and J. M. Lawrence, 1990, Phys. Rev. B **42**, 6842.
Hunt, M. B., M. A. Chernikov, E. Felder, H. R. Ott, Z. Fisk, and P. C. Canfield, 1994, Phys. Rev. B **50**, 14933.
Jaccarino, V., G. K. Wertheim, J. H. Wernick, L. R. Walker, and S. Arajs, 1967, Phys. Rev. **160**, 476.
Jarrell, M., 1992, Phys. Rev. Lett. **69**, 168.
Jarrell, M., H.-B. Pang, D. L. Cox, F. Anders, and A. Chattopadhyay, 1997, Physica B **230-232**, 557.
Jarrell, M., H.-B. Pang, D. L. Cox, and K.-H. Luk, 1996, Phys. Rev. Lett. **77**, 1612.
Kang, J.-S., J. W. Allen, M. B. Maple, M. S. Torikachvili, W. P. Ellis, B. B. Pate, Z.-X. Shen, J. J. Yeh, and I. Lindau, 1989, Phys. Rev. B **39**, 13529.
Kasuya, T., K. Takegahara, T. Fujita, T. Tanaka, and E. Banai, 1979, J. Phys. (Paris) **41-C5**, 308.
Kim, T. S., and D. L. Cox, 1994, Phys. Rev. Lett. **75**, 1622.
Kim, W. W., J.-S. Kim, B. Andraka, and G. R. Stewart, 1993, Phys. Rev. B **47**, 12403.
Kimura, S., M. Ikezawa, A. Ochiai, and T. Suzuki, 1996, J. Phys. Soc. Jpn. **65**, 3591.
Kimura, S., T. Nanba, S. Kunii, and T. Kasuya, 1994, Phys. Rev. B **50**, 1406.
Kimura, S., T. Nanba, M. Tomikawa, S. Kunii, and T. Kasuya, 1992, Phys. Rev. B **46**, 12196.
Kimura, S., A. Ochiai, and T. Suzuki, 1997, Physica B **230-232**, 705.
Kjems, J. K., and C. Broholm, 1988, J. Magn. Magn. Mater. **76-77**, 371.
Klassen, R. J., D. A. Bonn, T. Timusk, J. L. Smith, and Z. Fisk, 1987, J. Less-Common Met. **127**, 293.
Klein, O., S. Donovan, M. Dressel, and G. Gruner, 1993, Int. J. Infrared Millim. Waves **14**, 2423.
Kohn, W., 1964, Phys. Rev. A **171**, 133.

Lee, P. A., T. M. Rice, J. W. Serene, L. J. Sham, and J. W. Wilkins, 1986, Comments Condens. Matter Phys. **12**, 99.
Lenkewitz, M., S. Corsepius, G. F. v. Blanckenhagen, and G. R. Stewart, 1997, Phys. Rev. B **55**, 6409.
Ludwig, A. W. W., and I. Affleck, 1991, Phys. Rev. Lett. **57**, 3160.
Lunkenheimer, P., G. Knebel, R. Viana, and A. Loidl, 1995, Solid State Commun. **93**, 891.
Maldague, P. F., 1977, Phys. Rev. B **16**, 2437.
Mandrus, D., J. L. Sarrao, A. Lacerda, A. Migliori, J. D. Thompson, and Z. Fisk, 1994, Phys. Rev. B **49**, 16809.
Mandrus, D., J. L. Sarrao, A. Migliori, J. D. Thompson, and Z. Fisk, 1995, Phys. Rev. B **51**, 4763.
Maple, M. B., J. W. Chen, Y. Dalichaouch, T. Kohara, C. Rossel, and M. S. Torikachvili, 1986, Phys. Rev. Lett. **56**, 185.
Maple, M. B., M. C. de Andrade, J. Herrmann, Y. Dalichaouch, D. A. Gajewski, C. L. Seaman, R. Chau, R. Movshovich, M. C. Aronson, and R. Osborn, 1995, J. Low Temp. Phys. **99**, 223.
Maple, M. B., C. L. Seaman, D. A. Gajewski, Y. Dalichaouch, V. B. Barbetta, M. C. de Andrade, H. A. Mook, H. G. Lukefahr, O. O. Bernal, and D. E. MacLaughlin, 1994, J. Low Temp. Phys. **95**, 225.
Marabelli, F., 1989, in *Optical Spectroscopy of Intermediate Valence and Heavy Fermion Materials*, Ph.D. thesis, ETH Zurich.
Marabelli, F., G. Travaglini, P. Wachter, and J. J. M. Franse, 1986, Solid State Commun. **59**, 381.
Marabelli, F., and P. Wachter, 1990a, Phys. Rev. B **42**, 3307.
Marabelli, F., and P. Wachter, 1990b, Physica B **163**, 224.
Marabelli, F., P. Wachter, and E. Walker, 1988, Solid State Commun. **67**, 931.
Mattheiss, L. F., and D. R. Hamann, 1993, Phys. Rev. B **47**, 13114.
McEwen, K. A., M. J. Bull, R. S. Eccleston, D. Hinks, and A. R. Bradshaw, 1995, Physica B **206-207**, 112.
McEwen, K. A., U. Steigenberger, and J. L. Martinez, 1992, Physica B **186-188**, 670.
Metzner, W., and D. Vollhardt, 1989, Phys. Rev. Lett. **62**, 324.
Millis, A. J., 1992, in *Physical Phenomena at High Magnetic Fields*, edited by E. Manousakis, P. Schlottmann, P. Kumar, K. Bedell, and F. M. Mueller (Addison-Wesley, Reading), p. 146.
Millis, A. J., 1993, Phys. Rev. B **48**, 7183.
Millis, A. J., M. Lavagna, and P. A. Lee, 1987, Phys. Rev. B **36**, 864.
Millis, A. J., and P. A. Lee, 1987, Phys. Rev. B **35**, 3394.
Miranda, E., V. Dobrosavljevic, and G. Kotliar, 1996, J. Phys.: Condens. Matter **8**, 9871.
Miranda, E., V. Dobrosavljevic, and G. Kotliar, 1997a, Phys. Rev. Lett. **78**, 290.
Miranda, E., V. Dobrosavljevic, and G. Kotliar, 1997b, Physica B **230-232**, 569.
Mook, H. A., C. L. Seaman, M. B. Maple, M. A. Lopez de la Torre, D. L. Cox, and M. Makivic, 1993, Physica B **186-188**, 341.
Mörke, I., V. Dvorak, and P. Wachter, 1981, Solid State Commun. **40**, 331.
Mott, N. F., and E. A. Davis, 1971, in *Electronic Processes in Non-crystalline Materials* (Clarendon, Oxford), and references therein.
Nanba, T., H. Ohta, M. Motokawa, S. Kimura, S. Kunii, and T. Kasuya, 1993, Physica B **186-188**, 440.
Nozieres, P., and A. Blandin, 1980, J. Phys. (Paris) **41**, 193.
Nyhus, P., S. L. Cooper, and Z. Fisk, 1995, Phys. Rev. B **51**, 15626.
Nyhus, P., S. L. Cooper, Z. Fisk, and J. Sarrao, 1995, Phys. Rev. B **52**, R14308.
Nyhus, P., S. L. Cooper, Z. Fisk, and J. Sarrao, 1997, Phys. Rev. B **55**, 12488.
Oguchi, T., and A. J. Freeman, 1985, J. Magn. Magn. Mater. **52**, 174.
Ohta, H., S. Kimura, E. Kulatov, S. V. Halilov, T. Nanba, M. Motokawa, M. Sato, and K. Nagasaka, 1994, J. Phys. Soc. Jpn. **63**, 4206.
Ott, H. R., 1992a, Lecture on *f*-electrons in metals delivered at ETH Zurich (unpublished).
Ott, H. R., 1992b, Int. J. Mod. Phys. B **6**, 473.
Ott, H. R., 1996 (private communication).
Ott, H. R., E. Felder, and A. Bernasconi, 1993, Physica B **186-188**, 207.
Ott, H. R., and Z. Fisk, 1987, in *Handbook on the Physics and Chemistry of the Actinides*, edited by A. J. Freeman and G. H. Lander (Elsevier, Amsterdam), p. 85.
Ott, H. R., H. Rudigier, P. Delsing, and Z. Fisk, 1984, Phys. Rev. Lett. **52**, 1551.
Ott, H. R., H. Rudigier, E. Felder, Z. Fisk, and B. Batlogg, 1985, Phys. Rev. Lett. **55**, 1595.
Park, C.-H., Z.-H. Shen, A. G. Loeser, D. S. Dessau, D. G. Mandrus, A. Migliori, J. L. Sarrao, and Z. Fisk, 1995, Phys. Rev. B **52**, 16981.
Paschen, S., E. Felder, M. A. Chernikov, L. Degiorgi, H. Schwer, and H. R. Ott, 1997, Phys. Rev. B **56**, 12916.
Rice, T. M., 1987, Phys. Scr. **T19**, 246.
Rice, T. M., and K. Ueda, 1986, Phys. Rev. B **34**, 6420.
Riseborough, P. S., 1983, Phys. Rev. B **27**, 5775.
Rosch, A., A. Schröder, O. Stockert, and H. v. Löhneysen, 1997, Phys. Rev. Lett. **79**, 159.
Rozenberg, M. J., G. Kotliar, and H. Kajueter, 1996, Phys. Rev. B **54**, 8452.
Rozenberg, M. J., X. Y. Zhang, and G. Kotliar, 1992, Phys. Rev. Lett. **69**, 1236.
Sachdev, S., 1997a e-print cond-mat/9705266.
Sachdev, S., 1997b, e-print cond-mat/9705074.
Sachdev, S., N. Read, and R. Oppermann, 1995, Phys. Rev. B **52**, 10286.
Sacramento, P. D., and P. Schlottmann, 1989, Phys. Lett. A **142**, 245.
Saitoh, T., A. Sekiyama, T. Mizokawa, A. Fujimori, K. Ito, H. Nakamura, and M. Shiga, 1995, Solid State Commun. **95**, 307.
Sales, B. C., E. C. Jones, B. C. Chakoumakos, J. A. Fernandez-Baca, H. E. Harmon, J. W. Sharp, and E. H. Volckmann, 1994, Phys. Rev. B **50**, 8207.
Sarrao, J. L., D. Mandrus, A. Migliori, Z. Fisk, and E. Bucher, 1994, Physica B **199-200**, 478.
Schlesinger, Z., Z. Fisk, H. T. Zhang, M. B. Maple, J. F. DiTusa, and G. Aeppli, 1993, Phys. Rev. Lett. **71**, 1748.
Schlottmann, P., and P. D. Sacramento, 1993, Adv. Phys. **42**, 641.
Schoenes, J., and K. Andres, 1982, Solid State Commun. **42**, 359.
Schoenes, J., and J. J. M. Franse, 1985, Physica B **130**, 69.
Schultz, H. J., 1991, Int. J. Mod. Phys. B **5**, 57 and references therein.
Schweitzer, H., and G. Czycholl, 1991, Phys. Rev. Lett. **67**, 3724.

Seaman, C. L., M. B. Maple, B. W. Lee, S. Ghamaty, M. S. Torikachvili, J.-S. Kang, L. Z. Liu, J. W. Allen, and D. L. Cox, 1991, Phys. Rev. Lett. **67**, 2882.
Sengupta, A. N., and A. Georges, 1995, Phys. Rev. B **52**, 10295.
Sereni, J. G., and J. P. Kappler, 1994, J. Phys.: Condens. Matter **6**, 4771.
Severing, A., J. D. Thompson, P. C. Canfield, Z. Fisk, and P. Riseborough, 1991, Phys. Rev. B **44**, 6832.
Steglich, F., P. Gegenwart, R. Helfrich, C. Langhammer, P. Hellmann, L. Donnevert, C. Geibel, M. Lang, G. Sparn, W. Assmus, G. R. Stewart, and A. Ochiai, 1997, Z. Phys. B **103**, 235.
Stewart, G. R., 1984, Rev. Mod. Phys. **56**, 755.
Strange, P., and B. L. Gyorffy, 1985, Physica B & C **130**, 41.
Sulewski, P. E., and A. J. Sievers, 1989, Phys. Rev. Lett. **63**, 2000.
Sulewski, P. E., A. J. Sievers, M. B. Maple, M. S. Torikachvili, J. L. Smith, and Z. Fisk, 1988, Phys. Rev. B **38**, 5338.
Tajima, K., Y. Endoh, J. Fisher, and G. Shirane, 1988, Phys. Rev. B **38**, 6954.
Takagi, S., H. Yasuoka, S. Ogawa, and J. H. Wernick, 1981, J. Phys. Soc. Jpn. **50**, 2539.
Tanner, D. B., and T. Timusk, 1992, in *Physical Properties of High Temperature Superconductors III*, edited by D. M. Ginsberg (World Scientific, Singapore), p. 363, and references therein.
Thieme, St., P. Steiner, L. Degiorgi, P. Wachter, Y. Dalichaouch, and M. B. Maple, 1995, Europhys. Lett. **32**, 367; 1995, **32**, 783(E).
Thomas, G., J. Orenstein, D. H. Rapkine, M. Capizzi, A. J. Millis, R. N. Bhatt, L. F. Schneemeyer, and J. W. Waszczak, 1988, Phys. Rev. Lett. **61**, 1313.
Tinkham, M., 1975, in *Introduction to Superconductivity*, edited by R. E. Krieger (McGraw-Hill, New York).
Travaglini, G., and P. Wachter, 1984, Phys. Rev. B **29**, 893.
Tsvelik, A. M., and M. Reizer, 1993, Phys. Rev. B **48**, 9887.
Umeo, K., H. Kadomatsu, and T. Takabatake, 1997, Phys. Rev. B **55**, R692.
van Veenendaal, M. A., and G. A. Sawatzky, 1993, Phys. Rev. Lett. **70**, 2459.
van Veenendaal, M. A., and G. A. Sawatzky, 1994, Phys. Rev. B **49**, 3473.
Varma, C. M., 1984, in *Moment Formation in Solids*, edited by W. J. L. Buyers (Plenum, New York), p. 83.
Varma, C. M., 1985, in *Proceedings of the 8th Taniguchi Symposium on the Theory of the Valence Fluctuating State*, Solid State Science, Vol. 62, edited by T. Kasuya and T. Saso (Springer, New York).
Varma, C. M., P. B. Littlewood, S. Schmitt-Rink, E. Abrahams, and A. E. Ruckenstein, 1989, Phys. Rev. Lett. **63**, 1996.
von Loehneysen, H., 1995, Phys. Bl. **51**, 941.
von Loehneysen, H., F. Huster, S. Mock, A. Neubert, T. Pietrus, M. Sieck, O. Stockert, and M. Waffenschmidt, 1997, Physica B **230-232**, 550.
von Loehneysen, H., T. Pietrus, G. Portisch, H. G. Schlager, A. Schroeder, M. Sieck, and T. Trappmann, 1994, Phys. Rev. Lett. **72**, 3262.
Wachter, P., 1994, in *Handbook on the Physics and Chemistry of Rare Earths*, edited by K. A. Gschneidner, Jr., L. Eyring, G. H. Lander, and G. R. Choppin (Elsevier, Amsterdam), Vol. 19, p. 177.
Wang, C. S., H. Krakauer, and W. E. Pickett, 1985, Physica B & C **135**, 34.
Watanabe, H., Y. Yamamoto, and K. Ito, 1963, J. Phys. Soc. Jpn. **18**, 995.
Webb, B. C., A. J. Sievers, and T. Mihalisin, 1986, Phys. Rev. Lett. **57**, 1951.
Wertheim, G. K., V. Jaccarino, J. H. Wernick, J. A. Seitchik, H. J. Williams, and R. C. Sherwood, 1965, Phys. Lett. **18**, 89.
Willis, J. O., J. D. Thompson, J. L. Smith, and Z. Fisk, 1987, J. Magn. Magn. Mater. **63-64**, 461.
Wolfe, R., J. H. Wernick, and S. E. Haszko, 1965, Phys. Lett. **19**, 449.
Wooten, F., 1972, in *Optical Properties of Solids* (Academic, New York).
Wu, W. D., A. Keren, L. P. Le, G. M. Luke, Y. J. Uemura, C. L. Seaman, Y. Dalichaouch, and M. B. Maple, 1993, Physica B **186-188**, 344.
Wu, W. D., A. Keren, L. P. Le, G. M. Luke, Y. J. Uemura, C. L. Seaman, Y. Dalichaouch, and M. B. Maple, 1994, Phys. Rev. Lett. **72**, 3722.
Xu, J., P. J. C. Signore, B. Andraka, W. A. Acree, M. W. Meisel, and Y. Takano, 1994, J. Alloys Compd. **216**, 33.
Zlatic, V., G. Gruner, and N. Rivier, 1974, Solid State Commun. **14**, 639.
Zülicke, U., and A. J. Millis, 1995, Phys. Rev. B **51**, 8996.